

Shape measurement of the anterior eye surface

Citation for published version (APA):

Jongsma, F. H. M. (1998). *Shape measurement of the anterior eye surface*. [Doctoral Thesis, Maastricht University]. Universiteit Maastricht. <https://doi.org/10.26481/dis.19981126fj>

Document status and date:

Published: 01/01/1998

DOI:

[10.26481/dis.19981126fj](https://doi.org/10.26481/dis.19981126fj)

Document Version:

Publisher's PDF, also known as Version of record

Please check the document version of this publication:

- A submitted manuscript is the version of the article upon submission and before peer-review. There can be important differences between the submitted version and the official published version of record. People interested in the research are advised to contact the author for the final version of the publication, or visit the DOI to the publisher's website.
- The final author version and the galley proof are versions of the publication after peer review.
- The final published version features the final layout of the paper including the volume, issue and page numbers.

[Link to publication](#)

General rights

Copyright and moral rights for the publications made accessible in the public portal are retained by the authors and/or other copyright owners and it is a condition of accessing publications that users recognise and abide by the legal requirements associated with these rights.

- Users may download and print one copy of any publication from the public portal for the purpose of private study or research.
- You may not further distribute the material or use it for any profit-making activity or commercial gain
- You may freely distribute the URL identifying the publication in the public portal.

If the publication is distributed under the terms of Article 25fa of the Dutch Copyright Act, indicated by the "Taverne" license above, please follow below link for the End User Agreement:

www.umlib.nl/taverne-license

Take down policy

If you believe that this document breaches copyright please contact us at:

repository@maastrichtuniversity.nl

providing details and we will investigate your claim.

Shape measurement of the anterior eye surface

CIP-DATA KONINKLIJKE BIBLIOTHEEK DEN HAAG

Franciscus H. M. Jongsma

Shape measurement of the anterior eye surface

ISBN 90-5681-045-6

© 1998 ERIM (Eye Research Institute Maastricht)

© Review and classification of corneal topographers Springer-Verlag London Ltd.

© Development of a wide field height eye topographer: validation on models of the anterior eye surface the American Academy of Optometry.

© Corneal topography using a new moiré image-based system W.B. Saunders Company Limited.

Vormgeving omslag:

Geertjan van Zonneveld

Vormgeving binnenwerk en print:

Unigraphic, Universiteit Maastricht

Shape measurement of the anterior eye surface

PROEFSCHRIFT

ter verkrijging van de graad van doctor
aan de Universiteit Maastricht
op gezag van de Rector Magnificus
Prof. dr A.C. Nieuwenhuijzen Kruseman
volgens het besluit van het College van Decanen
in het openbaar te verdedigen
op donderdag 26 november om 16.00 uur

door

Franciscus Hermanus Maria Jongsma

geboren op 21 mei 1938 te 's-Gravenhage

Promotores:

Prof. dr F. Hendrikse

Prof. dr ir M.J.C. van Gemert (Universiteit van Amsterdam)

Co-promotor:

Dr H. Kingma

Beoordelingscommissie:

Prof. dr W. Th. Hermens (voorzitter)

Dr G.L. van der Heijde (Vrije Universiteit, Amsterdam)

Prof. dr ir A.P.G. Hoeks

Prof. dr L.H.E.H. Snoeckx

Dr ir C.H.F. Velzel (Technische Universiteit Eindhoven)

"All the arts are found by man. Man doesn't make them, but he finds them; and yet they haven't all been found. The finding of arts will never come to an end. Any day one of the arts could be found. Does the jester mention them all in the song? He doesn't mention them all, because in the world there are plenty of them that he doesn't know. From that song are missing many arts that are carried on beyond the mountains. Up there in Paris is a great art of carving and cutting precious stones, which is a great art there. And thus throughout the world there are many of them that you don't know, and yet they haven't all been found. Many of them have been found, but any day a new one could be found, and new ones are always being found".

Part of a sermon by friar Giordano at a meeting in 1305. Cited in E. Rosen, The invention of eyeglasses, Part I, Journal of History of Medicine 1956: 13-46

*To my loving wife Magda
and my daughters Hanneke and Sophia.*

Contents

1. Introduction and outline of the study	11
1.1 Introduction	13
1.2 Aim of the study	13
1.3 History of keratometry	13
1.4 Overview of the research, presented in this thesis	16
1.5 The fluorescent dye	16
1.6 Technical adaptations of the topographer	17
1.7 Technical validation of the MST	19
1.8 Clinical validation of the MST	19
2. Review and classification of corneal topographers	21
2.1 Abstract	23
2.2 History of corneal topography	23
2.3 Purpose and methods	25
2.4 Results	25
2.4.1 Literature search	25
2.4.2 Classification	26
2.4.2.1 Light-emitting Object/SPecular/INcoherent (OSPIN)	26
2.4.2.2 Projected Image/SPecular/INcoherent (PISPIN)	31
2.4.2.3 Projected Image/SPecular/COherent (PISPCO)	32
2.4.2.4 Projected Image/ScAttering/INcoherent (PISAIN)	37
2.4.2.5 Projected Image/ScAttering/COherent (PISACO)	38
2.4.2.6 Projected Image/DIFFuse/INcoherent (PIDIFIN)	39
2.4.2.7 Projected Image/SHadow/INcoherent (PISHIN)	41
2.4.2.8 Projected Image SPecular and DIFfuse/INcoherent (PISPDIFIN)	42
2.5 Discussion	43
2.5.1 The classification	43
2.5.2 Technical potential	43
2.5.3 Clinical potential	44
2.6 Conclusions	44
3. A model for testing fluorescein agents as a coating for the anterior eye:	
A feasibility study	47
3.1 Introduction	49

3.2	Assessment of fluorescent yield and opacity of different fluorescein staining agents in relation to layer thickness, fluorescein concentration and dilution medium using a phantom	51
3.2.1	Abstract	51
3.2.2	Materials and methods	51
3.2.3	Preparation of the samples	53
3.2.4	Results	53
3.2.5	Discussion	55
3.3	<i>In vivo</i> assessment of the fluorescent yield of fluorescein staining on the ocular surface	56
3.3.1	Abstract	56
3.3.2	Materials and methods	57
3.3.3	Results	57
3.3.4	Discussion	57
3.4	Comparison of phantom and <i>in vivo</i> results, conclusion	60
3.5	Conclusion phantom and <i>in vivo</i> studies	60
4.	System for determining the topography of a curved surface	63
4.1	Abstract	65
4.2	Introduction	65
4.2.1	General	65
4.2.2	Background of the invention	65
4.2.3	Limitations of Kawara's technology	65
4.3	Improvements on Kawara's technique	67
4.3.1	Improvement of measurement precision	67
4.3.2	Some methods for contrast control	67
4.3.3	Detection of the sign of the surface slope	69
4.4	Development of a new corneal topographer	69
4.4.1	Local frequency detection as an alternative to dynamic focusing techniques	71
4.5	The Maastricht Shape Topographer	72
4.5.1	Quality of the optics	74
4.5.2	The software	75
4.5.3	Precision of the pixel value	76
4.6	Discussion and conclusions	77
5.	Development of a wide field height eye topographer:	
	Validation on models of the anterior eye surface	79
5.1	Abstract	81
5.2	Introduction	81
5.3	Methods	83
5.3.1	Design considerations	83
5.3.2	The device	85
5.3.3	Calibration and validation of the MST	87
5.4	Results	88
5.4.1	Accuracy and precision in height	88

5.4.2 Reproducibility	90
5.4.3 Conversion of height values in radius of curvature	90
5.4.4 Depth of field	91
5.5 Discussion	91
5.6 Summary	93
6. Clinical evaluation of the MST	95
6.1 Abstract	97
6.2 Introduction	97
6.3 Corneal topography using a new moiré image-based system	97
6.4 Further developments	119
6.5 Further clinical validation	120
6.5.1 The subtraction modality	120
6.5.2 Localization of irregularities	120
6.5.3 Reproducibility of curvature determination	120
6.5.4 Wide field measurements	120
7. Concluding remarks	123
7.1 Introduction	125
7.2 Height measurements of the entire eye anterior surface	125
7.3 Limitations of height topography	126
7.4 Presentation of height data	126
7.5 Predicting contact lens fitting and behaviour	127
7.6 The MST compared to Placido disc-based CAVKs	127
7.7 Further research	128
Appendix 1 European patent EP o 551 955 B1 1997	131
List of symbols and abbreviations	149
Summary	153
Samenvatting	157
Dankwoord	161
Curriculum vitae	167
List of publications	171

Chapter 1

Introduction and outline of the study

1.1 Introduction

The optical part from the eye consists of a succession of transparent tissues with different refractive indices. Light entering from the outside passes the precorneal tear film, the cornea, the aqueous humor, the lens, the vitreous body and eventually reaches the retina. The first transition, from air to tear film, entails an optical density step of about 33% ($n = 1.00$ to $n = 1.33$). The posterior tissues deviate less than 10% from the refractive index of the tear liquid. Thus, the shape of the cornea, being the carrier of the tear film, is of paramount importance for the optical quality of the eye and consequently for good vision.

During the last twenty years, considerable progress has been achieved in the optical correction of this first refractive surface. In refractive surgery, there is wide acceptance today for the concept of precisely changing the outer corneal curvature by using laser photorefractive techniques. It requires accurate measurement of the corneal shape before and after surgery. Moreover the production of modern contact lenses has become highly sophisticated. With computer-assisted lathes not only spherical but also aspherical and torical (barrel-shaped) fittings and corrections can be made. Such torical surfaces are more curved in one particular direction, and may correct astigmatism.

Besides corneal contact lenses, also scleral contact lenses are made. To fit these lenses, not only the shape of the corneal surface but also the shape of the adjacent tissues (limbal area and sclera) must be taken into account. This requires a topographer that can measure the entire anterior eye surface. Today, many optometrists and ophthalmologists are looking for a device that can map the entire corneal surface and preferably also the adjacent tissues. These requirements form the background of the present study.

1.2 Aim of the study

To develop an instrument that measures the shape from the entire anterior eye. Measurement of irregularly shaped corneas and adjacent tissues must be possible. Data acquisition and presentation of results should be rapid and convenient in order to allow routine clinical application.

1.3 History of keratometry

The first "keratometers" (instruments to measure corneal curvature) were introduced in the mid-19th century and were based on the measurement of corneal refractive power. Refractive power of an optical medium causes deviation in propagation direction when a light ray passes the refractive boundary at an oblique angle. For instance, a specific shape composed of plane surfaces is a prism. The amount of deviation measured 100 cm from a refracting prism is expressed in "prism dioptres" (1 cm deviation = 1 prism dioptre). Another specific shape for which refractive power can be defined is a spherical surface. A parallel beam of light can be collected by a spherical refracting surface in a single point, the "focal point". The refractive power of such a surface is the reciprocal of

its "focal length" (f), or in inverse metres called "dioptries" (D), ($D = 1/f$ in metres). Conversion from height topography into Axial Radius Of Curvature (AROC) values can be done assuming the surface to be spherical (fig. 1.1a). The sagittal position (k -value) on which the height is measured determines the accuracy of the estimated AROC value and consequently dioptric value (fig. 1.1b).

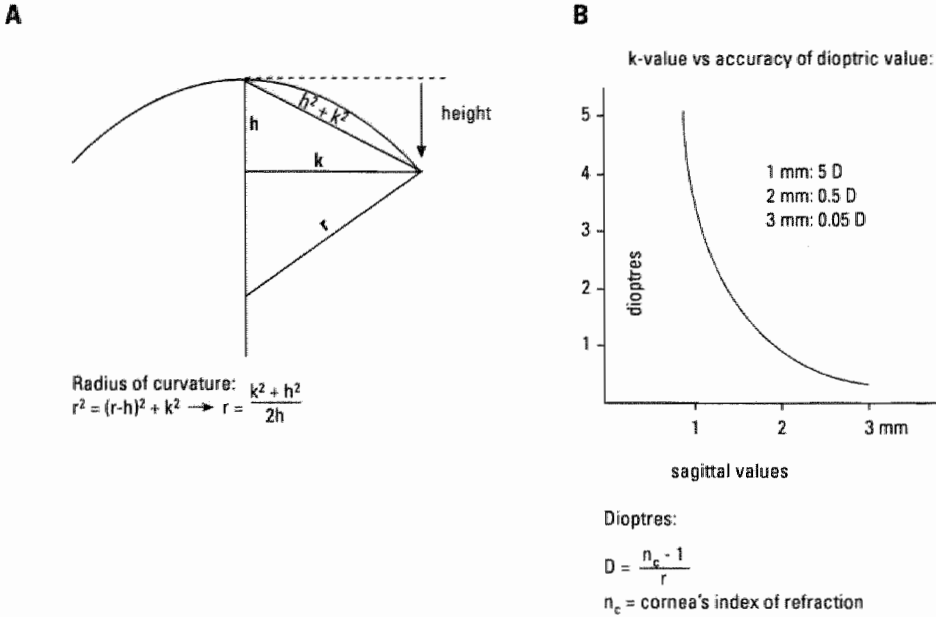


Figure 1.1

- a) Conversion from height (h) and sagittal value (k) into radius of curvature (r), and axial power according the lens makers equation (unit: m^{-1} = Diopter, D). The error in radius of curvature (or dioptries) depends on the position of the measurement with respect to the axis of the optical surface. (A more accurate estimation of the cornea's refractive power is obtained using Snell's law. It gives for any corneal position an indication of the first refractive surface's contribution to refraction).
- b) Relation between sagittal value (k) and accuracy of estimated dioptric value with an error in axial radius of curvature of 0.1 mm for a normal corneal surface.

A full treatment of the various optical principles and instruments used in this field is presented in Chapter 2 of this thesis. In order to explain the aims of the studies presented in this thesis, however, we will briefly discuss two different techniques, the Placido keratometer¹, introduced more than a century ago, and the keratometer introduced in 1979 by Kawara².

By considering the cornea as an optical equivalent to a spherical mirror, its radius of curvature can be estimated (fig. 1.2a). In 1880 Placido introduced a disc with concentric rings with a central hole through which he observed the image reflected by the subject's cornea (fig.1.2b). His device, later named "Placido keratometer", has been further developed into the computer assisted video keratometers (CAVKs) used today. However, this

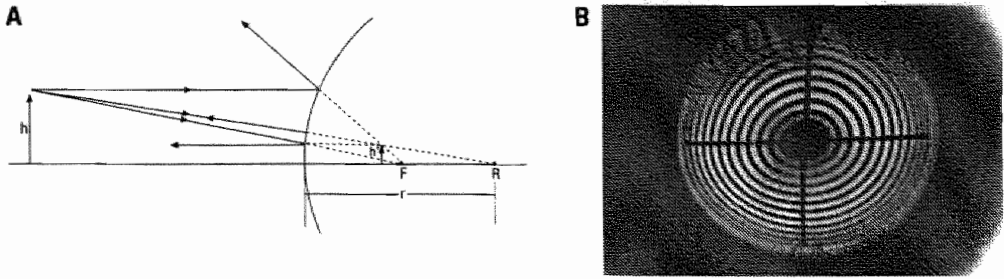


Figure 1.2

- a) The principle of keratometry is based on image formation with a convex mirror. The cornea is assumed to be a convex mirror of which the radius of curvature (r) determines the magnification (h/h') of the reflected images. The longer the distance between the object (h) and cornea, the closer h' is located to the focal plane of the corneal reflecting surface.
- b) Reflection of a Placido disc deformed due to corneal astigmatism.

specular reflection-based imaging technique has some shortcomings. The area on the corneal surface that is mapped depends on the shape of the "stimulator" (configuration of the light emitting pattern that is mirrored by the corneal surface) (fig. 1.3a) The surface topography of the adjacent non-corneal tissues is not obtained (fig. 1.3b). Imaging of abnormal corneas can lead to virtual images that are not properly focused due to a lack of depth resolution or due to concave areas on the corneal surface. As a consequence, the recorded image may contain unresolved or ambiguous parts.

To obtain reliable topographic data from an irregular surface, it is necessary that the surface itself is imaged. This excludes most of the measurement techniques based on specular reflection, such as Placido disc-based techniques that visualizes indirect surface properties such as the axial radius of curvature (see fig. 1.3a). The keratometer intro-

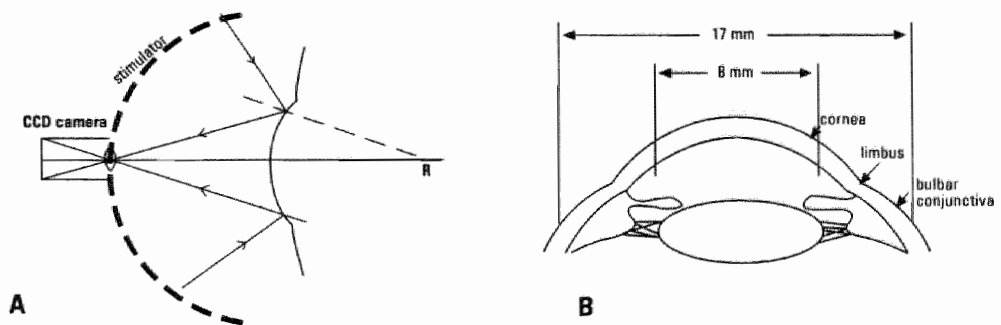


Figure 1.3

- a) Principle of a Placido disc-based CAVK. The cornea's area that is mapped depends on the shape of the stimulator.
- b) Current Placido disc-based CAVK's map the central 8 mm of the cornea's surface. In chapter five it is shown that the "Maastricht Shape Topographer" is able to map an area of 17 mm. This includes the adjacent tissues limbus and bulbar conjunctiva.

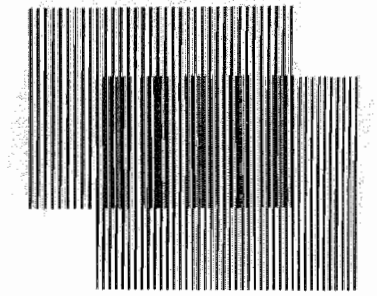


Figure 1.4

Two gratings with different spatial frequency cause moiré interference when superimposed.

duced by Kawara was an important step forward in this direction. Kawara made use of "moirés", wavy patterns that appear when two periodical structures (gratings) with different orientations or different spatial frequencies are superimposed (fig. 1.4). This kind of interference between gratings can be introduced by a three-dimensional object on which a grating is projected at an angle with respect to the viewing axis. To change the reflecting cornea into a light-emitting surface, Kawara added some fluorescein in the lacrimal fluid of his subjects. After excitation of the fluorescein in the precorneal tear film with a blue-coloured grating, a yellow fluorescent image is created which, after comparison with a reference grating, visualizes a height mapping of the corneal surface.

1.4 Overview of the research, presented in this thesis

In order to satisfy the requirements outlined above, a number of fundamental properties of the technique introduced by Kawara had to be adapted, changed and evaluated. The main aspects were:

- 1) Better characterization of the fluorescent dye used for imaging (Chapter 3).
- 2) Enlargement of the measurement field from the corneal surface to the entire anterior eye, and reduction of the time required for the collection and presentation of clinically relevant data (Chapter 4 and Patent description (Appendix)).
- 3) Evaluation of the new instrument, the "Maastricht Shape Topographer" (MST) using phantoms (Chapter 5).
- 4) Clinical evaluation of the MST (Chapter 6).

1.5 The fluorescent dye

The dye applicated to the cornea transforms the specular reflecting surface in a diffusely radiating one and should have a sufficient high quantum yield to enable imaging of a fluorescent pattern in the thin tear film. It should also absorb excitation light sufficiently well to prevent backscatter from underlying tissues such as the iris. Several commercially available fluorescent dyes were tested on yield and absorption with respect to

layer thickness and concentration. Tests with a phantom, using saline or methylcellulose as artificial tear fluid, and *in vivo* tests, using natural tear fluid or methylcellulose were performed. Dependence on excitation wavelength was also tested with a phantom as well as *in vivo*.

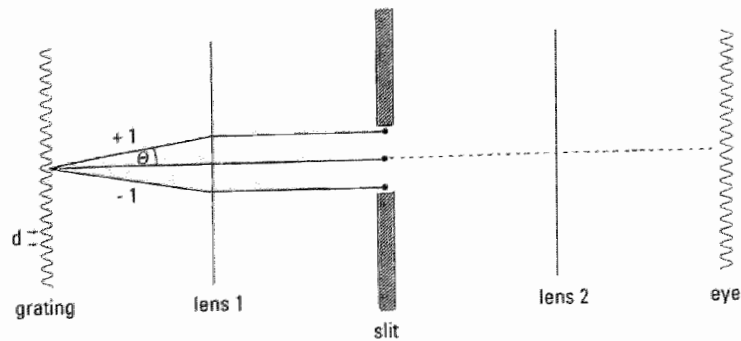
1.6 Technical adaptations of the topographer

Kawara used 35 mm photographic film on which the eye could be imaged with an 1:1 imaging ratio. The laborious procedure of taking a photograph, processing the film, and measuring its density on a microdensitometer, can be circumvented by applying a video-camera connected to a (personal) computer. For this a standard CCD camera can be used. Such a camera contains about a quarter of a million pixels (picture elements). Each has a capacity to assume 256 values the standard dynamic range of a PC connected to an imaging device. The pixel density and dynamic range is still less than available on a 35 mm photographic film frame, resulting in diminished lateral intensity and resolution.

A normal corneal diameter is 12 mm. For mapping the anterior eye, a standard $\frac{1}{2}$ " CCD camera takes at for instance an imaging ratio of 1:3.5, a 22.4×16.8 mm² area. In a horizontal direction, about 600 pixels are available being just enough to see Kawara's 12 lp/mm (on a flat surface) over 22.4 mm, however with a poor Signal to Noise Ratio (SNR). Lowering the spatial frequency of the projected fringes will increase the SNR of the image but decrease lateral and depth resolution. Replacing the standard CCD camera by a high resolution camera with for instance 1200 pixels in a horizontal direction, exposes a physical limit to Kawara's technique.

A large depth of field requires a small aperture (the diameter of the opening that determines the light throughput of a lens), whereas, due to the wave character of light, a high definition of the projected image (e.g. a fine grating pattern) can only be reached by using a large aperture. The aperture is determined by the width of the slit in the grating projectors (see fig. 1.5). In order to reach 2 mm depth of field, slit width has to be restricted to 1.5 mm. In order to reach 5 micrometres depth resolution, Kawara had to use the fine grating pattern of 12 line pairs/mm. In this situation the slit just allows passage of the zero-order and two first-order diffraction maxima, and an optimal (diffraction limited) result is obtained.

For assessment of the topography of the entire anterior eye, depth of field had to be increased to 6 mm, while preserving the depth resolution of ± 5 μ m. Therefore, Kawara's technique using projected fringes that are superimposed on a reference grating is replaced in the "Maastricht Shape Topographer" (MST) by projection of two stereoscopically projected fringe patterns. With a double flash technique, both projected sine-wave fringes are made suitable for Fourier analysis. This configuration is shown in figure 1.6. By superimposing the fringes, moiré contrast is also present (insert fig. 1.6) but the moiré fringes are not used for the calculation. In contrast to the usual moiré technique, where a shift over a full line width is the fundamental unit for height differences, Fourier analysis can discern much smaller shifts, provided that a sufficient number of fringes are present in the total image.



$$d \sin \Theta = m \lambda \quad (m=0,1,2,3,\dots)$$

Figure 1.5

Spatial filtering of a sine-wave signal. When a grating is placed in a monochromatic parallel beam of light, its diffraction pattern will appear in the focal plane of a transforming lens (lens 1). According to Abbe, at least two diffraction pattern are necessary to reconstruct the grating. Consequently, when a slit is placed in the focal plane of lens 1, its minimal width that passes information from the grating is dictated by the focal length of the lens, the wavelength of the light used, and the spatial frequency of the grating.

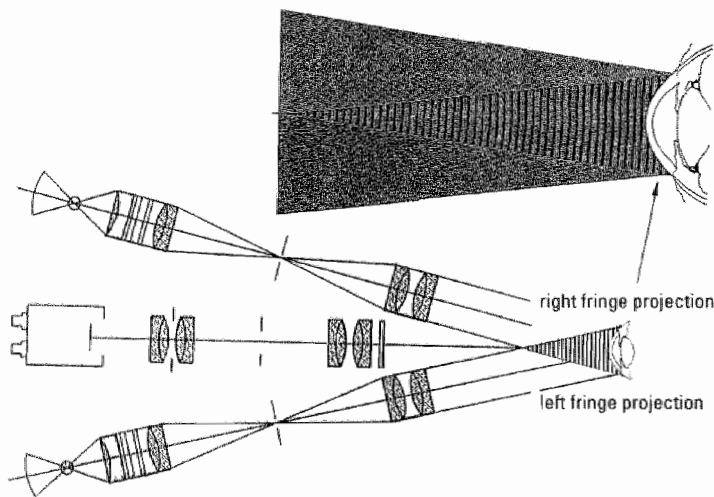


Figure 1.6

Schematic of the optical layout of the MST. Two orthoscopically projected beams form a measuring volume in which an eye is situated. The superimposed beams form a moiré pattern resulting in height contours on the corneal surface (insert). By applying a double flash technique, both projected fringe patterns are separately available for Fourier analysis.

In this way, relatively higher depth resolution is obtained with coarser gratings. In chapters 4 and 5 it will be shown that by applying this technique, the 36 x 24 mm² photographic negative used by Kawara could be replaced by a CCD camera with a 6.4 x 4.8 mm² target with 603 x 575 pixels to reconstruct the shape of the anterior eye with a latitude in depth of 6 mm and a depth resolution of $\pm 5 \mu\text{m}$.

1.7 Technical validation of the MST

Using fluorescent bispherical shapes as a surrogate for the anterior eye, the MST is tested on accuracy and reproducibility of its height measurements. This is described in Chapter 5, also presenting parametrical data (Axial Radius Of Curvature, or AROC values) in order to facilitate comparison with existing measurement techniques. Conversion from height topography into AROC values can be done assuming the surface to be spherical (fig. 1.1a)

The meridians (cross-sections) obtained with the MST are about 17 mm long. Remarkably, the meridian obtained from an anterior eye *in vivo* is quite different from the meridian obtained from the surrogate. The *in vivo* meridian is composed of a cross section of which the slope has no discontinuities in the limbal area. The entire anterior eye could be better described as an aspherical surface.

1.8 Clinical evaluation of the MST

A clinical evaluation of the MST has been performed at St Thomas' Hospital in London, UK and is described in chapter six. Measurements were carried out on patients with corneal pathologies and patients who underwent photorefractive surgery. The measurements were made with both the MST and a commercially available Placido disc-based Computer-Assisted VideoKeratometer (CAVK). Advantages of the MST over the Placido disc-based CAVK were demonstrated in a detailed analysis of three patients. However, there were also problems typical for fluorescence-based corneal topography. For instance, the predominantly blue-eyed British patients produced an image-disturbing backscatter of blue excitation light. By replacing the (visible) moiré-based focusing and alignment light by an infrared radiation-based device, pupillary constriction could be avoided and backscatter was reduced to acceptable levels. This evaluation yielded a variety of suggestions for improvements of the MST. Some improvements were realized during the evaluation, other modifications were implemented in the commercial version of the MST, the "Euclid ET-800". Moreover, some preliminary results of other clinical evaluations have been added to this chapter.

References

1. Placido A. Novo instrumento de exploracao da cornea. Periodico d'Ophthalmologica Practico. Lisbon, 1880;5:27-30. Cited in: Arch Ophthalmol 1981;99, Rouwsy JJ, Reynolds AE, Brown R. Corneal topography, Corneoscope 1093-1100.
2. Kawara T. Corneal topography using moiré contour fringes. Applied Optics 1979 18:3675-3678

Chapter 2

Review and Classification of Corneal Topographers

F.H.M. Jongsma, J.de Brabander, and F. Hendrikse

Lasers in Medical Science (in press)

2.1 Abstract

Corneal topography has, due to developments in refractive surgery and contact lens fitting, become a widely used diagnostic tool. Many types of topographers have been introduced, but there is some confusion on classification and subsequent principle possibilities of the various devices offered to the practitioner. The purpose of the study reported here was to make an inventory of developed devices, analyse the basic principles and create a classification based on optical principles. A literature search was done using Medline, the IBM Patent Server, and references found in articles and patents. This search resulted in a variety of descriptions that could be classified into 12 groups according to their use of light source and light-matter interaction of which 4 groups have representatives on the commercial market. This classification can be used by researchers and practitioners to gain insight into the possibilities of a given device in relation to the desired application.

Keywords: Corneal topography; Fluorescence; Holography; Interferometry; Moiré; Partial coherence

Table 1. List of symbols and subscripts

Symbol/subscript	Meaning
CAVK	Computer Assisted Video Keratometer
CCD	Charge Coupled Device, a light-sensitive chip used in miniature video cameras
LED	Light Emitting Diode
mire	Light emitting pattern of which the reflection on the corneal surface is used to estimate the corneal radius of curvature
moiré	Pattern that can appear when two periodic patterns are superimposed (fig. 2.7)
NA	Numerical Aperture, the half angle of the cone of light accepted by the objective lens
PC	Personal Computer
Placido disc	A flat disc with concentric black and white circles
Purkinje image	Virtual image, seen when a pattern is reflected by the eye
TGI	Twyman-Green Interferometer

2.2 History of corneal topography

For centuries ophthalmologist, optometrist, and others involved in eye care, have been using the first refractive surface of the eye to obtain a qualitative impression of the integrity of the cornea. This simple diagnostic tool is based on the fact that the boundary air-precorneal tear film acts as a mirror.

The basis for quantitative corneal topography was described by Helmholtz¹, Placido² and Gullstrand³ in the 19th century. Helmholtz measured the local slope of the cornea by observing the reflection of a pair of objects positioned at a known place with respect to the subject's eye. The virtual image obtained in this way is called "first Purkinje image". (Table 1 lists terms and symbols referred to in this review.)

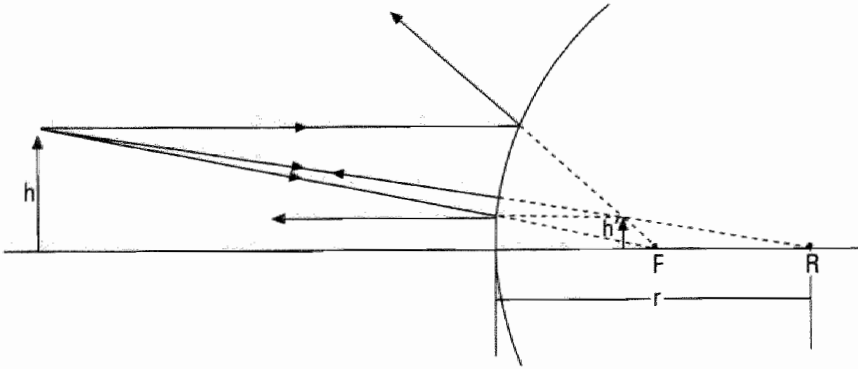


Figure 2.1

The principle of keratometry is based on image formation with a convex mirror. The cornea is assumed to be a convex mirror of which the radius of curvature (R) determines the magnification (h/h') of the reflected images. The longer the distance between the object (h) and cornea, the closer h' is located to the focal plane of the corneal reflecting surface.

By considering the cornea as an optical equivalent to a spherical mirror its radius of curvature can be estimated (fig. 2.1). Javal (1889) designed an instrument in which the objects could be rotated around the optical axis. In this way it is possible to find the orientation of the steepest and flattest radius of curvature, the so-called "principal meridians" of the cornea. Although Javal called it "ophthalmometry", this technique is known, as "keratometry". Instead of pairs of small objects, Placido² used a disc with concentric rings with a central hole through which he observed the image reflected by the subject's eye. This extended the observation to more meridians, and it covers an area rather than two or more points on the cornea. With this simple but ingenious invention, the practitioner is able to make a qualitative diagnosis of corneal irregularities, and very importantly, corneal astigmatism (fig. 2.2). Gullstrand³ took a major step in quantification of corneal topography by placing a photographic camera in the central hole of the Placido disc. Measuring the size of the rings on the photographs, enabled Gullstrand to estimate the corneal radius of curvature quantitatively. A century after the invention of photography, the first television was developed leading to the small and cheap Charge Coupled Device (CCD) television systems that are common today. The modern personal computer has had a comparable history. Coupling these two devices has made it possible to collect and process a quarter of a million data in a very short time. After the development of algorithms for surface reconstruction and translation of the acquired image into clinical relevant data in the 1980s⁴⁻⁶, the Computer Assisted Video Keratometer (CAVK) was born.

Today many CAVKs exist but most of them are still based on the old Placido disc principle. The inherent limitations of imaging by specular reflection led to the development of alternatives. These alternatives, utilize for instance the light scattering properties of the corneal tissue or alter the specularly reflecting surface of the precorneal tear film in a fluorescent layer that do not contain the directional information of the impinging light, open new possibilities but also introduce other limitations. This has led to a some-

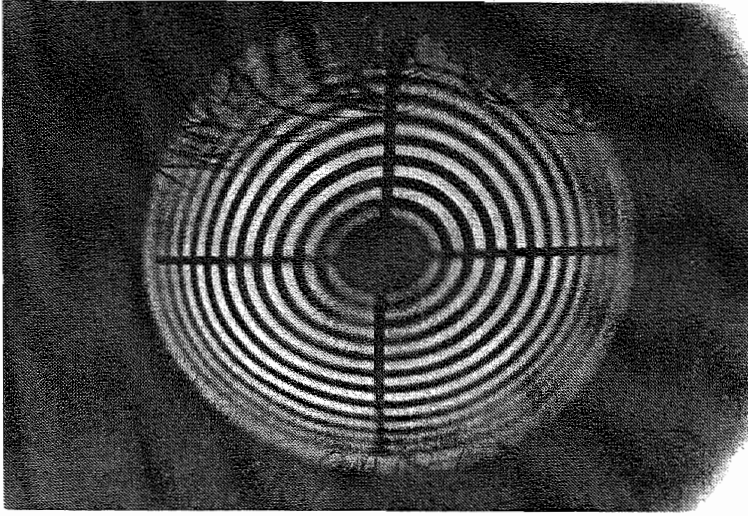


Figure 2.2 Reflection of a Placido disc deformed due to corneal astigmatism.

what confusing situation where it is not always possible for the user to link modalities of a given device to what is desired in research or in the clinic.

2.3 Purpose and methods

The aim in the present study was to provide more insight into the possibilities and limitations of devices for corneal topography. To do so, we first made an inventory of devices described in the literature and in patents. Second we looked for an adequate parameter to classify the devices found. Then we compared technical potential of the various devices within the groups.

To avoid confusing the reader, we describe the results of this search on the basis of the classification system developed. The first part of the results section is dedicated to an explanation of the classification system, followed by a description of major groups with subgroups. At the end of each group we specify in detail the technical potential of the group and particular devices within the group.

2.4 Results

2.4.1 Literature search

Corneal topography has led to the publication of a vast number of papers. Most of these were not suitable for our purpose since they were more concerned with clinical application than technical description. Only a limited number of papers linked technical possibilities and clinical application. The search for articles that could be used in the present study yielded 50 papers. Patents are much easier to handle from a technical point of view but results of clinical application are not given. We found 18 patents relating to

the subject. In total, information on 24 devices based upon essentially different principles was found.

2.4.2 Classification

The analysis of the designs to map the corneal surface optically revealed a tight coupling between the light source(s) and the optics of the receiving part. This principle underlying the design of all devices is, therefore, used to set up our classification system. It was found that all devices would fit into a system which makes a discrimination between the combination of light source used and light-matter interaction.

The parameters given in the literature descriptions of the keratometers yielded a classification of 12 modalities as shown in Table 2. The light source may be a light-emitting object (O), e.g. a Placido disc, or a projected image (PI). The light used can be incoherent (IN) or coherent (CO). The light-matter interaction results in specular reflection (SP), Scattering (SA), diffuse reflection (DIF), Shadow projection (SH) or a combination (SP/DIF). For example, in Table 2 the Placido disc-based CAVK is labelled "OSPIN". Feasibility, experimental and/or commercial availability for each group is given in Table 3.

Table 2. Classification

Light-matter interaction	INcoherent (IN)	COherent (CO)
Light-emitting object (O) e.g. back lightened transparant		
SPecular (SP)	OSPIN	n.a.
Projected image (PI)		
SPecular (SP)	PISPIN	PISPCO
ScAtter (SA)	PISAIN	PISACO
DIFfuse (DIF)	PIDIFIN	PIDIFCO
SHadow (SH)	PISHIN	PISHCO
SP/DIF	PISPDIFIN	PISPDIFCO

2.4.2.1 Light-emitting Object/SPecular/INcoherent (OSPIN)

The use of specular reflection is the oldest technique for corneal mapping. In keratometry, the reflected image of small light-emitting targets, usually called "mires", formed by the anterior surface of the cornea is used to determine the outer corneal radius for one meridian. This is established by measuring the size of the specularly reflected image of the targets. (fig. 2.1)⁷. By rotating the instrument about its optical axis, the principal meridians can be found. Present-day keratometers observe the virtual image at infinity by using a telescopic configuration of the objective. The angle between the incoming ray from the mires and the reflected ray from the cornea, called "collimator angle", is normally about 17°. However, some autokeratometers work with different collimator angles in order to measure the asphericity along meridians. The same can be accomplished by using off-axis fixation targets, to induce rotation of the eye over a known angle⁸⁻¹⁰. Instead of two mires, a ring-shaped configuration of mires can be used to obtain information on several meridians without rotating the instrument. The modified Placido disc consisting of concentric light-emitting rings led eventually to mea-

surements based on local radii of curvature⁴.

The power of a cornea as a refracting surface is generally expressed in diopters (D). $D = \text{metres}^{-1}$ ($D = 1/f_{\text{in metres}}$). Even today there is still debate in the literature about the proper figure to be used for refractive index (n). One could use 1.33 being close to water or tear fluid, or 1.376 being the average for the corneal tissue. The selection depends on the purpose to calculate curvature to optical power. Generally, 1.3375 has been taken as the figure in keratometry.

Consequently, by using the radius of curvature (r) in metres for corneal power calculation, the formula $D = (n-1)/r$, can be substituted simply by $D_{\text{cornea}} = 0.3375/r$.

Scanning and point measuring devices

In the Troutman surgical keratometer¹¹, the target consists of 12 equally spaced mires. The surgeon can estimate the corneal refractive power by means of the first Purkinje image of the 12 mires by looking through a special eyepiece which includes a measuring reticule, called "comparator" (fig. 2.3).

A computerized surgical keratometer was developed by Feldon et al.¹². This system makes use of a light-emitting ring as an optical stimulator to obtain a Purkinje image from the surface of the eye. The ring is coaxially aligned with respect to the centre point of the entrance pupil of an operating microscope. Keratometric values of the cornea can be estimated by the signals of a number of Light-Emitting Diodes (LEDs) that can be activated individually. As the LEDs are equally spaced at 10° or 5° radial positions on the light ring, 36 or 72 keratometric values can be measured sequentially by activating the appropriate pair of LEDs. For that, a rather complex light guiding system of prisms and

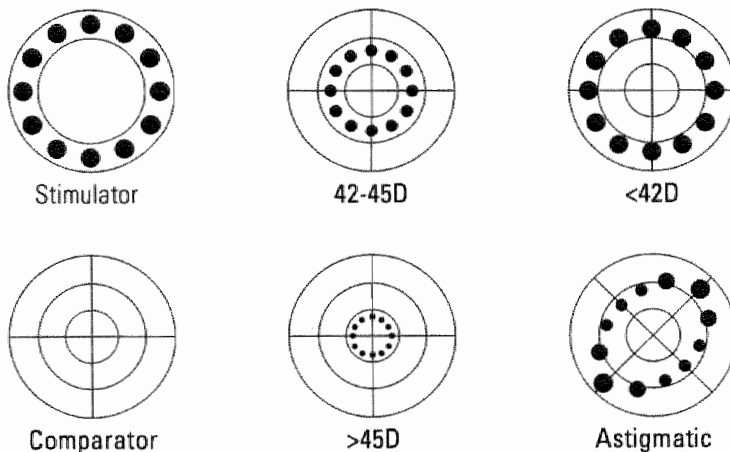


Figure 2.3

Keratometer after Troutman et al. The image of the 12 light-emitting diodes in the stimulator is specularly reflected by the corneal surface and re-imaged on a reference target (comparator). The optical power of a cornea is normally expressed in diopters (D). Normal eyes are in the range of 42 to 45 D. A flat cornea can have a power smaller than 42 D and a "steep" (having a short radius of curvature) cornea will have a power exceeding 45 D.

lenses has to be positioned in the optical axis of the surgical microscope. Each measurement contains the peak-to-peak distance of the mirrored LEDs. The collected data are stored in a RAM that thus contains information about maximum and minimum values of peak-to-peak distance and their corresponding axes (corneal astigmatism and axis). Subsequently, corneal curvature or dioptric values are calculated by a microprocessor.

In a configuration described by Nakamura and Yano³, the directions of view of the surgical (stereo) microscope and keratometer are chosen to be coincident (fig. 2.4). During focusing for the measurement, only the Purkinje image from the ring-shaped mire (M2) is visible. Therefore, the corneal reflection image of the illuminating light source from the surgical microscope is suppressed. After the Purkinje image of M2 is focused, a short flash with the circular flash lamp (M1), acting as a mire, is given. The sensor consists of three linear CCD arrays oriented in meridian directions which intersect one another at 60° crossing through the optical axis. The mire image is reflected by the beam splitter (BS) and optically divided by two half-mirrors (HM) to be imaged on the three linear CCD sensors (L1, L2, and L3). The shape of the mire image is detected by

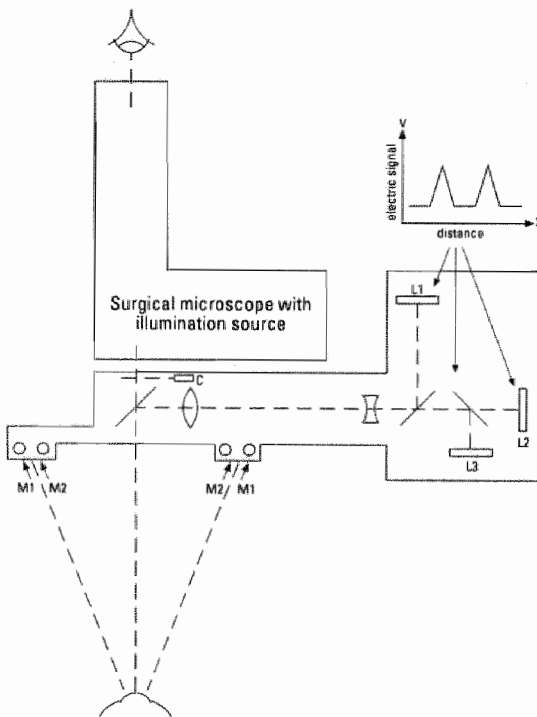


Figure 2.4

Schematic view of the computerised keratometer after Nakamura and Yano, attached to a surgical microscope. The device works with a mire (M1) and a ring stroboscope (M2) to freeze movements during each measurement. A chopper (C) prevents interference between microscope illumination and the measurements. L1, L2, and L3 are linear CCD arrays for measurements in three meridians which intersect one another at 60° relative to a point on the optical axis. A diagram of the electrical signal vs distance is given in the insert.

the coordinates of points of intersection. In this way each array detects the position of two points that is used to estimate the keratometric value of the corresponding meridian. By substituting the coordinates of the three pairs of points (insert fig. 2.4), a general equation is obtained and solved by a microprocessor yielding curvatures, refractive power and degree of astigmatism of the cornea.

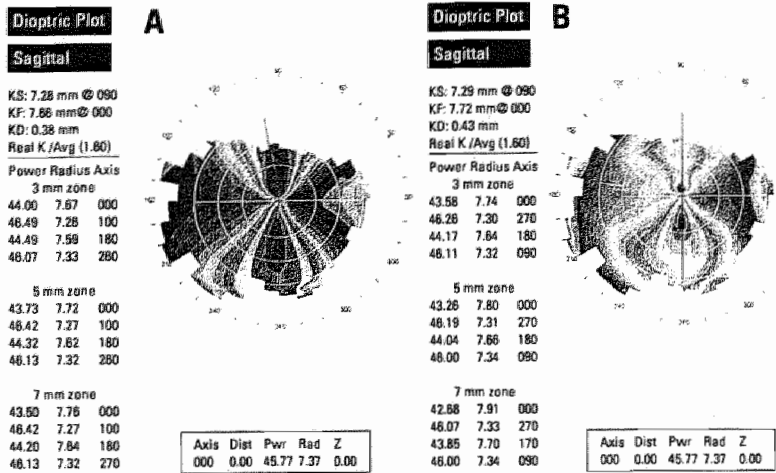
Keratometers, belonging to this subgroup, can measure any number of meridians. However, the curvature of each meridian is estimated on the basis of discrete point measurements.

Snap shot devices

A huge number of simultaneous measurements can be obtained by using a mire consisting of concentric rings rather than point-like structures. To avoid movement artifacts, the "picture" can be taken by a single short exposure ("snap shot") rather than by scanning.

Placido disc techniques

In Placido disc-based devices, light-emitting Placido rings are used. The objective lens of the recording system, centrally positioned in the Placido disc, only receives rays that are parallel¹⁴ or nearly parallel to its optical axis. In order to increase the field of view without changing the restricted entrance pupil of the receiving lens, the flat illuminated Placido disc was transformed in a conical light-emitting stimulator by Dekking in 1930¹⁵. In present-day devices spherical, ellipsoidal, or cylindrical stimulators are also used to increase the area measured. As the three-dimensional shape of the Purkinje image depends on the shape of cornea and stimulator, even a stimulator with the shape of a cigar was proposed to get a flat Purkinje image¹⁶. The photographic trendsetters for the modern devices, such as the Nidek Model PKS 1000 or the Corneascoper, enabled clinicians to examine, on a qualitative basis, disorders such as moderately advanced keratoconus or severe (irregular) astigmatism. Unfortunately, its sensitivity to corneal astigmatism is limited to about 3 D¹⁷. A much higher sensitivity and accuracy is obtained in present-day Placido disc-based CAVKs. In these devices, a CCD camera is placed in the centre of the stimulator to capture the reflected image of the mires. The camera is connected to a personal computer for analysing the data. CAVKs offer colour-coded maps in which axial power is indicated either representing surface areas of which the centre of curvature lies on the keratoscopic axis (fig. 2.5a), or as local curvature. In the latter case the centre of radius of curvature of the indicated area is related to either the keratoscopic axis or the best fit spheres fitting to the local characteristics (fig. 2.5b). Together with the coloured map, data concerning the value of the local radius, the position in degrees of the meridian or location in millimetres from the center can also be extracted using a cursor. Programs for simulated fluorescein maps for contact lens fitting, topographic 3-D and height maps and so on have been developed. A variety of books have been published explaining how to learn to read and interpret these corneal maps^{17,18}. The first CAVK was the Corneal Modeling System (CMS, now TMS-2)^{19,20}, soon followed by the EyeSys from Corneal Analysis System (CAS)¹⁴, the Alcon Eye Map EH 270²¹, the Humphrey MasterVue²², the Optikon Keratron²³, the TechnoMed C-Scan²⁴, and the Topcon CM-1000²⁵. With the manufacture of many other devices that



reflection-based devices is that considerable loss of data does occur as the Purkinje image can be distorted in the case of irregular corneas (fig. 2.6a). Due to the shape of the current Placido stimulators only a limited part of the cornea can be measured. The radius of curvature of the corneal surface determines the size of the image that can be focused (fig. 2.6b). For applications in which the shape rather than the optical properties of the corneal surface needs to be known, many researchers have developed alternatives in an attempt to beat the Placido disc-based CAVK on the weak points mentioned.

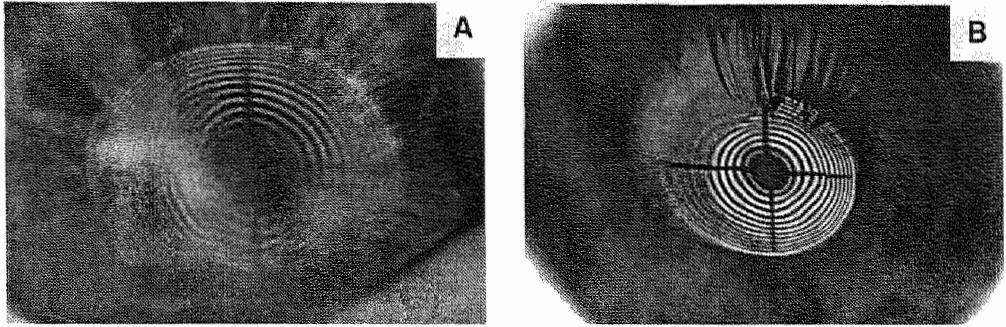


Figure 2.6

- a) Placido disc photograph from a cornea with an irregular corneal surface. Quantitative interpretation of this distorted image is difficult if not impossible.
- b) Placido disc photograph from a cornea with a very steep apex, a flat superior part and a steep inferior part (keratoconus).

2.4.2.2 Projected Image/SPecular/INcoherent (PISPIN)

Fujii et al.²⁸ arranged a series of collimated light beams in a semicircle to acquire 18 discrete slope values. The Purkinje images of these reflected beams on the corneal surface were photographed to reconstruct one meridian.

Moiré techniques

Instead of using a light-emitting Placido stimulator, concentric rings can be projected on the corneal surface. After specular reflection, the projected rings are re-imaged on a reference target. In this way a "moiré" contrast image can be obtained.

The word "moiré" means "a watered or wavy appearance"²⁹. Moiré interference occurs when periodic structures are superimposed at different orientations. When these gratings are viewed against a light background, dark fringes can be observed (fig. 2.7). An on-axis projection and viewing eye topographer, using moiré contrast between the projected image and a reference image to visualize lines of equal slope, was described in 1965³⁰. The projection and re-imaging part of the device works on-axis by using the same objective for both tasks. The images are superimposed by using a half-silvered mirror for combining projection- and viewing-axis.

Mandell³¹ also described a technique using moiré patterns in 1966. Adachi et al.³² developed a computerized specular reflection-based moiré device. This device was designed to measure the corneal as well as the limbal contour. (The limbus forms the transition

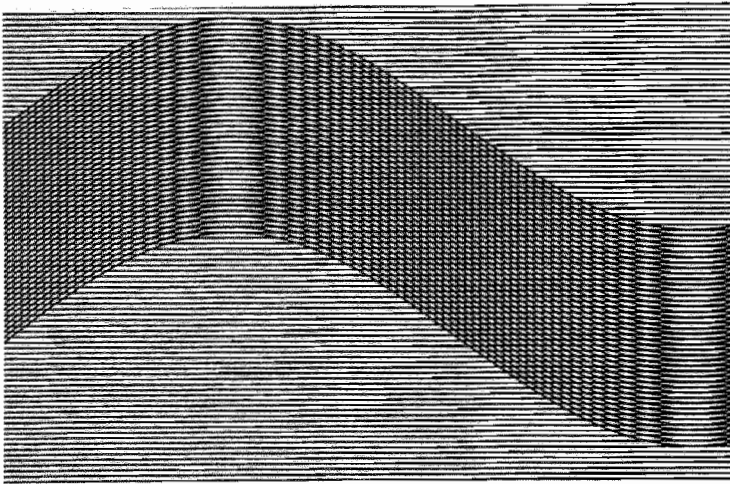


Figure 2.7

Moiré pattern composed of a sine wave and a linear grating.

area between cornea and sclera.) As the area on which the target is reflected depends on the aperture of the optics of the device, a $NA=0.6$ projection and receiving objective was used. (The "NA" or "Numerical Aperture" of a objective indicates the sinus value of the half angle of the cone of light accepted by the objective lens.) By placing the fixation point off-centre, the area of the eye that is measured can be extended to 14 mm diameter. To compensate for the small depth of field due to the high NA used, the stimulator surface and a fibre plate, acting as a reference grating, are curved as a conjugate of a spherical curvature with a $r=7.5$ mm. The moiré pattern contains a transverse line pattern indicating the differences between the actual corneal and the 7.5 mm spherical reference curvature.

Technical potential of PISPIN

The projection device from Fujii et al.²⁸ yields 18 discrete data to reconstruct a single meridian. By replacing the photographic film by a CCD-camera interfaced with a PC, the restricted amount of measuring points facilitates real-time measurements. However, using this principle to acquire 2-D measurements, requires a complex configuration. The moiré keratometer is a snap shot device and is consequently a potential candidate for the clinical office. This device can produce measurements of the central part of the corneal surface. However, no commercial versions of these devices are known by the authors of this article.

2.4.2.3 Projected Image/Specular/COherent (PISPCO)

For specific applications, a laser offers an adequate light source. For instance, a He-Ne laser can be used when a diffraction limited point source is needed. The temporal coherence makes the laser an ideal source for interferometry.

Strictly speaking, generally there is no difference between the light - matter interaction of coherent and incoherent light. However, in an interferometric set-up the observer

sees a difference. With coherent light, absolute values for the radius of curvature or local height can be obtained when the distance between eye and camera is known by comparing a wavefront with a substantially error-free flat reference wave³¹.

Deflection techniques

Bille³⁴ described a device for mapping corneal topography in which aberrations on the cornea are mapped against a spherical surface. A beam of laser light is focused toward the cornea as a converging spherical wavefront. The light reflected from the spherical part of the cornea is again collimated by the focusing lens. The deviations that are present in the collimated beam (caused by deformations of the corneal surface) are visualized with an image dissection technique comparable with that in high speed photography³⁵. (Presently this technique is referred to as "wave front sensing"). A matrix of focusing lenses is made by a sandwich of two layers composed of juxtaposed cylindrical lenses. The longitudinal axes of the lenses of the first layer are perpendicularly positioned with respect to the longitudinal axes of the lenses of the second layer. The matrix of foci indicate whether the incident rays are parallel or not. In this way the local slope of the corneal surface is mapped. (Today, one would use an array of lenses rather than crossed cylindrical lenses).

Interferometric techniques

Hochberg³⁶ described a method for extracting "long-equivalent wavelength" (notation of Hochberg) interferometric information to obtain the surface topography of a cornea. Interferometric comparison of a flat wavefront with a curved wavefront (due to the corneal surface) yields detailed information about the surface topography of the eye. However, there are only adequate sensors for visible and near-infrared light. An interferogram made with this kind of radiation is difficult to store due to the tremendous quantity of fringes. By using a two-wavelength interferometer the frequency beat of two frequencies from the visible spectrum can be applied as a long-equivalent wavelength. The basic principle of two-wavelength interferometry is that a phase beat is generated when waves with a different wave length travel a certain distance³⁷. When, for example, the two laser lines at 514nm and 488nm from an Argon laser are applied, a destructive interference results after about ten wavelengths, a constructive interference after about 20 wavelengths. For these two lines, a beat is produced at every $(514 \times 488 \text{ nm}) / (514 - 488 \text{ nm}) = 9648 \text{ nm}$. As the light travels twice the distance, the reflected interference pattern has a fringe value of half that value. This "long-equivalent wavelength" can be extracted when the two-frequency interferogram is recorded on a non-linearly responding high resolution photographic film.

Photographic films act as a low-pass spatial filter. The spatial modulation transfer characteristics, which indicate the effects on the microstructure of the image caused by diffusion of light within the emulsion, decrease in amplitude at higher spatial frequencies³⁸ (see insert fig. 2.8).

Hence, the envelope of the beat pattern forms a better modulated frequency than the high frequency carrier wave. In a second step this film is spatially filtered. As the intensity of the diffraction pattern in the spatial filtering depends on the modulation of the photographic image, the envelope of the frequency beat dominates, and forms the

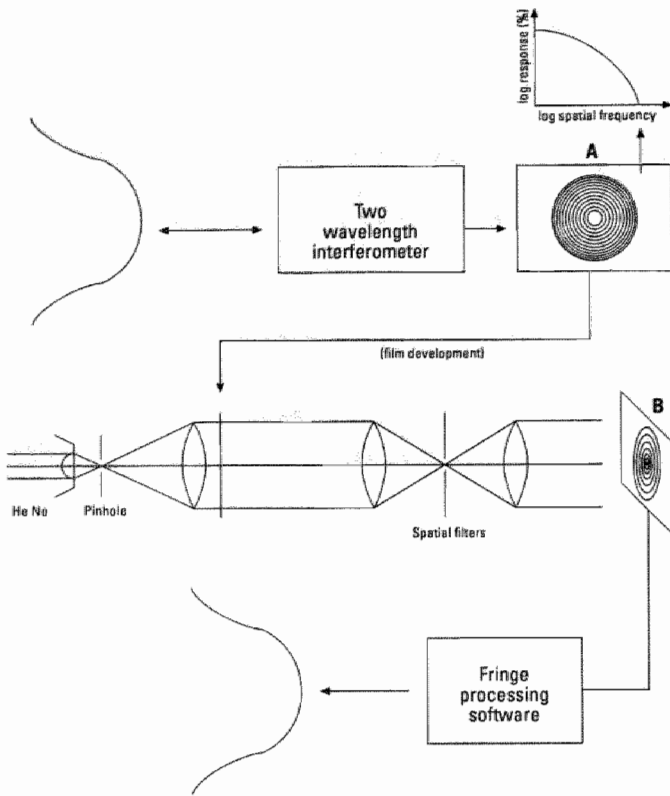


Figure 2.8
Block diagram of an aspheric testing scheme after Hochberg. The two-wavelength interferogram is recorded on a high resolution film (A) and optically filtered to obtain the low frequency component (envelope of the frequency beat of the two wavelengths) on the sensor (B). The lines of equal height obtained can be subsequently processed for reconstructing the features of the measured surface.

"long-equivalent wavelength" (fig. 2.8). This long-equivalent wavelength interferogram can be recorded on a normal CCD-camera and fed into a PC for further (digital) processing.

Another way to reduce the quantity of fringes is to compare two curved wavefronts. This technique was applied by Kasprzak et al³⁹. They used a Twyman-Green Interferometer (TGI) to obtain real-time subtraction interferograms from the human cornea in vivo with a best fit sphere. A HeNe laser at a 632.8 nm wavelength is used as a light source. By converging the laserbeam on the corneal surface, a range of spherical wavefronts are thus available as a reference. Recordings are made at a position of the eye where the minimum of fringes is observed. In this way the fine corneal topography in a 5 mm area can be measured. The absolute value of the corneal curvature can be estimated with an accuracy equal to that to which the distance from the subject's eye to interferometer is known. To obtain an implicit measurement of the distance, Jongsma et al.⁴⁰ used infrared light with a coherence length of about 30 μm in a TGI similar to Kasprzak et

al.'s configuration. Instead of a flat reference mirror, they used a spherical reference mirror with a radius of curvature of 7.5mm. In this way the radius of curvature of the cornea can be visualized as an interferogram with fringes showing the difference between the 7.5mm sphere and the actual curvature of the corneal surface. The radius of curvature can be estimated with an accuracy that is determined by the coherence length of the light used.

Hochberg and Baroth⁴¹ used a TGI with a white light source and estimated the local height by spectral analysis of the polychromatic interference pattern.

Hellmuth and Wei⁴² described a raster scanning technique that also used partially coherent light. An infrared super luminescent diode beam is collimated and projected on the eye and a helical reference mirror. By rotating the helical mirror, the reference arm length of the interferometer is changed periodically. Transverse scanning of the collimated beam is done by two orthogonally positioned scanner mirrors which are mounted on a pair of galvanometers for rotation. Local height is measured by matching the object beam length with the reference beam length, using the interference beat as a length mark.

Holographic techniques

The holographic technique facilitates interferometry as it works with two mutually coherent beams. In this way sub μm sensitivity to height variations can be obtained. For example, an interferogram can be obtained by comparing the object beam from a subject's cornea in its initial state with the object beam from the cornea after a change. This can be accomplished by a double exposure technique or with real-time holographic interferometry. In this way a stress test analysis using the intra-ocular pressure difference after a heart beat was used to detect structurally weak areas in the cornea. A weakened region of a wound that stretches only 1 μm could be easily detected⁴³.

Besides these differential measurements that may be helpful in the diagnosis of corneal alterations under a load, a topographic contour analysis of a cornea can also be obtained in a holographic way using a two-wavelength technique³⁷. The phase beat, which is generated when the reconstructed waves travel a certain distance, can be used to visualize contours of equal height. In 1977, Politch⁴⁴ described a system and method to obtain contour fringes from a living human cornea by applying a two-wavelength technique. The Argon laser lines 514 and 488nm were used. When a cornea is placed in a convergent beam from the interferometric device at a distance where the curvatures of wavefront and cornea match, the non-sphericity of the cornea is visualized in the holographic reconstruction at contour intervals of 4.8 μm . A commercialized version using this technology was developed by Kera Metrics Corp.

Technical potential of PISPCO

In contrast to the OSPIN techniques, this specular reflection-based technique reveals either the local slope or the local height (or local height difference). When only the spatial coherence is used (to obtain a diffraction limited spot), as Bille did in his deflection technique, the local slope is mapped. However, when the temporal coherence also plays a role, the wavelength of the light used acts as a yardstick to measure the distance from corneal surface to a reference plane and consequently the local height is mapped.

Bille's design is an interesting alternative to Placido disc-based measurements as the deflection is measured in two directions with a good SNR. The precise localisation of the foci on the sensor might be solved with Position Sensitive Detectors (PSD's).

Interferometric laser technologies can yield height information with a sub μm accuracy. To reduce the amount of data, subtraction of a spherical shape can be done. In fact, the actual shape is compared with a spherical wavefront travelling from a point source. Hence this wavefront has a place-dependent radius of curvature. Due to this subtraction, radius of curvature values can only be obtained if the precise position of the subject's eye with respect to the taking lens is known.

Instead of subtraction by using a curved wavefront, a two-wavelength technique with collimated beams can be used to reduce the amount of data with respect to visible light interferometry. Due to the spatial invariance of flat wavefronts, absolute height data can be obtained. However, even with a $10\ \mu\text{m}$ long-equivalent wavelength as proposed by Hochberg an entire corneal surface will be mapped with about 500 contour fringes. Its holographic equivalent, proposed by Politch, is a parametric measurement. It reveals the differential contour lines of the corneal surface compared with the surface of a sphere of unknown radius of curvature. By using partially coherent light as proposed by Jongsma et al.⁴⁰, the position of the eye is known to a high degree of precision and hence its radius of curvature can be estimated. What the interferometric and holographic techniques have in common is that they are based on the projection of, in general, a collimated or convergent beam of coherent light. Although the primary information is height information, the local slope on the cornea plays an important role. Reflection at irregular corneas, which cause strong deviations of direction, may not pass the entrance pupil of the sensor, resulting in recordings of poor quality. Alignment in interferometric technologies yielding local height information is critical. A much less critical alignment was demonstrated in an *in vivo* precorneal tear film study by Licznarski et al.⁴⁵ introducing an optical wedge in a Twyman-Green interferometer. Through this "lateral shearing technique" alignment is much less critical but at the cost of loss of sensitivity. In sum, the accuracy of height measuring interference techniques for *in vivo* applications is not as high as generally assumed. Biological surfaces, such as the corneal surface, can deform the reflected wavefront considerably. Confusion in regard to the interpretation of the interferogram arises when the plane of observation is not conjugate with the surface studied. The principle problem here is that the wavefront shape changes as the wavefront travels⁴⁶. Such a confusion can, in a limited way, be avoided in holographic measurements. At irregular corneal surfaces the reflected wave can be so distorted that it does not focus within the pupil of the imaging system. By applying a holographic speckle interferometry technique, such a cornea could be illuminated by a diffuser that is coherently illuminated by a laser. This diffuser, acting as an extended light source, prevents some parts of the corneal surface being "in shadow" with respect to the point of observation. The characteristics of the interference then change from unlocalized fringes to the localized fringes obtained with an extended source⁴⁷. However, holographic configurations are complex and consequently expensive.

2.4.2.4. Projected Image/ScAttering/INcoherent (PISAIN)

Profile photography

Mandell appears to be one of the early workers who developed alternatives to the Placido disc-based systems. In 1961 he gave a detailed report on profile photography with a slit-lamp illumination system based on Rayleigh scattering in the anterior eye tissues⁴⁸. A computerised version of the slit-lamp illumination system was developed by Orbtex Inc. The "Orbscan" device is not only a real corneal topographer (measuring height, presented in Cartesian coordinates, instead of slope, presented in polar coordinates), but also incorporates a pachymeter^{49,50}. It utilizes a series of sequentially projected pairs of slits as a "Scheimpflug corrected"⁵¹ optical sectioning of the corneal tissues.

The "Scheimpflug correction" is an optical technique to provide critical focus for all illuminated portions of the cornea. This principle states that if a tilted object plane (S) at object distance intersects at one point (R) with the tilted lens plane and the projection plane (located at imaging distance), the entire tilted object plane will be conjugated to the projection plane, and consequently sharply focused in the image plane (fig. 2.9). If the projection screen is not flat but for example convex, the surface of this convex curvature must be inside the focusing volume of the camera. The focusing volume is determined by the depth of field of the imaging lens.

Scattering in the corneal tissue is used for imaging of the corneal contours. The Purkinje images that are formed at each optical surface are used for alignment and as compensation parameters for eye movement during the scanning process. Purkinje images are formed due to the reflection not only on the air-tear film boundary, but also, although with much weaker contrast, on the posterior corneal surface or the lens surfaces⁵².

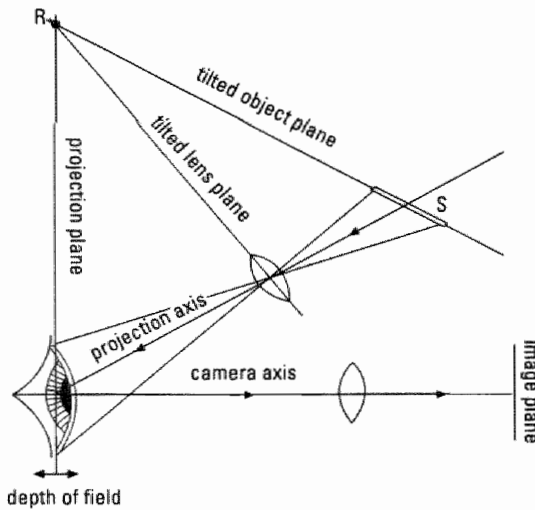


Figure 2.9

Schematic view of a Scheimpflug correction. The tilted object plane (S) is conjugated to the projection plane when the tilted lens plane meets object plane and projection plane at the same point (R).

Technical potential of PISAIN

Profile technologies based on scattering are often used for standard clinical examinations. Most qualitative direct observations are done with a normal slit lamp or bio-microscope. An advantage of these technologies is that they measure the real surface instead of a virtual image and that they measure the corneal thickness as well. There are no problems with irregular surfaces or scattering surfaces (e.g. as are present with dry eyes). A disadvantage is that these technologies require a series of measurements to map the entire corneal surface. A very sophisticated scattering-based CAVK, using a short data collecting time, the "ORBSCAN", is commercially available for use both as a surgical keratometer and as a keratometer for the clinical office.

2.4.2.5 Projected Image/ScAttering/COherent (PISACO)

An intriguing technology, developed by Soroko, combines coherent projection and detection method with measuring the scattering in a point on the optical axis of a confocal observation system⁵³. The axial intensity modulation is obtained by applying the interference pattern of two mutually coherent and coaxial beams that are oriented obliquely with respect to the observation axis of the device.

The Rayleigh scatter of the illuminated part of the reflecting surface of the eye is scanned and only transmitted at a point on the optical axis of the detection system that is confocally focused in a point photodetector⁵⁴. A disadvantage of the configuration described is that the object profile must be smooth. Discontinuities of the surface can induce ambiguities in the interpretation of the output signals. By applying two mutually coherent beams with different vergencies (either convergent or divergent), the angle between the two wavefronts varies along the observation axis of the device (fig. 2.10).

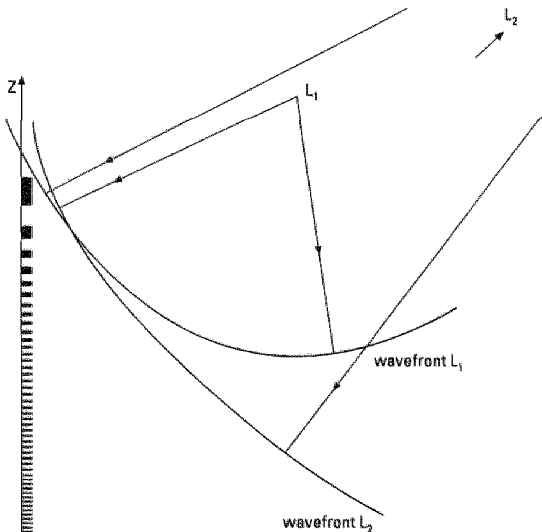


Figure 2.10

Interference pattern of two mutually coherent beams (L_1 , L_2) with different vergencies. The spatial intensity modulation varies along the optical axis (Z).

Hence the longitudinal modulation that yields the signal varies during travel along the optical axis of the devices. This enables one to discriminate structures along the optical axis of the detector.

Technical potential of PISACO

Soroko's devices were developed for surgical microscopes. Scatter-based reflection techniques do not depend on a precorneal tear film and are therefore not prone to the disturbances that can deteriorate the images of specular reflection-based systems. Soroko's device may be useful in modern photorefractive surgery where the target area on the corneal surface is "dry". It is not clear whether these devices can also be used in other circumstances. The data collection time is about 10 ms, short enough to freeze eye movement of an awake patient. The combination of coherent projection and scattering looks promising. Unfortunately, to the authors' best knowledge, no clinical evaluation has been performed.

2.4.2.6. Projected Image/DIFFuse/INcoherent (PIDIFIN)

Fringes projected on a diffusely reflecting surface are distorted by the surface curvature when the axis of observation is different from the axis of projection. This distortion of the fringes is a measure of the local height of the surface.

Stereo photogrammetry

In 1965 Friedberg and Dimond described a method for stereo photogrammetry of the surface contours of an eye to be fitted with a contact lens⁵⁶. They transformed the specular reflecting corneal surface in a "Lambertian" (a perfectly diffusing) surface by adding a biological fluorescent stain to the precorneal tear film. To obtain randomly scattered photons, the energy of the photon was affected ("inelastic scattering"). Some fluorescent molecules can act as an effective inelastic scattering medium. Friedberg and Dimond obtained such a medium by instilling fluorescein in the precorneal tear film. It was possible to put the invention into practice by using a conventional slide projector that projects a blue pattern to excite a fluorescent image on the surface to be measured. This fluorescent image, that follows the curvature of the surface, was photographed in three dimensions with a stereo camera.

Raster photogrammetry

About 20 years after Friedberg and Dimond described their system, it was modified into a raster photography system by Warnicki et al.^{6,57} and Cambier and Strods⁵⁸. This led to several patents and a commercial version, the "PAR Corneal Topography System"⁵⁹. The PAR system is a biostereometrical device using raster photogrammetry to obtain a real topographic mapping of the entire corneal surface⁶⁰. This device is mounted on a modified stereo biomicroscope (slit lamp). One side of the stereo device is modified to support a grid projection system for projection of a raster on the corneal surface consisting of horizontal and vertical lines about 200 μm apart. The other side comprises a video camera and optics that are aligned with a support for a head and chin rest. A personal computer connected to the video camera is used to reconstruct the topography of the cornea.

As this raster photogrammetry CAVK is based on a single flash exposure technique, thus reducing the risk of movement artefacts greatly, it is adaptable to different clinical environments. This technique requires no precise spatial alignment for accurate reconstruction of the corneal topography⁶¹.

Phase shifting techniques

Lange and Thall described a method and apparatus for measuring corneal topography based on diffuse reflection⁶². They found an alternative to fluorescein as a diffusing agent. A thin white teflon tape, cut into small circles having the same diameter as the cornea or a part of the cornea, served as a diffusing membrane. The method is claimed to be effective intraoperatively when used in conjunction with a fringe contouring device described by Lange entitled "Phase shifting device and method"⁶³. Phase shifting is a well-known technique in interferometry to obtain a sub-wavelength accuracy. However, this technique can also be used in a non-coherent light set-up. By projecting a sine wave grating and displacing the projector slide a fraction of a contour interval between each measurement, the same kind of information is obtained⁶⁴. The method needs a series of exposures with a known phase shift of the projected gratings and is therefore only suitable for an immobilized eye as is present during surgical procedures. Windecker and Tiziani developed an accurate phase evaluation algorithm by combining a temporal algorithm with a spatial algorithm⁶⁵. They used the interlaced mode of a CCD-camera to acquire four frames for phase evaluation in 80 ms. This technique enabled corneal height mappings in quasi real-time to be obtained using a spatial carrier fringe measuring system.

Moiré techniques

To create a diffusely radiating corneal surface Kawara used the fluorescein staining technique that was earlier recommended by Friedberg and Dimond. He obtained real-time moiré fringes on the corneal surface indicating lines of equal height⁶⁶ (fig. 2.11). The stained precorneal tear film is illuminated with a cobalt blue grating that is projected at an angle relative to the viewing axis. The viewing part of the device is aligned with the visual axis of the subject's eye. In this part a reference grating is placed on which the projected grating, distorted by the subject's eye, is re-imaged. The beat of the lines from these two periodic structures form moiré contours with a fringe interval of 148 μm . This moiré pattern is photographed and the negatives are analysed on a microdensitometer. Kawara claimed a topographical precision of 5 μm on a spherical surface.

Jongsma modified Kawara's device to a double-fringe projecting system. This system is suitable for local frequency reconstruction of the spatial frequency of the projected fringes, rather than using the height contours that are obtained by the moiré interference itself⁶⁷. For this CAVK an image reconstruction program was developed by Stultiens et al.⁶⁸. It allows the use of lower spatial frequency projection sine-wave fringes than Kawara used, resulting in a larger depth of field. The measured area is therefore not restricted to the corneal surface but extended to the adjacent tissues. The latter is relevant for (semi-)scleral contact lens fitting, for example.

The raster photogrammetry sub-group has a commercially available CAVK, the PAR Corneal Topography System. Recently, the double-fringe projection technique, as

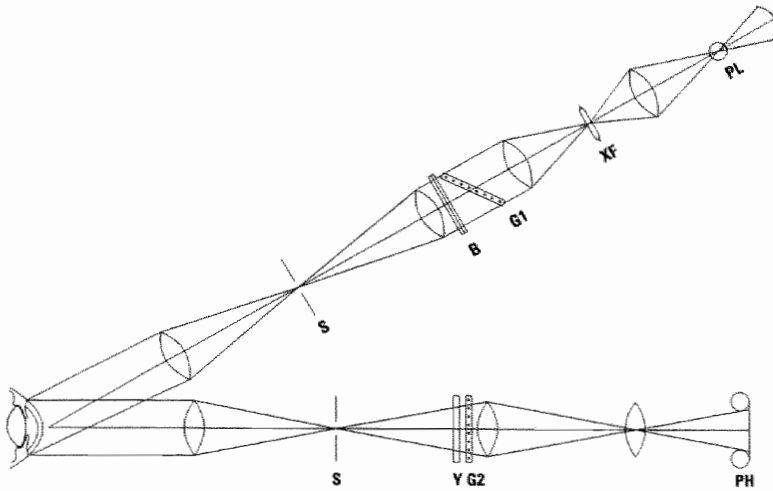


Figure 2.11

Schematic view of the orthoscopic projection and viewing optics of the corneal topographer after Kawara. The projection part consist of a pilot light (PL) in cascaded arrangement with a pulsed flashlamp (XF) for short exposure. The obliquely placed grid (according to the Scheimpflug correction) (G_1) is telecentrically projected via a 1.5mm wide slit (S) on the fluorescence stained precorneal tear film. The light in the projection beam is spectrally filtered by a cobalt blue filter (B). The modified fluorescent grating pattern is subsequently telecentrically re-imaged via a slit (S) on a reference grating (G_2). The excitation light is blocked by a yellow filter (Y). The obtained moiré image is photographed on the film (PH).

described by Jongsma, has yielded a commercially available device, the Euclid ET-800 Corneal Topography System.

Technical potential of PIDIFIN

Fringes that are observed on a diffusely radiating surface map a corneal area of which the size depends on the distance and the angle of view of the sensor. This surface quality makes it possible to obtain the topography of a variety of shapes with all kinds of curvature.

With diffuse reflection-based techniques, the measurement is located on the surface itself rather than derived from a virtual image that might introduce ambiguity.

A disadvantage of diffuse reflection-based devices is that they require a diffusing agent, e.g. sodium fluorescein to obtain the required optical quality (having a diffusely radiating and opaque surface) of the cornea. The sodium fluorescein can be replaced by a flexible membrane. The advantage of a diffusing membrane over fluorescein is the modality to cover the (fluorescein absorbing) stromal layer during a surgical procedure. For normal clinical examination the membrane technique might be too cumbersome.

2.4.2.7. Projected Image/SHadow/INcoherent (PISHIN)

Mandell investigated a set-up using shadow projection. The corneal surface is illuminated under an angle for suitable for shadow projection. The corneal shadow is pho-

topographed to measure its contour, with poor results however⁴⁸. What is salient is that this principle was incorporated later, with success, by the Corneal Analysing System as a technique for automatic centring and focusing the EyeSys CAVK⁶⁹.

Technical potential of PISHIN

Mandell considered the shadow projection technique as not accurate enough. Only one year before Mandell did his investigation on the total reflection method, Mayman finished the first laser ever made⁷⁰. This ruby laser was not suitable as a point source but the He-Ne laser that was developed shortly thereafter could very well act as a diffraction limited point source. In conjunction with high resolution photographic film, this technique can reach a micrometre precision in measuring the corneal profile. However, for practical use Mandell's set-up is too laborious.

2.4.2.8. Projected Image SPecular and DIffuse/INcoherent (PISPDIFIN)

Surgical corneal topographers (scan technologies)

Baron⁷¹ described a method for measuring the topography of an anaesthetised eye. The apparatus works simultaneously with diffusely reflected light using fluorescent radiation of sodium fluorescein and specularly reflected light. During the measurement, a blue excitation spot is scanned in the x-y plane to cover the entire cornea and adjacent tissues. The location of the spot is monitored by two orthogonally-oriented continuous position sensitive silicon detectors that are sensitive to the fluorescent emission of the stained precorneal tear film. The location of the eye is monitored by a reference beam that is simultaneously focused on the surface of the eye. Its specular reflection is monitored by a quadrant position sensitive detector (that is sensitive to the incident light) to detect deviations of an illuminated area away from the optical axis of the instrument. The reference and sampling beams are modulated in intensity with different frequencies to enable discrimination between these beams and to suppress interference of ambient light with the signal. The locally measured topography of the eye in one meridian can be determined by triangulation. This is done by comparing the sampling spot with the both diffusely and specularly reflecting, centrally projected reference spot that monitors the position of the eye. As the eye moves, the specularly reflected part of the reference spot changes position. To measure the entire corneal and scleral surfaces of the eye, more meridians are scanned. The information can be analysed with a computer to make the required topographic information accessible to the ophthalmic practitioner.

Technical potential of PISPDIFIN

Scanning devices with a hybrid data collecting system that combine the features of specularly reflected light for alignment and diffusely reflected light for the measurement of shape were developed for surgical microscopes. However, the accuracy that can be obtained based on specular reflection on the precorneal tear film-air boundary during surgery is poor. These devices, although sophisticated from an optical point of view, seem therefore impractical.

2.5 Discussion

2.5.1 The classification

Table 3 gives an overview of the techniques according to the physical classification principles described in this paper. For each principle the first step (feasibility), the second step (prototype built), and the third step (commercial availability) is rated "yes", "?" (status unknown by the authors of this review) or "no". It is assumed (by the authors of this review) that descriptions given in a patent are based on experimental work. The rating "-" is given when the proceeding step is negative.

Table 3

principle	feasibility	prototype	commercial
1. OSPIN	yes	yes	Placido disc-based
2. OSPCO	no	-	-
3. PISPIN	yes	?	no
4. PISPCO	yes	yes	holography-based
5. PISAIN	yes	yes	slit-scan-based
6. PISACO	yes	?	no
7. PIDIFIN	yes	yes	stereo photogrammetry-based
8. PIDIFCO	no	-	-
9. PISHIN	yes	no	-
10. PISHCO	no	-	-
11. PISDIFIN	yes	?	-
12. PISDIFCO	no	-	-

Although the feasibility of 8 groups was proven, only four principles have been used to build a commercial version. Representatives were found of 8 groups. With this table in mind it is easy to imagine configurations according to some groups that have no representatives. For instance, in the PIDIFIN group an incoherent projection of a sinus wave has been applied to obtain moiré fringes. If, instead of this incoherent projection, an interferogram of two mutually coherent laser beams was projected on the corneal surface, the PIDIFCO would have a representative. The same laser, used as a perfectly collimated beam, would alter Mandell's shadow technique PISHIN into PISHCO, as a result of which 10 groups would have their representative. And finally PISDIFCO is feasible if instead of a coherent point source a coherently illuminated diffusing screen is used as light source. It would give an image with a good SNR; however, interpretation of the fringes from a single exposure can lead to errors⁴⁷.

In PISPCO interferometers were used to measure local height. It is also possible to measure local slope by using a common-path interferometer⁷². The latter has the advantage that, as the waves follow nearly the same path, the measurement is less affected by a deviating curvature of the corneal surface.

2.5.2 Technical potential

None of the techniques described are without inherent shortcomings. Techniques based on specular reflection require optical characteristics of the anterior surface of the eye

that are not always present. The central part of the eye can be mapped interferometrically with a high spatial resolution in x,y, and z directions. However, due to its critical alignment, this method does not appear feasible for routine examinations in patients. As the modulation of the specularly reflecting surface slope determines the minimum allowable aperture of the viewing optics, it is difficult, if not impossible, to map the entire corneal surface including the limbal area in a single exposure unambiguously. Technologies based on scattering cannot image the entire corneal surface in one exposure under physiological conditions. The problem remains of the movement artefacts that can occur during long exposure times. Technologies based on diffuse reflections need a diffusing agent (fluorescent label or membrane) to obtain the required optical properties of the anterior surface of the eye. It is not yet proven whether these semi-invasive technologies alter the surface features or not.

2.5.3 Clinical potential

The question which of all the technologies mentioned is the best cannot be answered easily. It largely depends on the aim of the application. Corbett et al. raised questions on four subjects: the kind of measurements, the kind of corneas, the kind of situation, and the kind of presentation⁷³. If the corneal surface is considered to be an optical surface, a parametrical measurement might be indicated with the advantage that considerable sensitivity is gained. Most devices based on specular reflection, the Placido disc-based CAVKs included, measure parametrically. If the local corneal anatomy is important in the diagnosis, devices based on scattering can offer interesting modalities, e.g. pachymetry (measurement of thickness with a bio-microscope). Should it not be the optical performance but the shape that is the object of the diagnosis, e.g. for pre- and post-operative evaluation or for contact lens fitting, devices based on diffuse reflection offering direct height measurements are indicated. Sometimes a diffusing membrane may be useful. Dry corneas, for example, exclude effective use of specular reflection, whereas during surgery no fluorescein must be used as this penetrates the stromal tissue. Scanning techniques may be applied during surgery, but the accuracy is mostly poor due to the condition of the patient's eye. They can be subject to movement artefacts in other circumstances. For corneas with a regular surface, a mirrored image, which is easy to acquire with a Placido disc-based CAVK, is adequate. For irregular corneas of which the shape is to be known, detailed height mapping might be more accurate when obtained with a non-parametrical measurement⁷⁴.

2.6 Conclusions

The inventory of keratometers based on the literature search revealed a variety of techniques. Placed in a classification matrix based on optical principles, unexplored techniques emerged that, from a theoretical point of view, seem reasonable starting points for the development of new devices. The information found is not limited to the 4 groups that are commercially available (Table 3). The search revealed 24 devices based on essentially different principles that could be classified according to 8 groups (Table 3). For some devices, especially the keratometers described by Soroko⁵³, it is not clear to

the authors of this review why they are not represented on the commercial market.

References

- Helmholtz H von. Graef's Archiv für Ophthalmologie. 1854. 2:3
- Placido A. Novo instrumento de exploracao da cornea. Periodico d'Ophthalmologica Practico. Lisbon, 1880, 5:27-30
- Gullstrand H. Helmholtz's Treatise in Physiologic Optics, Vols I and II (Appendix), Ed. Southall JPC, New York-Dover 1962
- Klyce SD. Computer-assisted corneal topography; high resolution graphic presentation and analysis of keratoscopy. Invest Ophthalmol Vis Sci 1984 25:1426-35
- Warnicki JW, Rehkopf PG, Curtin SA et al. Corneal topography using computer analysed raster stereographic images. Appl Opt 1988, 27:1135-40
- Wang JY, RICE DA, Klyce SD. A new reconstruction algorithm for improvement of corneal topographical analysis. Refract Corneal Surg 1989 5:379-87
- Rubin ML. Optics for clinicians 2nd Edn. 1974:319
- Wilms KH. Ein einfaches Messverfahren zur Erfassung der Corneaform mit dem klassischen Ophthalmometer. Die Kontaktlinse 1973 1:24-30
- Wilms KH. Zur Vermessung von Kontaktlinzenflächen mit dem Ophthalmometer. Die Kontaktlinse 1975, 9:3-6
- Wilms KH. Verbesserte Methoden zur Auswertung topometrischer Messergebnisse. NOJ 1982, 24:71-75
- Kon YP. The keratometer and corneal measurement. Contact Lens Journ 20(7):14-7 (Troutman et al. US patent 1977)
- Feldon SE, Broome BG, and Wallage DA. Keratometer. US patent No. 4,597,648 1 July 1986
- Nakamura Y and Yano K. Ophthalmic apparatus. US patent No. 4,795,250 3 January 1989
- El Hage SG. A computerized corneal topographer for use in refractive surgery. Refract & Corneal Surg 1989, 5:418-24
- Dekking HM. Zur Photographie der Hornhautoberfläche. Graefes Arch Ophthalmol 1930, 124:708-30
- Rouwen AJP. Corneal alterations with contact lens wear. Kugler Publications Amsterdam/New York 1992
- Klyce S. Introduction to keratoscopy. In: Burato L. (ed) Corneal topography, the clinical atlas. Thorofare, NJ: Slack Inc 1996: Chap 1
- Drummond AE (ed) Corneal topography, the state of the art. Thorofare NJ: Slack Inc 1995
- Gormley DJ, Gersten M, Koplin RS, and Lubkin V. Corneal modeling. Cornea 1988 7(1):30-5
- Mammone RJ, Gersten M, Gormley DJ, et al. 3-D Corneal modeling system. IEEE Trans Biomed Engineer 1990 37:66-72
- Kuhn WP and Baker PC. Device and method for mapping objects. US Patent No 5,592,246 7 January 1997
- Campbell C. Reconstruction of the cornea shape with the MasterVue Corneal-Topography System. Optom Vis Sci 1977 74(1):899-905
- Mattioli R, Tripoli NK. Corneal geometry reconstruction with the Keratron Videokeratopher. Optom Vis Sci 1997 74(11):881-94
- Jean B, Bende T, Mathhana-Kielmann M. Process and device for determining the topography of a reflecting surface. US Patent No 5,640,962 24 June 1997
- Tsukada H, Sato T, Hatanaka , Kamiya M, Kato, T. Corneal shape measuring apparatus. US Patent No 5,694,197 2 December 1997
- Klein SA. Uniqueness of corneal shape from Placido ring images. Vision Science and its applications. Vol Technical Digest Series. Washington DC: Optical Soc of Am 1996:204-7
- Applegate RA, Howland HC. Noninvasive measurement of corneal topography IEEE Eng Med Biol 1995 14:30-42
- Fujii T, Maruyama S. Determination of corneal configuration by the measurement of its derivatives. Optica Acta 1972 19(5):425-30
- Gove PB (Ed) Webster's Third New Int. Dictionary of the English Language, G & C Merriam Co, Springfield, Mass, 1976
- UK patent 1,145,721, 8 March 1966. (Application made in the USA, USA patent 439,749 on 15 March 1965)
- Mandell RB. Corneal curvature measurements by the aid of moiré fringes, A O A 1966 373930:219-42
- Adachi IP, Adachi Y, and Frazer RE. Real-time analysis keratometer. US patent No. 4,692,003, 8 September 1987
- Steel WH. Interferometry, second edn. Cambridge, Cambridge University Press, 1983: Chap 7
- Bille JF. Device for mapping corneal topography. US patent No 5,062,702, 5 November 1991
- Schardin H. Über die Grenzen der Hochfrequenzkinematographie. Proc sixth int congress on high speed photography, The Hague, 1962:1-29
- Hochberg EB. Method for extracting long-equivalent wavelength interferometric information. US patent No. 5,054,924 8 October 1991
- Hildebrand BP, Haines KA. Multiple-wavelength and multiple-source holography applied to contour generation, J Opt Soc of Am 1967, 57:155-162
- James TH (Ed). The theory of the photographic process, The Macmillan Company, New York 1966: Chap 23
- Kasprzak H, Kowalik W and Jarónski J. Interferometric measurements of fine corneal topography. Proceedings of the SPIE conference on Optical and Imaging Techniques in Biomedicine, Lille, 1995 2329:32-39

40. Jongsma FHM, Brabander J de, Hendrikse F. Meten aan het hoornvlies, Nederlands Tijdschrift voor Natuurkunde 1997, 63(2):39-43 (English abstract: Microtopography of the central area of the cornea, Invest Ophthalmol & Vis Sci 1997 38(4):S851)
41. Hochberg EB and Baroth EC. Method and apparatus for white-light dispersed-fringe interferometric measurement of corneal topography. US patent No. 5,317,389, 31 May 1994
42. Hellmut T and Wei J. Optical coherence tomography corneal mapping apparatus. US patent No. 5,491,524, 13 February 1996
43. Calkins JL, Hochheimer BF, and Stark WJ. Corneal woundhealing: holographic stress-test analysis. Invest Ophthalmol Vis Sci 1981, 20(2):322-34
44. Politch J. Optical and long wave holography: potential application. Doc Ophthalmol 1977, 2113-8
45. Licznarski TJ, Kasprzak HT, Kowalik W. The results of in vivo assessment of the tear film stability on a cornea and a contact lens by use of the Twyman-Green interferometer and the lateral shearing techniques. Vision Research 1996, 36(5):200
46. Malacara D. Twyman-Green Interferometer. In: Malacara D (Ed) Optical shop testing, Second Edn, New York: John Wiley and Sons 1992: Chap 2
47. Steel WH. Interferometry, second edn. Cambridge, Cambridge University Press, 1983: Chap. 12
48. Mandell RB. Profile methods of measuring corneal curvature. J Amer Opt Soc 1961, 32:627-31
49. Snook RK. Pachymetry and true topography using the Orbscan system. In: Drummond AE. Corneal topography, the state of the art. Thorofare NJ Slack 1995: Chap 7
50. Sandler G. Elevation mapping technology gives enhanced corneal view. Ocular Surgery News Int Ed 1996, 7(11):40-3
51. Scheimpflug T. Der Photospectrograph und seine Anwendung. Photograph Kor 1906, 43:516-31
52. Barry J-C, Brannmann K, Dunne MCM. Catoptric Properties of Eye With Misaligned Surfaces Studied by exact Ray Tracing. Inv Ophthalmol Vis Sci 1997, 38:1476-84
53. Soroko LM. Meso-optics, Foundations and Applications, Singapore: World Scientific, 1996:288-95
54. Soroko LM. Keratometer. USSR patent No. SU 1,680,058, 15 December 1988
55. Soroko LM. Keratometer. USSR patent No. SU 1,806,588, 12 October 1990
56. Friedberg MA and Dimond WJ. Method for determining surface contours of an eye. US patent No. 3,169,459 16 February 1965
57. Warnicki JW, Rehkopf PG, Cambier JL, and Strods SJ. Method and apparatus for obtaining the topography of an object. US patent No. 4,995,719 26 February 1991
58. Cambier JL, Strods SJ. Method and apparatus for obtaining the topography of an object. Patent PCT/US91/04960 15 July 1991
59. Arffa RC, Warnicki JW and Rehkopf PG. Corneal topography using raster stereography. Eur J Implant Ref Surg 1989, 1:45-8
60. Belin MW. Intraoperative raster photogrammetry - the PAR corneal topography system. J Cataract Refr Surg supplement 1993, 19:188-97
61. Belin MW, Zloty P. Accuracy of the PAR corneal topography system with spatial misalignment. The CLAO journal 1993, 19(1):64-8
62. Lange SR and Thall EH. Method and apparatus for measuring corneal topography. US patent No. 5,116,115 26 May 1992
63. Lange SR. Phase shifting device and method. US patent No. 4,984,893 15 January 1991
64. Thall EH, Lange RS. Preliminary results of a new intra operative corneal topography technique. J Cataract Refr Surg 1993, 9(5):193-7
65. Windecker R and Tiziani HJ. Semispatial, robust, and accurate phase evaluation algorithm. Appl Opt 1995 34(31):7321-26
66. Kawara T. Corneal topography using moiré contour fringes. Appl Opt 1979, 18:3675-8
67. Jongsma FHM. System for determining the topography of a curved surface. US patent No. 5,406,342 on 11 April 1995
68. Stultiens BAT. Frequency modulation as an alternative for local phase in 3D corneal topography. Proceedings of the SPIE Conference on Ophthalmic Technologies IV, Los Angeles, 1994, 2126:174-84
69. El Hage SG. Apparatus and technique for automatic centering and focusing a corneal topographer. US patent No. 5,526,072 11 June 1996
70. Maiman HT. Stimulated optical radiation in ruby masers. Nature 1960, 187:493-4
71. Baron WS. Apparatus and method for determining corneal and scleral topography. US patent No. 4,761,071 2 August 1988
72. Mantravadi MV. Lateral shearing interferometers. In: Malacara D. Optical Shop Testing, New York: John Wiley and Sons Second edn 1992: Chap. 4
73. Corbett MC, Marshall J, O'Brart DPS, Rosen ES. New and future technology in corneal topography. Eur J Implant Ref Surg 1995, 7:372-86
74. Jongsma FHM, Brabander de J, Hendrikse F, and Stultiens BAT. Development of a wide field height eye topographer: Validation on models of the anterior eye surface. Optom Vis Sci 1998, 75(1):69-77

Key words: Corneal topography; interferometry; holography; moiré; fluorescence; partial coherence

Chapter 3

A model for testing fluorescein agents as a coating for the anterior eye: a feasibility study

3.1 Introduction

Since 1882 fluorescein has been used for clinical diagnosis and research in ophthalmology¹⁻⁸. Its fluorescent characteristics, such as yield, spectral absorption and emission have been extensively investigated. When exposed to light, fluorescein absorbs the blue and violet parts of the spectrum and emits fluorescent light of longer wavelength after about 10^{-9} seconds⁷. With a spectrophotofluorometer the absorption and emission of a solution of sodium fluorescein in a buffer can be measured⁷. For low fluorescein concentrations, it shows a maximum absorption at 490 nm. When exposed to this wavelength, the highest intensity of fluorescence is at about 530 nm⁹.

Traditionally the ophthalmologist observes the eye after instilling fluorescein from a unit dose container or a specially prepared strip, in order to look for absorption of the dye in damaged tissue. Research has shown that fluorescein is capable of staining interruptions in corneal epithelium by diffusing between cells^{2,3,5}, even devitalized¹⁰ or living¹¹ cells. In both animal and human healthy eyes, daily variability and differences between right and left eyes have been observed¹²⁻¹⁵.

Furthermore, variation in intensity and location of the staining for both pathological and normal eyes has led to the development and use of grid type of grading systems (use of coloured reference images to determine nature and progress of a process)¹⁵⁻¹⁸.

In contact lens fitting, fluorescein is used to estimate the thickness of the tear layer between the posterior lens surface and the corneal epithelium (fig. 3.1, c-e). In this case transparency must be sufficient for the excitation light to penetrate a tear layer several hundred micrometres thick on the anterior lens surface and the lens itself.

For assessment of tear quality, Tear film Break Up Time (TBUT) and wettability of the eye (fig. 3.1, a,b) or contact lens surface (fig. 3.1 e-g), one would like the tear film to be visible easily contrasted from the underlying "dry" substance. This requires limited optical penetration (opacity) rather than transparency.

In 1965 Friedberg and Dimond suggested the use of fluorescein as a diffusing coating for corneal topography¹⁹. In this application the dye must perform two tasks. One task is to destroy the directional information of the excitation light by transforming the impinging light into a (diffusely) fluorescing image of sufficient luminance. The other task is to make the transparent precorneal tear film opaque for the excitation light. When the tear film is insufficiently opaque to the excitation wavelength, backscatter from underlying eye tissues can disturb the fringe pattern, especially from the posterior corneal surface and iris (e.g. from the iris in blue-eyed individuals). Sometimes, also the bulbar conjunctiva that covers the white scleral tissue must be mapped, implying that requirements concerning the opacity are high for all types of eyes. This suggests the use of fluorescein solutions of high concentrations (high absorption of excitation light) with consequently a reduced fluorescent yield due to concentration quenching. Fortunately, fluorescein is a fluorescent agent with a high quantum yield²⁰. Nevertheless, it would be helpful to know the behaviour of the fluorescent label under controlled circumstances for example layer thickness and fluorescein concentration.

The aim of the present phantom (3.2) and *in vivo* (3.3) studies was to explore the feasibility of quantifying the efficiency of fluorescein applications using various types of fluorescein, concentrations and dilution fluids.

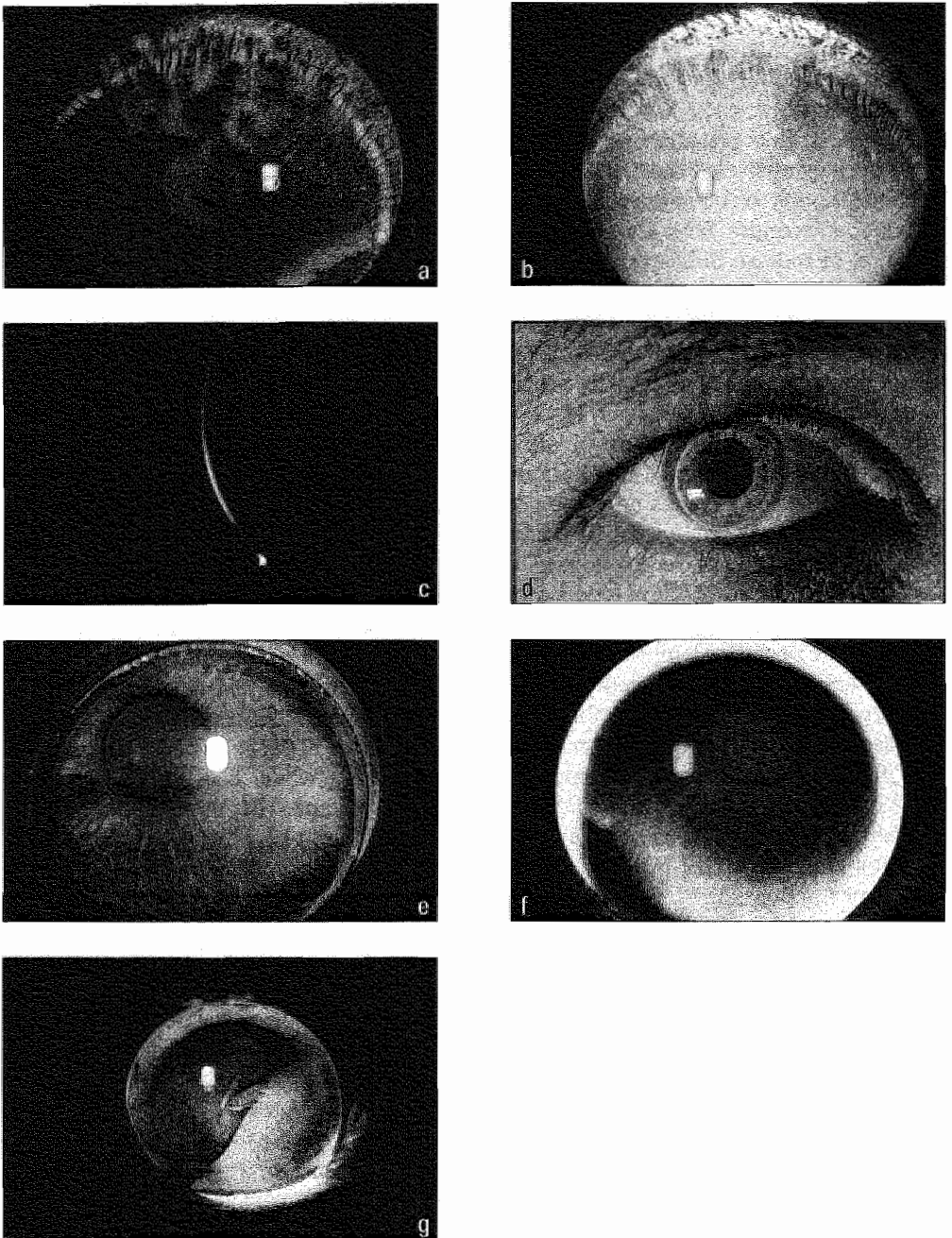


Figure 3.1
Various applications of fluorescein in contact lens fitting and assessment of tear quality and wetting (see text).

3.2 Assessment of fluorescent yield and opacity of different fluorescein staining agents in relation to layer thickness, fluorescein concentration, and dilution medium using a phantom

F.H.M. Jongsma, J. de Brabander, G.G.C. Mols, and F. Hendrikse

3.2.1 Abstract

This study aimed to investigate the yield and opacity of several fluorescein solutions to be used as a fluorescent coating for measurement of the topography of the anterior eye. Phantom measurements were performed using frontal illumination on 40 μm thick layers of fluorescein samples with three different concentrations in saline or methylcellulose 2%. Fluorescent yield was measured at various excitation wavelengths ranging from 440 to 510 nm, using a barrier filter and a radiometer as detector. To quantify the opacity, a wedge-shaped chamber was used that provided a variation in layer thickness starting from an average of 5 μm to about 500 μm . The layer thickness beyond which fluorescent yield no longer increased defined the layer thickness of 100% opacity. In this explorative study it was found that yield and opacity varied considerably with wavelength, type of fluorescent label and dilution medium. We found that high molecular weight strip fluorescein solution in methyl cellulose provided relatively high fluorescent yield with a nearly 100% opacity in 40 μm thick layers at all concentrations measured.

3.2.2 Materials and Methods

The measurements were carried out with front illumination on a measuring chamber that was developed by Van den Biessen et al.²¹. It consisted of a black acrylate cone with a slope of 3° with respect to a 1 mm thick fixed cover glass. In this way a measuring chamber with a thickness varying from 0 to 500 μm was obtained (fig. 3.2). The excitation source was provided by a filament of a 12 Volt/50 Watt halogen tungsten lamp (1) that was projected with a F/2.4 focused input on a 1 mm circular diaphragm (2) positioned close to a spectral wedge (3) linear variable interference filter (Oriel Corp. Stratford, CT, USA). In this way a beam with about 10 nm Full Width Half Maximum

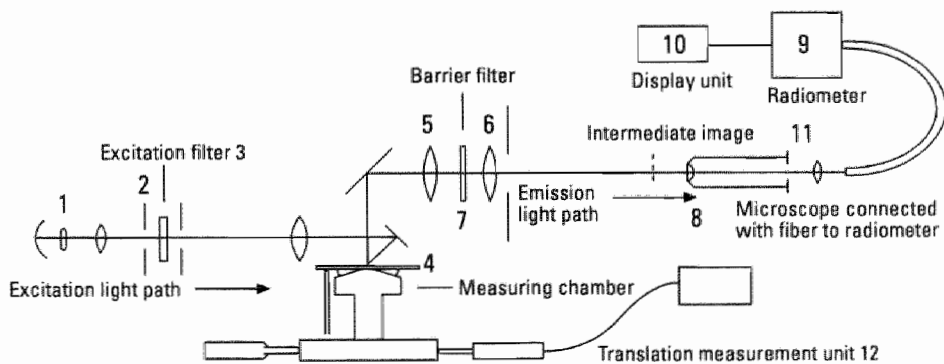


Figure 3.2

Scheme of the set-up that was used to measure the fluorescent yield and the opacity vs. layer thickness.

(FWHM) bandwidth was transmitted. The 1 mm diameter spot on the spectral wedge was 1:1 re-imaged on the rear side of the cover glass (4) of the measuring chamber. The excitation beam was projected at about the same angle (18°) with respect to the detection axis as is used in the MST²². The emitted fluorescent light passed through a 40 nm bandpass filter (barrier filter) with a centre wavelength of 550 nm (7, Melles Griot 03 FIV 044) positioned in between two 160 mm achromat relay lenses (5 and 6). The re-imaged spot using the relay lenses served as an intermediate image for a microscope (EE&G model 585-38-11) with a $2.5/\text{NA}=0.1$ objective (8, Melles Griot) coupled with a fibre optics probe (EE&G model 385-35-13). The detector consisted of an EE&G radiometer model 585-63 high sensitivity head (8), and a model 580-13 indicator unit (9). The excitation spot had a diameter of about 1 mm within the sample. The aperture of the relay optics was restricted by a diaphragm to match the etendue of the microscope and to prevent specularly reflected light entering the radiometer. The fluorescent spot (and for one measurement also the scattered spot) was projected through the microscope objective on a field aperture with a diameter of 1 mm (11). Due to the 2.5x magnification provided by the microscope objective, the effective diameter with respect to the measuring chamber was about 0.4 mm. The 0.1 NA microscope lens provided enough depth of field to catch a cylindrical volume with a diameter of about 0.4 mm over the whole measuring chamber.

Measurements were done with lateral intervals of 800 μm resulting in an increase in depth for each step of 40 μm (fig. 3.3). The first two steps were 400 μm apart to find a reliable reference point for the second (40 μm depth) measurement. Positioning was measured with a Heidenhain digital length gauge (11, model MT 30) with a precision of 5 μm .

The radiometer was calibrated for wavelength response.

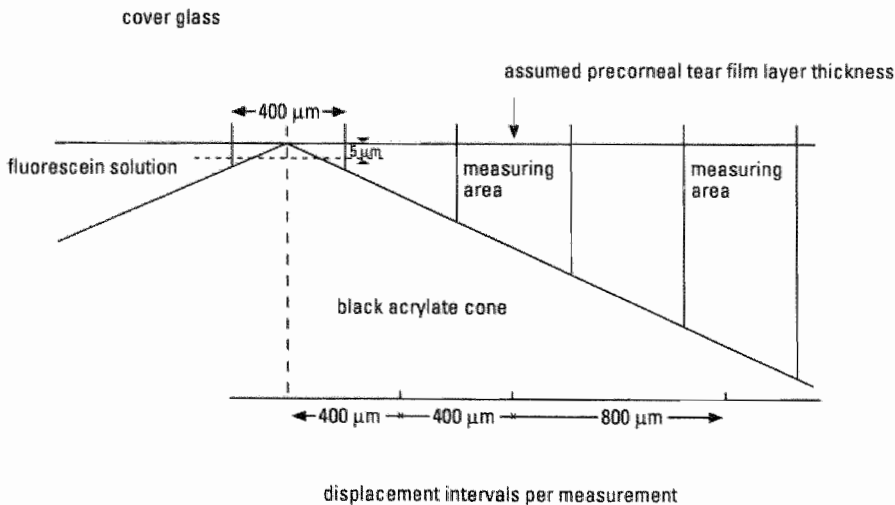


Figure 3.3

Schematic set-up of the fluorescein wedge. The central sample measures an average layer thickness of 5 μm .

Reproducibility of the measurements on one type of fluorescein (Fluor-I-Strip[®] A.T.) in one solution (methylcellulose) was tested. Opacity (%) of the layers was defined as the ratio between yield at 40 μm thickness and maximum yield (found at thicker layers). Figure 3.5 shows fluorescent yield vs layer thickness of several types of fluorescein. The 40 μm layer thickness was chosen because Prydal²³ estimated this as the average thickness of the precorneal tear film.

3.2.3 Preparation of the samples

The following samples were tested;

1. Fluor-I-Strip[®] A.T. (Small molecular Strip, "SS")
2. Fluor large molecule strip (Large molecular Strip, "LS").
3. Fluoresoft 0.25% Ciba (Small molecular Unit, "SU").
4. Fluorescéine 0.5% Faure (Large molecular Unit, "LU").

The dry strips were immersed in 0.5, 1 or 2 ml saline during 60 seconds. The contents of the units were diluted with one or three parts of saline or methylcellulose 2%.

3.2.4 Results

The reproducibility of ten fluorescence intensity measurements on Fluor-I-Strip[®] A.T. (SS) in 2 ml saline at 200 μm thickness showed $\pm 4\%$ reproducibility (these data are: 213, 207, 207, 207, 210, 196, 187, 207, 193, and 196). Fluor-I-Strip[®] A.T. in 1 ml methylcellulose 2% at 200 μm thickness showed $\pm 2\%$ reproducibility (these data are: 187, 193, 196, 196, 196, 187, 185, 187, 187, and 185).

Figure 3.4 shows the measured intensity (Arbitrary units, AU) vs excitation wavelength for SS in 1 ml saline at 100 μm layer thickness. The curve has two peaks. The first peak centred around 490 nm represents the fluorescent yield of the sample. The second peak at 550 nm is due to leakage of the excitation light through the barrier filter. Maximum yield for all types of fluorescein was found at excitation wavelengths between 483 nm

Intensity vs wavelength

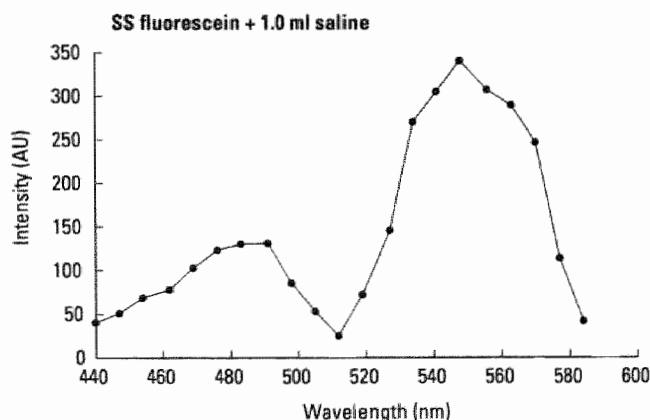


Figure 3.4

Fluorescent yield vs. excitation wavelength for a solution of Fluor-I-Strip[®] A.T. (SS) in 1 ml saline.

and 490 nm. Wavelength selection was achieved by manual displacement of the spectral wedge resulting in a wavelength precision of 5 nm.

Figure 3.5 shows the yield at average layer thicknesses between 10 and 240 μm for the four types of fluorescein using 483 nm excitation wavelength. Measured yield at the centre of the cone is not at zero thickness due to the dimensions of the measuring spot (see fig. 3.3). The present types of fluorescein have been selected on maximum yield at 40 μm layer thickness (see table I).

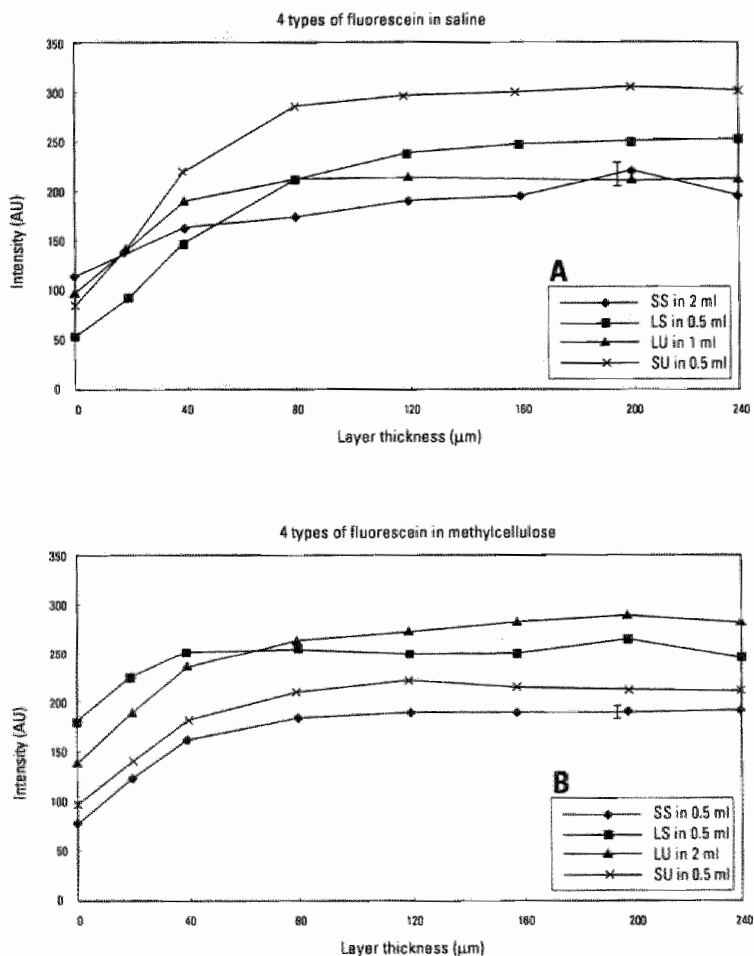


Figure 3.5

- Fluorescent yield as a function of the four types of fluorescein in saline. The concentrations used were selected from the highest yield at 40 μm layer thickness (see Table I). Error bar ($\pm 4\%$) is given for SS at 200 μm layer thickness.
- Fluorescent yield of the four types of fluorescein in methylcellulose. The concentration chosen were selected from the highest yield at 40 μm layer thickness (see Table I). Error bar ($\pm 2\%$) is given for SS at 200 μm layer thickness.

Table 1

Fluorescent yield from 40 μm layer at various concentrations in saline and methylcellulose. Figures indicate measured intensity in arbitrary units.

In saline	+0.5ml	+1ml	+2ml
Small Strip (SS)	158	139	161
Large Strip (LS)	145	74	43
Large Unit (LU)	116	188	216
Small Unit (SU)	152	167	147
In methylcellulose 2%	+0.5ml	+1ml	+2ml
Small Strip (SS)	166	138	106
Large Strip (LS)	258	250	215
Large Unit (LU)	134	169	244
Small Unit (SU)	186	174	158

In figure 3.5a saline is used as substrate and in 3.5b methylcellulose 2%. Both figures show that one of the curves has a steep increase of yield up to about 40 μm layer thickness and subsequently the flattest saturation curve. In saline this is LU in 1 ml (the increase of SU is steeper, although its saturation is achieved at about 80 μm layer thickness). In methylcellulose (3.5b) LS in 0.5 ml shows the best performance.

Figure 3.6 shows opacity vs concentration for the four types of fluorescein diluted in saline (A) and methylcellulose (B) at 40 μm layer thickness. These results followed from similar measurements as shown in figure 3.5 for the other concentrations, varying between 0.5 ml and 2 ml solutions of one unit or stripe. In saline the LU performed best at dilutions with 0.5 ml and 1 ml, whereas in methylcellulose LS performed best at all dilutions tested. If one assumes a reproducibility of about 4% in all fluorescent yields (fig. 3.5) this would yield a reproducibility of about 8% in the opacity due to uncertainty of estimation of opacity (fig. 3.6). However, this would hardly affect the conclusions.

3.2.5 Discussion

For clinical topography the opacity at a 40 μm tear layer thickness is crucial for corneal surface reconstruction and is based on fluorescence from the precorneal tear film.

The *in vitro* measurements show that for increasing layer thicknesses the yield increases until saturation occurs at thicker layers. However, some scatter of the data points was observed (fig. 3.5). For SS, reproducibility measurements were done at layer thickness of 200 μm , having a variation of $\pm 4\%$ (indicated in fig. 3.5). This suggests a $\pm 8\%$ uncertainty in the opacity data. The contrast in behaviour of LS in saline vs LS in methyl cellulose is remarkable. The dilution medium may play an important role for this type of fluorescein.

Opacity is shown in fig. 3.6. Here, the LS curve in fig. 3.6a is quite different from the LS curve in fig. 3.6b. To a lesser degree similar behaviour can be seen in the SS curves in figs. 3.5a and b.

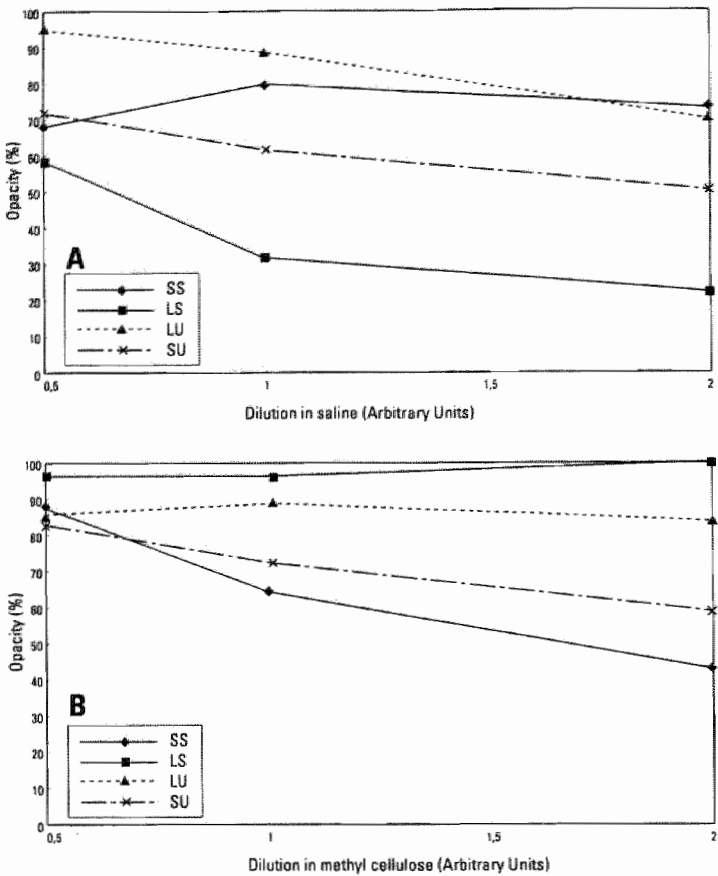


Figure 3.6
a. Opacity vs concentration of 4 types of fluorescein in saline.
b. Opacity vs. concentration of 4 types of fluorescein in methyl cellulose. Opacity is defined as the ratio between yield at 40 μm layer thickness and maximum yield (found at thicker layers).

3.3 *In vivo* assessment of the fluorescent yield of fluorescein staining on the ocular surface

J. de Brabander, F.H.M. Jongsma, and F. Hendrikse

3.3.1 Abstract

In contact lens fitting, the topical application of fluorescein is used for a variety of reasons. The most important ones are assessment of tissue integrity, qualitative analysis of the tear layer, wettability of the eye or contact lens surface and evaluation of the contact lens fit. The clinician observes the eye after instilling high or low molecular weight fluorescein from a unit dose container or a specially prepared strip. The eye is illuminated by blue excitation light and in some cases viewed through a barrier filter in order to sup-

press unwanted emissions and enhance visibility. A special application of fluorescein exists in shape topography of the anterior eye surface. The fluorescein is used to change the specular reflecting tear layer into a diffusely fluorescent layer. In this application the excitation wavelength used, type of fluorescein, and dilution fluid are of particular importance, since the tear film should be made completely opaque. The purpose of this study was to investigate the effects of excitation wavelength, type of fluorescein and type of dilution fluid on transparency/opacity of the tear film *in vivo* by using photographic visibility as a criterion. Results show that an excitation wavelength of 489 nm is most effective in obtaining high fluorescent yield. The use of an excitation wavelength of 450 nm, because of its reduced absorption in fluorescein, made deeper structures in the scleral part of the eye visible. Low molecular weight fluorescein was superior in creating opacity compared to high molecular weight fluorescein. Using methylcellulose as a dilution fluid increased yield and opacity.

3.3.2 Materials and methods

Photographs of a volunteer's eye were taken using a Zeiss 75SL photo slitlamp. Within the illumination path of the slitlamp, excitation filters with a centre wavelength of 450 and 489 nm and a 10 nm Full Width Half Maximum bandwidth were placed. Large and small molecular fluorescein was used from strip and unit dose. Saline and methylcellulose 0.5% and 2% served as dilution fluids.

In this explorative study, photographs were taken of a blue eyed subject using the slitlamp without barrier filter on a 200 ASA colour positive film. The photographic material was visually analysed on visibility of the underlying tissue (transparency/opacity) and on colour (fluorescence).

3.3.3 Results

Figures 3.7 (top a, b) show a pair of photographs taken with different excitation wavelength of an eye with sodium fluorescein (small molecular strip) diluted in saline in the tear film. The left picture was taken with 450 nm excitation wavelength and the right picture with 489 nm excitation wavelength. As the chromatic extinction coefficient for 450 nm is less than for 489 nm, the deeper structures at the scleral part of the eye are more clearly visible with the shorter wavelength.

In figures 3.7 (bottom c, d) the difference between the photographic result after instilling a solution in saline of small molecular strip (c) and large molecular strip (d) is shown. The small molecular strip shows a higher opacity than the large molecular strip.

Figure 3.8 shows four pictures where methylcellulose instead of saline was used as solvent for fluorescein. For both the methylcellulose 2% (b) and 0.5% (d), the small molecular strip (a,c) outperforms the large molecular strip (b,d) concerning yield and opacity.

3.3.4 Discussion

Better visibility of the deeper structures in the scleral part of the eye at shorter wavelength excitation (fig. 3.7a) can be explained by the lower light absorbance for 450 nm than for 489 nm. Probably, the same result can be obtained using longer wavelengths at a more diluted solution. In clinical practice it is rather difficult to control exactly the concentration of the fluorescein in the eye. One could, by rinsing the strip before uti-

Transparency/Opacity with saline

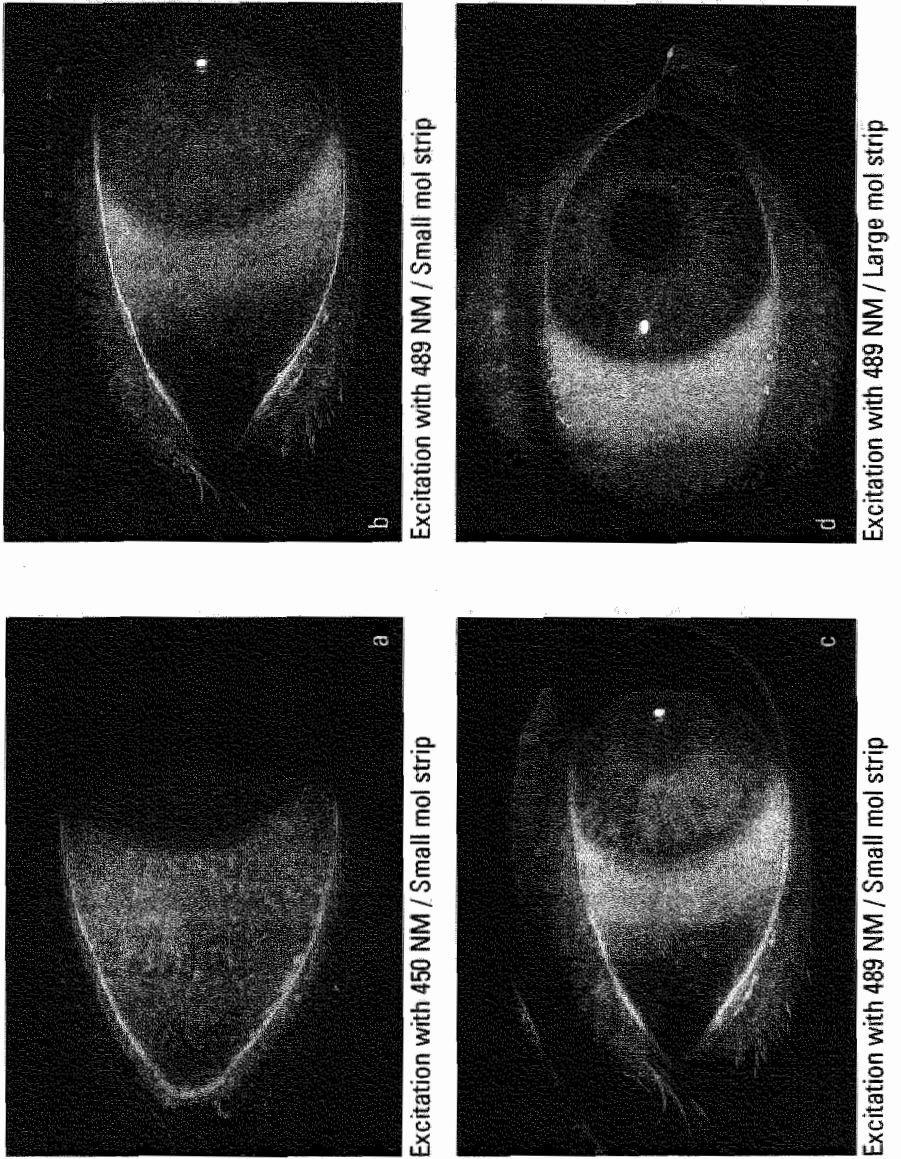


Figure 3.7

Transparency/opacity with saline. The top pictures show the difference in opacity between excitation with 450 nm (a) and 489 nm (b) using a small molecular strip as fluorescent dye. Note the better visibility of the underlying episcleral tissue in a. The bottom pictures show the difference in opacity using strips of small (c) and large (d) molecular fluorescein with saline.

Transparency/Opacity with methylcellulose

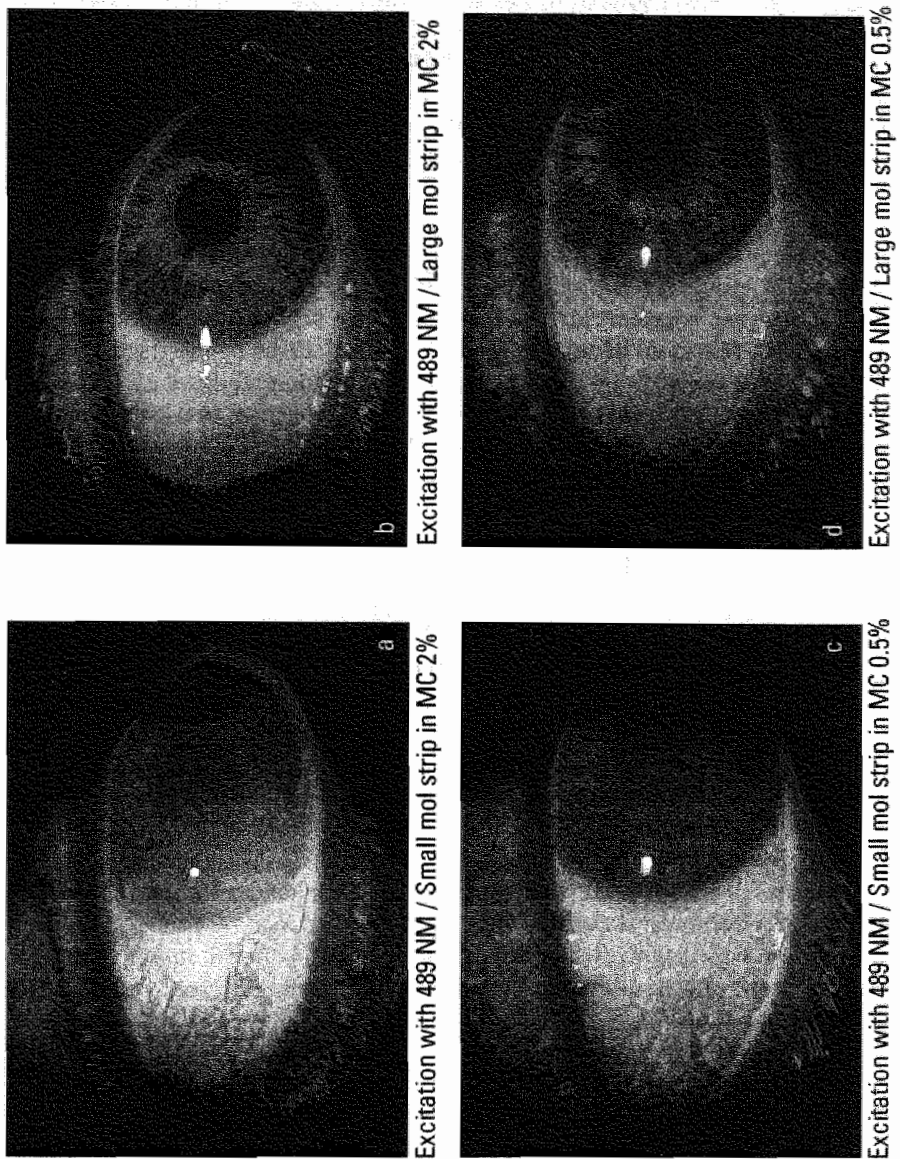


Figure 3.8

Four photographs of a fluorescent label in methyl cellulose with 489 nm excitation wavelength. The left pictures were taken using small molecular strip as fluorescent label, for the right pictures the large molecular strip was used. In the upper pictures methyl cellulose 2% served as substrate, in the lower pictures the substrate was methylcellulose 0.5%. Note the remarkable higher opacity with small molecule fluorescein in the left picture.

lization, reach a lower concentration or wait until the tears dilute the fluorescein. A practical solution allowing observations at wavelengths of not only 489 nm but also 450 nm would be to incorporate a 450 nm filter into the slitlamp filter disk. It would be of interest to investigate this aspect further since no clinical assessment of the scleral/conjunctival structures with a viewing system at 450 nm wavelength has been performed. From figure 3.8 it is clear that small molecular fluorescein results in better opacity. This is in accordance with our general observations in performing height topography with the MST.

It is also clear from figure 3.8 that the addition of methylcellulose increases opacity considerably. Theoretically this would be an advantage in topographic measurements. It is unclear, however, whether this increase is due to a higher fluorescence efficiency of the fluorescein or due to an increase of layer thickness caused by the viscosity of the methylcellulose. With the addition of methylcellulose the increase in the thickness of the tear film could obscure distinct height differences. The balance between detection of small height differences vs the better possibility of obtaining height measurements over the entire eye needs further study.

3.4 Comparison of phantom and *in vivo* results, conclusion

The use of a fluorescent label in topography of the anterior eye, to make its surface diffusely fluorescing rather than specularly reflecting, gives reliable surface data if the yield is sufficient for imaging the projected fringe pattern and if opacity prevents light reflected from deeper structures, e.g. iris or sclera, from interfering with the surface pattern. Both the phantom study and the *in vivo* study indicate that it is quite possible to achieve such conditions. Furthermore in both studies significant differences between the various types of fluorescein and substrates were found. However, the data obtained from the phantom experiments are not in agreement with the *in vivo* data. For instance, in contrast to good phantom performance of the large molecular fluorescein in methylcellulose, the *in vivo* study showed a very poor performance. A problem in the phantom investigation was that artificial dilution fluids had to be used, rather than body fluids¹². It seems, from our results, that these fluids react quite differently on fluorescein than the *in situ* tear film.

3.5 Conclusion phantom and *in vivo* studies

Our *in vivo* experiments show that opacity of the tear layer can be decreased by using a shorter excitation wavelength (450nm) enhancing visibility of fluorescence of deeper structures in the bulbar conjunctiva/episclera.

Both phantom and *in vivo* studies showed that it is possible to create opacity in a thin layer by using fluorescein.

Saline and methylcellulose used as solvent do not provide a good model for the phantom study on the behaviour of fluorescein in the tear film.

References

1. Maurice DM. The use of fluorescein in ophthalmological research. *Inves Ophthalmol* 1967;6(5):464-477
2. Fromm, Groenouw. Ueber die diagnostische Verwendbarkeit der fluoresceinfärbung bei Augenerkrankungen. *Arch Augenheilkd* 1891;22:247-57
3. Reitsch. Färbung der oberflächliche erkrankten Hornhaut mit Fluorescein und biebrichler Scharlachrot. *Graefes Arch Ophthalmol* 1915;89:299-307
4. Passmore JW, King JH. Vital staining of conjunctiva and cornea. *Arch Ophthalmol* 1955;55:568-574
5. Norn MS. Vital staining of cornea and conjunctiva. *Acta Ophthalmol (Kbh)* 1962;40:389-401.
6. Bailly EA, Rollefson GK. The determination of the fluorescent lifetimes of dissolved substance by a phase shift method. *J Chem Phys* 1953;21:1315-1322
7. Pflueger. Zur Ernährung der Cornea. *Klin Monatsbl Augenheilkunde* 1882;20:69-81
8. Romanchuk KG. Fluorescein. Physicochemical factors affecting its fluorescence. *Surv of Ophthalmol* 1982;26(5):269-283
9. Delori F, Ben-Sira I, Trempe C. Fluorescein angiography with an optimized filter combination. *Am J Ophthalmol* 1976;82(4):559-566 (1976)
10. Tabery HM. Dual appearance of fluorescein staining in vivo of diseased human corneal epithelium. A non-contact photomicrographic study. *Br J Ophthalmol* 1992;76:43-4.
11. Feenstra RPG, Tseng SCG. Comparison of fluorescein and rose bengal staining. *Ophthalmology* 1992;99:605-17.
12. Kikkawa Y. Normal corneal staining with fluorescein. *Exp Eye Res* 1972;14:13-20.
13. Caffery BE, Josephson JE. Corneal staining after sequential installation of fluorescein over 30 days. *Optom Vis Sci* 1991;68:467-9.
14. Schwallie JD, McKenney CD, Long WD Jr, McNeil A. Corneal staining patterns in normal non-contact lens wearers. *Optom Vis Sci* 1997;74:92-8.
15. Josephson JE, Caffery BE. Corneal staining characteristics after sequential instillation of fluorescein. *Optom Vis Sci* 1992;69:570-73.
16. Korb DR, Herrman JP. Corneal staining subsequent to sequential fluorescein instillations. *J Am Optom Assoc* 1979;50:361-7.
17. Josephson JE, Caffery BE. Corneal staining after instillation of topical anesthetic (SSII). *Invest Ophthalmol Vis Sci* 1988;29:1096-9.
18. Schwallie JD, Long WD Jr, McKenney CD. Day to day variations in ocular surface staining of the bulbar conjunctiva. *Optom Vis Sci* 1998;75:55-61.
19. Friedberg MA and Dimond WJ. Method for determining surface contours of an eye. US patent No. 3,169,459 (1965)
20. Pringsheim P, Vogel M: Luminiscence of liquids and solids and its practical applications. Interscience, New York (1943)
21. Van den Biesen PR, Jongsma FHM, Tangelder GJ and Slaaf DW. Shear rate and hematocrit dependence of fluorescence from retinal vessels in fluorescein angiography. *Ann of Biomed Eng* 1994;22:456-463
22. Jongsma FHM, de Brabander J, Hendrikse F, and Stultiens BAT. Development of a wide field height eye topographer: Validation on models of the anterior eye surface. *Optom Vis Sci* 1998;75:69-77
23. Prydal JI, Artal P, Woon H, Campbell FW. Study of human precorneal tear film thickness and structure using laser interferometry. *Invest ophthalmol and Vis Sci* 1992;33:2006-2011

Chapter 4

System for determining the topography of a curved surface

F.H.M. Jongsma

Published as: US Patent no. 5, 406, 342, 1995

European Patent EP 0 55195581, 1997

4.1 Abstract

A new Computer-Assisted VideoKeratometer (CAVK) has been developed. It is based on the principle of a moiré-based corneal topographer as previously described by Kawara¹. Hardware and software techniques have been adapted to circumvent the drawbacks inherent to moiré techniques. The device comprises a CCD camera interfaced with a computer for fast presentation of the data. An area of $22.4 \times 16.8 \text{ mm}^2$ is mapped. This requires a depth of field of about 6 mm that was obtained by applying a stereoscopic projection technique providing two fringe images of the surface in conjunction with Fourier analysis of the spatial frequency of the fringes projected. In order to exclude movement artefacts between the video signals from the left and right hand images, a double flash technique was implemented providing two tv fields (the odd and even frames) within 8 milliseconds. A real time topographic moiré picture of a living eye, as well as a reconstructed meridian, and a reconstructed topographic mapping of a living eye, are shown as examples. The local precision in height is $5 \mu\text{m}$.

4.2 Introduction

4.2.1 General

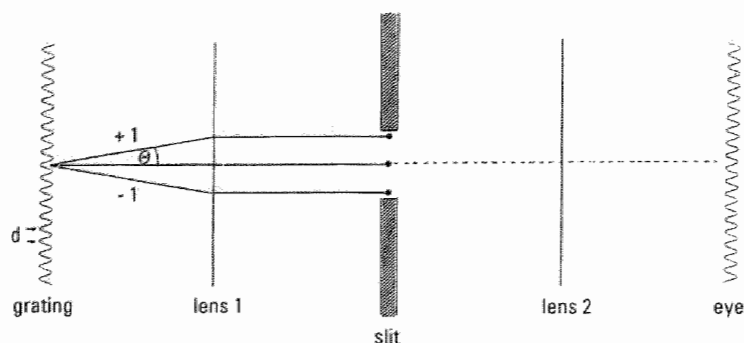
In this chapter a more general description is given of the author's patent "System for determining the topography of a curved surface". This patent is enclosed in appendix 1. Performance figures, given in this chapter, are tentatively estimated figures, and actual validation of the "Maastricht Shape Topographer" (MST), based on measurements on bispheric models, will be presented in chapter 5. Words marked with an asterisk (*) are further explained in the list of symbols and subscripts.

4.2.2 Background of the invention

As described in chapter 2, there is a variety of optical techniques to obtain a topographic mapping of the cornea. The device developed by Kawara¹ served as a starting point for the development of a CAVK* that measures primarily shape, described in this chapter. In order to make Kawara's device suitable for computer-assisted interpretation and to extend the area of measurement, some limitations connected with Kawara's device had to be overcome.

4.2.3 Limitations of Kawara's technology

In Kawara's technique a fringe pattern is projected on the eye. What is important for good moiré contrast is that fringes are projected with sufficient depth of focus*. For re-imaging this pattern on a reference grating, depth of field* is the crucial factor. An inherent limitation of a moiré projection system is that a small diaphragm is needed to obtain sufficient depth of focus, whereas a large diaphragm is required to project a fine grating, for sufficient depth resolution. The system described by Kawara obtained sufficient depth of focus by using a 1.5 mm telecentric* slit in the projectors. These slits allowed only the zero-order and \pm first-order diffraction maxima of the gratings to pass, making the projectors therefore diffraction-limited (fig. 4.1). Kawara's technique sup-



$$d \sin \Theta = m \lambda \quad (m=0,1,2,3,\dots)$$

Figure 4.1

Spatial filtering of a sine-wave signal. When a grating is placed in a monochromatic parallel beam of light, its diffraction pattern will appear in the focal plane of a transforming lens (lens 1). According to Abbe, at least two diffraction orders are necessary to reconstruct the grating. Consequently, when a slit is placed in the focal plane of lens 1, the minimal width that passes information from the grating is dictated by the focal length of the lens, the light used, and the spatial frequency of the grating. Lens 1 performs a Fourier transform of the grating (from the spatial domain to the frequency domain) whereas lens 2 performs an inverse Fourier transform (the part of the diffraction pattern projected by lens 1 that passes the slit, or another spatial filter, is back transformed to an image).

ports a 2 mm depth of field combined with 10 μm depth resolution, but this is insufficient to map the entire anterior eye. By increasing the projection angle of the fringes with respect to the observation axis, a higher resolution of depth may be obtained with the same fringe pattern. A serious drawback of this approach, however, is that large surface inclinations tend to broaden the fringe pattern on the surface, lowering its effective spatial frequency. When the distance between fringes on the surface increases over twice the distance of the bars in the reference grating, the lower mode moiré overlaps with the high moiré frequencies characterizing this surface and aliasing moiré patterns emerge² (fig. 4.2). Moreover, shadows are introduced on a corneal surface at projection angles larger than 35°, also a factor contributing to deterioration of the moiré image.

Another limitation follows from the kind of moiré technique used. The height lines are displayed at the reference grating in the viewing axis instead of on the surface to be analysed. This means that the flexibility of the instrument with regard to alternative data extraction is limited. The sign of the surface slope remains unknown, implying that we do not know whether a convex or concave surface is present (the "hill-or-valley" dilemma). The final outcome of Kawara's corneal topographer is a photograph. The translation of the height lines into AROC* (Axial Radius Of Curvature), IROC* (Instantaneous Radius Of Curvature, in this chapter referred to as "local radius of curvature"), eccentricity*, etc., start from these data.

Application of digital image analysis techniques can reduce the data acquisition time, increase the depth of field and solve the hill-or-valley dilemma, as further discussed below.

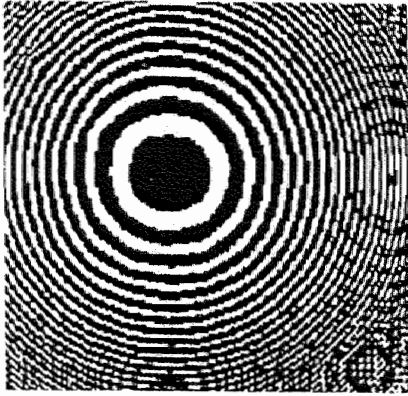


Figure 4.2

Moiré pattern of a spherical object. The faintly visible concentric rings on the right and bottom parts of the image are aliasing moiré patterns.

4.3 Improvements on Kawara's technique

4.3.1 Improving of measurement precision

In the patent a variety of techniques to improve measuring are discussed. Only the techniques potentially relevant for the Maastricht Shape Topographer (MST) are described in this chapter.

"Additive moiré": Instead of placing the reference grating in the viewing axis, the grating can also be placed in a second projector and projected simultaneously with another grating. In this way an additive moiré image is obtained that is located on the surface itself rather than on a reference grating.

Distinguishable planes, appearing in the volume in space, are parallel to the optical axis (fig. 4.3a). When parallel (collimated) beams are used to form moiré contours, the patterns represent equal-depth contours (fig. 4.3b). An object placed in the intersection volume of both projected fringe patterns is alternately intersected by fringe patterns and areas without intensity modulation (fig. 4.4).

4.3.2 Some methods for contrast control

The contrast of the additive moiré image can be enhanced by spatial or temporal filter techniques.

The spatial filter technique is accomplished in a two step procedure. The additive moiré fringes are formed in the first step, constituting a transparent image (fig. 4.4). Then, a collimated beam of monochromatic light back illuminates this image. The parallel light passing the image will be partly diffracted (see fig. 4.1). Focusing the beam after passing the moiré image, zero order and higher order diffraction spots will appear in the focal plane of lens 1. When also the undiffracted zero order is blocked (not indicated in figure 4.1), only the diffracted orders focused by lens 1 are back-transformed by lens 2. After this spatial filtering process the grey parts in the image are black, resulting in enhanced moiré contrast. As the contribution of the zero order is lacking, the fringes in the enhanced image have half the periodicity of the original images. This is demon-

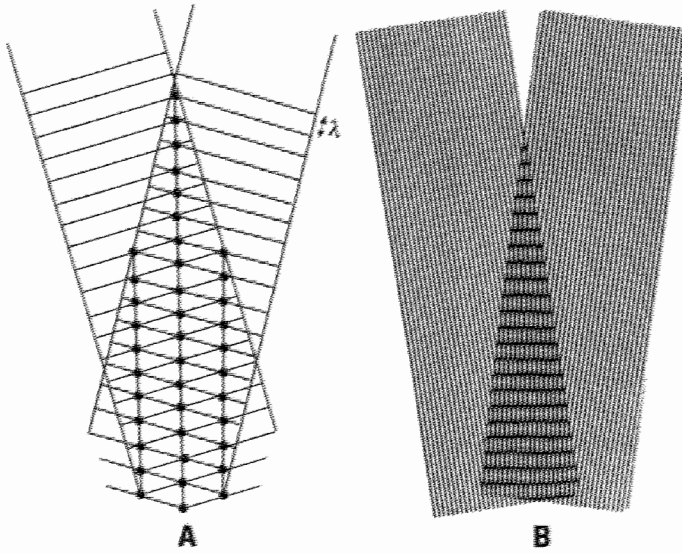


Figure 4.3

- a) When two mutually coherent beams are projected on a surface, bright and dark fringes appear where the interfering waves are in phase and out of phase respectively. The in phase positions (maximum intensity) are marked by black dots. The maxima and minima form a fringe pattern parallel with the bisectrix of the two interfering beams. As the waves travel with equal speed, the local phase relations do not change. Only the local intensity is modulated with the frequency of light, being for visible light about 10^{14} Herz.
- b) When the interference patterns of two pairs of interfering beams are projected on a surface, additive moiré contours are formed that are perpendicular to the bisectrix between the two pairs of beams.

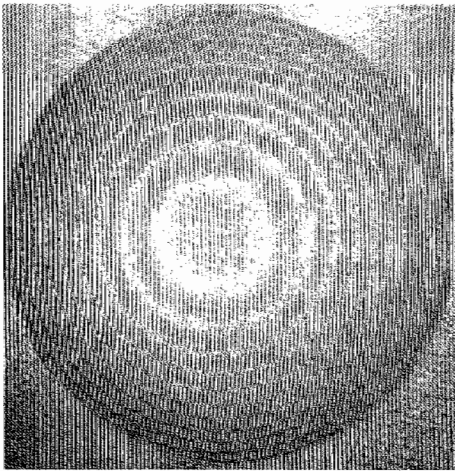


Figure 4.4

Additive moiré pattern on a spherical object. Concentric circles consisting of the fringes of the projected grating are separated by more or less grey circles, indicating the surface's contours of equal height where the projected left and right grating fringes are 180° out of phase.

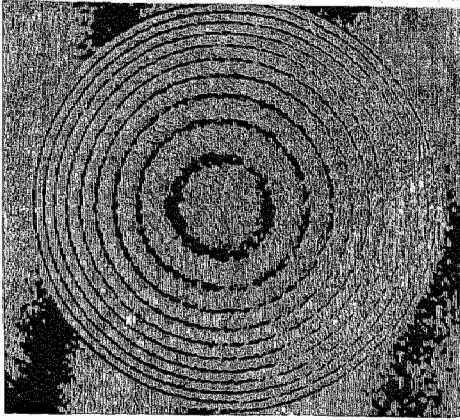


Figure 4.5

Moiré pattern that indicates lines of equal height on a spherical surface. This moiré contrast was obtained by a spatial filtering technique. The photographic recording of an additive moiré pattern (fig. 3.4) was placed in a parallel monochromatic beam of light. After passing the recording, the beam was focused yielding a zero order and higher diffraction orders of the image. After spatial filtering, where only the ± 1 diffraction orders were allowed to pass, and re-imaging of the recording, a contrast that is comparable to a multiplication contrast was obtained. Due to this kind of spatial filtering the fringe frequency is doubled compared to the grating frequency (compare projected grating fringes of figure 4.4 with the fringes in this enhanced image).

strated in fig 4.5 which represents the additive moiré image from fig. 4.4 after the spatial filtering process. Temporal filtering can be accomplished by selecting the fringe frequency from the video signal and blocking the less modulated frequencies produced by the beating of the left-hand and right-hand projected fringes, the selected fringes appear white against a black background on the tv-screen (fig. 4.6).

4.3.3 Detection of the sign of the surface slope

The "hill-or-valley" dilemma can be solved by avoiding moiré in the recording process ("fixed encoding")⁶. Then the bending of the projected fringes remains visible and indicates the sign of the slope.

4.4 Development of a new corneal topographer

To meet the requirements for temporal and spatial resolution we redesigned the hardware. We excluded moving parts such as for instance used for dynamic focusing⁶ or phase shifting⁷. In the image reconstruction we also excluded analogous methods such as moiré contrast by interference of two gratings. However, contrast-enhanced additive moiré was incorporated for focusing the device on the eye of the patient, using electronic moiré filtering described earlier (fig. 4.7).

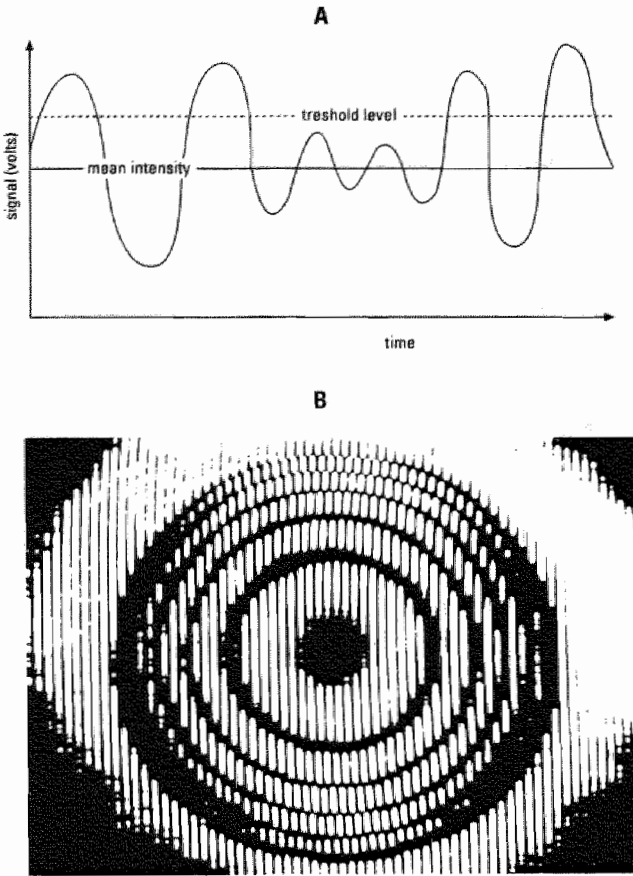


Figure 4.6.

Tv line representing an amplitude modulated signal (a). By blocking the low voltage part of the signal, contrast enhancement of an additive moiré pattern can be obtained (b).

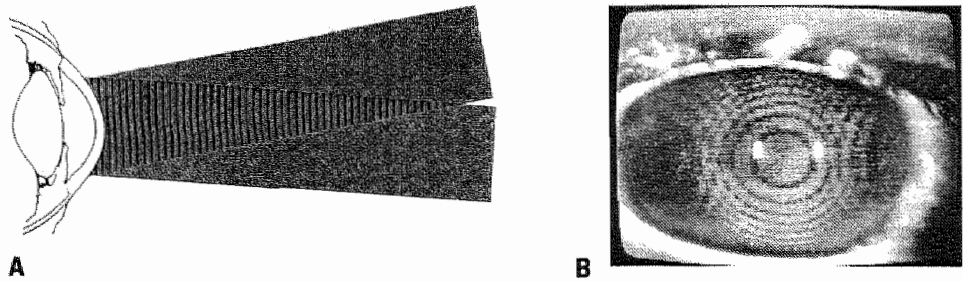


Figure 4.7

By projecting an additive moiré pattern on the eye (a), a real-time enhanced moiré image can be obtained by filtering the tv signals electronically (b).

4.4.1 Local frequency detection as an alternative to dynamic focusing techniques

Figure 4.8 shows a tv-line representing the intensity modulation from an additive moiré image. The points of minimal modulation (A) are lost for detailed (on pixel* level of the camera) analysis of the projected fringe itself. It would be nice if all camera pixels* could be fed with explicit height data. This can be accomplished by applying a Fourier analysis technique. This technique enables a periodic function, e.g. a fringe pattern, to be decomposed into a sum of sinusoidal functions. As these functions are integral sub-multiples of the original periodic function, the technique offers a way to measure the local characteristics of a single period. For example, the first part of a single sine wave of a projected sine-wave grating on an irregular surface will be compressed by a steep slope of a surface, whereas the second part is decompressed due to an adjacent part of the surface's flat slope. In this case, the first part of the sine wave represents a higher frequency component in the Fourier analysis than the second part. These local characteristics ("local frequency") are a measure of the local height. Fig 4.9 shows how the surface curvature of an object changes the local frequency of a orthoscopically fringe pattern projected. The local contraction or expansion of the projected fringe pattern at an area on the object surface reflected can be measured by calculating its local frequency. Thus the local frequency of the sine wave represents the surface's local slope. In fact each CCD camera pixel contains information over the average surface slope when compared to the information from neighbouring pixel. When the surface's slope contains no discontinuities within a pixel distance, the local height can be reconstructed by straightforward calculation.

The local characteristic of a single period, however, is changed when two gratings are superimposed (fig. 4.8) as will happen with moiré. To avoid this complication the following solution was chosen. Two fringe patterns are labelled in time by using a double

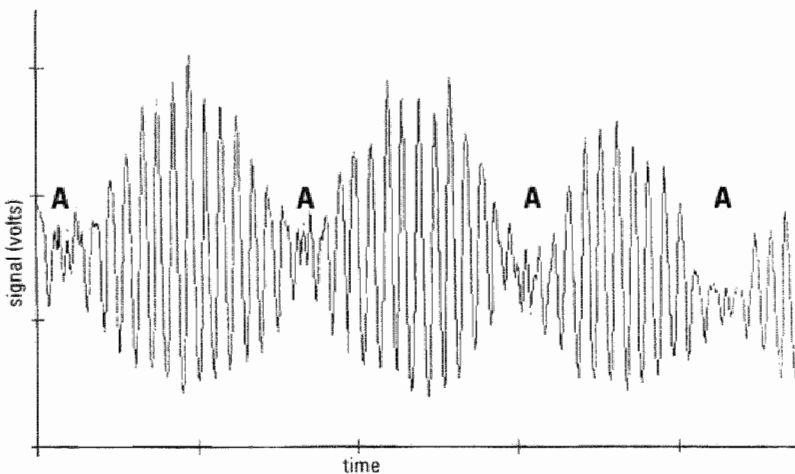


Figure 4.8

A tv-line of the CCD camera on which the intensity modulation of an additive moiré pattern formed by the left-hand and right-hand projection on a oblique surface is given. To avoid low modulation due to moiré (A), the left-hand and right-hand projections must be sequentially illuminated.

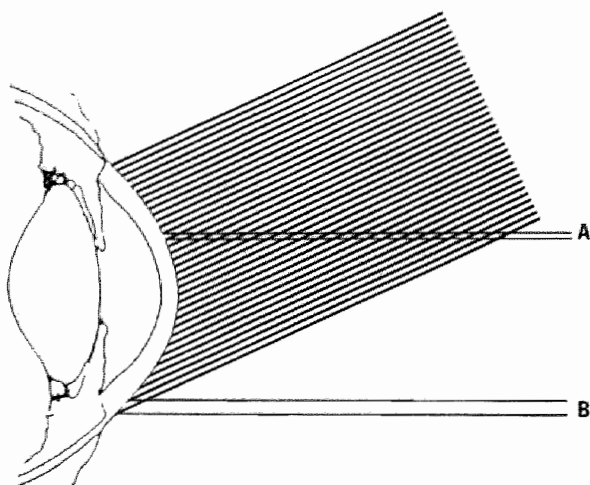


Figure 4.9

A fringe pattern projected on the cornea's surface is frequency modulated according to the surface's slope relative to the viewing axis.

flash technique described by Tangelder et al.⁸. We labelled within 8 ms to exclude eye movements during the measurements. The two flashes are synchronized with a CCD camera. The first flash is triggered at the end of the first field of the camera (odd frame) and the second flash is triggered at the beginning of the second field (even frame). This synchronization scheme is depicted in the insert of fig. 4.10. As the exposure time of the camera is controlled by the duration of the flash (0.1 ms) and the interval between both flashes, the total integration time can be considerably reduced by this technique. With the labelling in time, the unwanted amplitude modulating moiré interference is avoided. The odd and even frames can be distinguished by the computer and Fourier-analysed. The final result is a detailed height map composed of both Fourier-analysed frames. By applying Takeda's method of analysis⁹, automatic discrimination can be achieved between elevation and depression of the object's surface. The method also works with relatively coarse gratings which permit correspondingly larger diaphragms in projector and sensor.

4.5 The Maastricht Shape Topographer (MST)

The MST (fig. 4.10) comprises two projectors (3) set up at an angle of 18° to the optical axis (1) of a camera (2). Both projectors hold a slide (4) containing a line pattern of about 5 lp/mm, where the lines run at right angles to the plane through the projection axes. Projection lamps (5) are used as the light source in the projectors. In order to "freeze" rapid eye movements, the double flash technique with the flash lamps (6), which are synchronized (13) with the tv camera's framing frequency, is used. The lamps, continuously on, in the projectors are shut off during the measurement. Filters (7), positioned

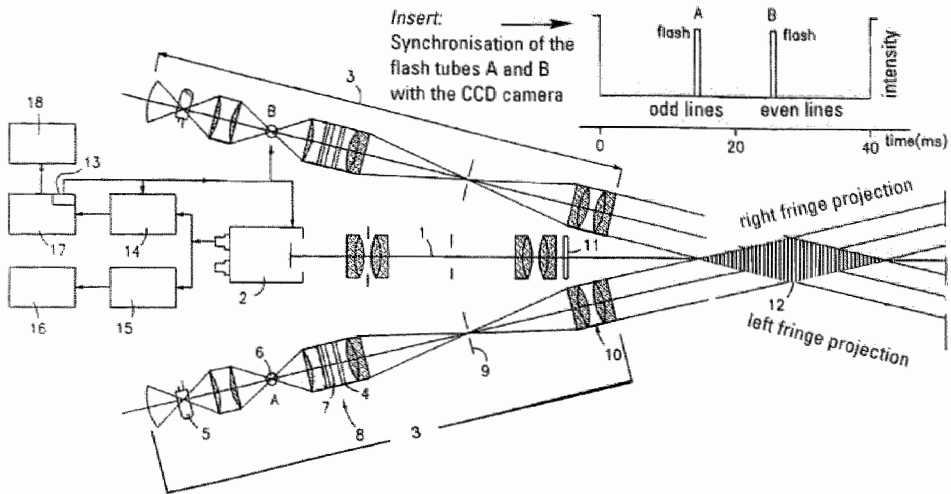


Figure 4.10

Scheme of the optical layout of the MST. Two orthoscopically projected beams by the telecentric grating projectors (3) form a measuring volume (12) of which a moiré monitor image can be obtained when illuminated by continuous light (5), or two fringe patterns (see fig. 4.11) when sequentially illuminated by flash tubes 6A and 6B. The MST consists of a CCD camera (2) connected to an electronic moiré filter (15) with monitor (16), and framegrabber (14), synchronizing device (13), personal computer (17) and monitor (18). In the insert the synchronization scheme of the flash tubes with the CCD camera is given. A = flash forming the odd frame and B = flash forming the even frame.

between the lamps and the slides, reflect the heat of the light source and all colours except blue-green (8), restricting the radiation load on the eye to that of the blue-green excitation light. To project the grating, the projection device is provided with a projection objective (10). A 3 x 20 mm² rectangular diaphragm (9), of which the long sides run parallel to the lines of the grating, is placed in the focal plane of the projection objective, at the object's side. The aperture of the diaphragm along the narrow side is small enough to project the 5 lp/mm gratings with sufficient depth of focus. The relatively large aperture of the diaphragm along the long side contributes to the desired light intensity of the projected pattern.

The distance setting takes place with the aid of an image observed via a pilot monitor (16) using an electronic analogue filter (15). When the cornea is placed completely in the depth of field of the sensor, concentric rings will appear on the entire cornea (fig. 4.7b). As the Fourier analysis is very sensitive to local over-exposure, for instance due to specular reflection of the excitation light on the cornea, a yellow barrier filter (11) is fitted in front of the camera. This filter blocks the blue excitation light and transmits only the yellow fluorescence light.

For the calculations, the unfiltered data of the frequency modulated grating image, as are present in the pair of frames (left and right hand projections respectively or odd and even frames) of the CCD camera, are used (fig. 4.11).

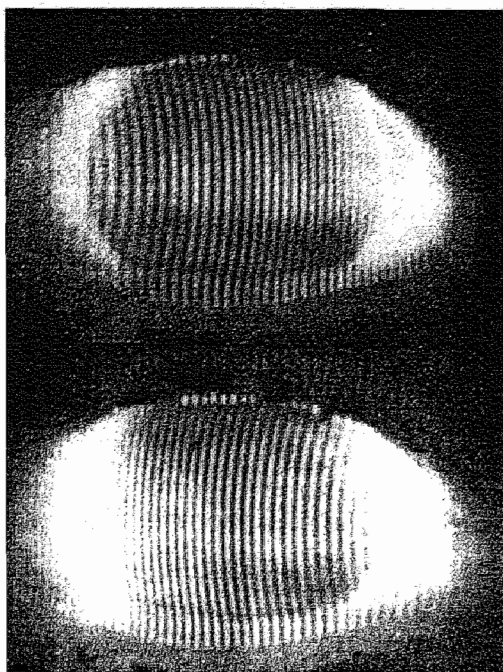


Figure 4.11

The left and right fringe projections on the cornea that are imaged as odd and even frames respectively are used as a starting point for the Fourier analysis.

As soon as the instrument is set, a frame grabber (14) sees to the digitalization and transmission of the signal to a monitor (18) coupled to a computer (17). There, the signal is analysed line by line. In this way, any missing information in one image can be supplemented through the other image. This also compensates possible defocusing effects of the peripheral right part of the left projection and the left part of the right projection.

The unfiltered moiré image (left and right fringe projections) at the location of each CCD camera field (fig. 4.11) contains pixel information on the spatial coordinates x , y , and z . With the aid of digital image processing, it is possible to reconstruct the shape of the anterior eye in detail. For example, a height (fig. 4.12) or local curvature meridian, or a height contour mapping can be displayed (fig. 4.13).

4.5.1 Quality of the optics

The projectors have the task to project gratings with enough depth of focus to provide a measuring volume (12 in fig. 4.10) adapted to the depth of field of the viewing system. Although it concerns low frequency gratings, the optics must be of high quality to ensure height measurements with μm accuracy. To achieve this, Spindler & Hoyer diffraction-limited achromats were used to project the gratings with a 1:1 ratio on the anterior eye. The 160mm achromats (10 in fig. 4.10) have been completely corrected for the C, d, and F lines ($C = 656.27\text{nm}$, $d = 587.6\text{nm}$ and $F = 486.13\text{nm}$). As the maximum

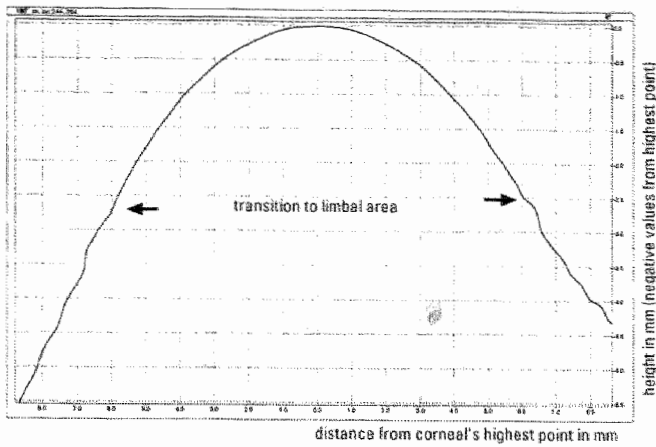


Figure 4.12
Reconstruction of a meridian.

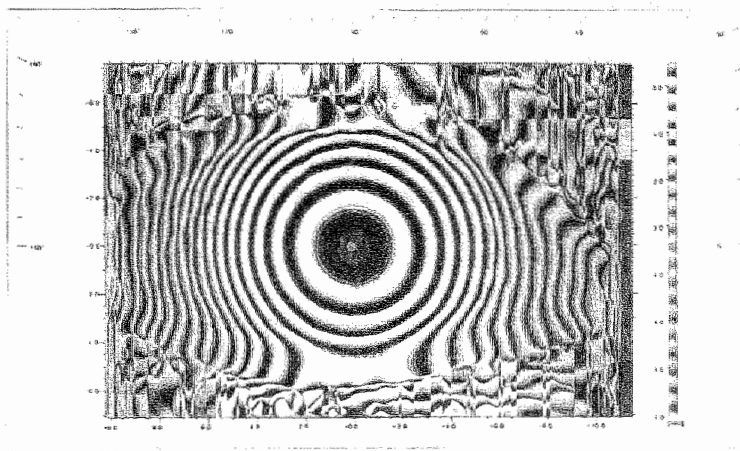


Figure 4.13
2-D reconstruction. The measurement includes adjacent tissue such as the bulbar conjunctiva. It clearly shows the concave surface of the lacrimal fluid in the lower fornix.

absorption for sodium fluorescein is at about 490 nm, the F correction is advantageous for the projection of the excitation light. The achromats are incorporated in an aplanatic configuration according minimum deviation requirements to minimize spherical aberration.

4.5.2 The software

A reconstruction image of 512 x 512 points defining a 22.4 x 16.8 mm² area is available after combination of the separately illuminated left and right projection images (fig. 4.13).

Although the spatial grating frequency induces mainly a horizontal carrier wave modulation, a two-dimensional analysis has to be performed to reveal a consistent image that contains the required information of the three-dimensional object. Digital filters were used to limit the local frequency to the equivalent of $\pm 60^\circ$ slope of the corneal surface. The left and right hand projected gratings are vertically oriented. Thus the highest spatial frequency (the modulated carrier frequency) is present along the tv lines. However, the bent fringes on the convex surface introduce a low spatial frequency component in the vertical direction. The reconstruction by Fourier analysis is done either in 1 dimension (following the tv lines) or in 2 dimensions¹⁰.

The patient's eye is aligned by bringing the visual axis in line with the optical axis of the instrument. When some misalignment is present, correction can be obtained by rotating the 3D-reconstruction guided by the surface features of the eye. For estimation of radii of curvature of a reconstructed image it is possible to use, for instance, elliptical or polynomial curve fitting. Corneal eccentricity*, astigmatism*, and so on, can be estimated or calculated from these fittings. The determination of fittings can also be carried out in a two- dimensional or three-dimensional manner. A "best fit sphere" algorithm was developed to calculate the central radius of curvature. Using an index of refraction value for the corneal tissue, the height or curvature mappings can be translated into dioptric values by applying Snell's law for refraction.

4.5.3 Precision of the pixel value

In case of fringe projection, the height information is coded in the local intensity distribution on the surface. The yardstick, a pair of fringes ("black" and "white"), is divided in subdivisions by the pixel values in the CCD camera incorporated in the viewing axis. The grating period (p) is translated in a fringe period on a surface perpendicular to the viewing axis (α) according $d = p/\cos\alpha$ (fig. 4.14). A shift along the viewing axis over a

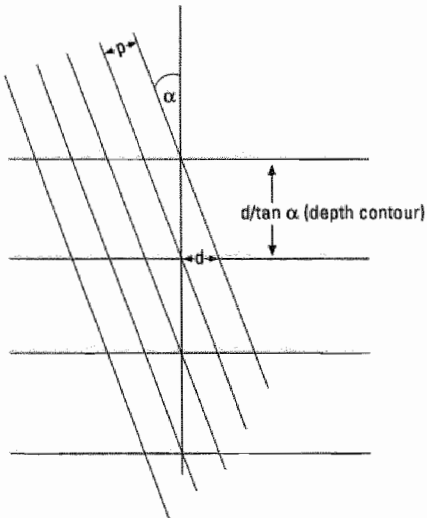


Figure 4.14

Relation between spatial grating frequency, projection angle, and resolution in depth.

fringe period will occur at $d/\tan\alpha$. For the MST $\alpha = 18^\circ$ and $p = 5$ lp/mm. (later on p was decreased to about 2.5 lp/mm in order to gain in depth of field and SNR of the image in the CCD camera.) For 5 lp/mm, $d/\tan\alpha = 616 \mu\text{m}$. Assuming pixel values between 0 and 256, the average depth interval for each pixel value is $2.4 \mu\text{m}$. For 2.5 lp/mm this average interval increases to $4.8 \mu\text{m}$. A lower (more realistic) SNR in the image decreases the precision. Estimation of precision of parametrical values, however, can be increased by averaging over more pixels for instance by shape matching (best fit sphere, elliptical shape, or other shapes). A tentative conclusion on the base of these considerations is that the MST allows height estimation with a precision of $5 \mu\text{m}$.

4.6 Discussion and conclusions

The hybridization of Kawara's technique¹ as explained above and the double grating technique introduced by Wasowski³ offers the following advantages. The resolution in depth will be mainly determined by the bandwidth (amount of pixels) and signal-to-noise ratio of the CCD camera in conjunction with the frame grabber rather than by the depth of field of the sensor optics. The contours of a moiré pattern do not play a role here; they have a lower lateral resolution because it is a beat pattern by definition. Movement artefacts are excluded by synchronizing the flash tubes with the end of the odd frame and the beginning of the even frame of the CCD camera. Depth of field is considerably increased compared to Kawara's technique. (The 5 lp/mm gratings used give, compared with the 12 lp/mm gratings used by Kawara, 2.4 times more depth of field of the viewing optics with the same aperture and imaging ratio.) Effective depth of focus of the fringes pattern on the surface is increased by projecting two gratings from opposite directions at an angle of 18° instead of only one grating at an angle of 35° . Some parts of the grating image on the surface may be out of focus due to the oblique projection angle. However, as the out-of-focus parts of the gratings in the odd and even projections (fig. 4.10) are projected from opposite directions, one image can supplement the information which has been lost (due to lack of depth of focus of the projectors) in the other image.

Focusing on the subject's eye is achieved with a pilot monitor showing a real time moiré pattern on the corneal surface. As out-of-focus parts of the image appear black on the monitor and the in-focus gratings are orthoscopically projected and recorded, the quality of corneal mapping is independent of the operator¹¹. This projection technique makes the system suitable for providing the information requested by, for instance, an optician, contact lens specialist or ophthalmologist.

Most commercially available corneal topographers are designed to "see" the cornea as an optical element, only characterized by its dioptric value. However, in a variety of applications, it is not the dioptric value but the shape of the cornea which plays an important role. This is, for example, the case in contact lens fitting and in evaluating the results of photorefractive surgery. The MST is designed to measure the local height with respect to a reference plane. Therefore, assumptions concerning the shape are not necessary. Especially when in the case of abnormal corneas, this is advantageous as assumptions may lead to false conclusions.

Therefore, the MST was developed as a "true shape" measuring device. It measures the surface itself with a sample density equal to the pixel density of a CCD tv camera, resulting in shape information with a lateral resolution of about $40\text{ }\mu\text{m}$ and an estimated local height precision of $5\text{ }\mu\text{m}$. Experimental verification of these figures has been done in a technical validation of the MST. This is described in chapter five of this thesis.

The modification of Kawara's device has been achieved without affecting the basics of the optical configuration such as telecentric projection and recording. With the latter reconstruction technique, the precision of the topographic mapping of $5\text{ }\mu\text{m}$ obtained by Kawara is maintained, while the depth of field is increased from approximately 2 mm to more than 6 mm . High spatial sampling and the image enhancement filtering, implemented by Stultiens¹⁰, also improved the lateral resolution.

The MST can be used for real-time height data acquisition of the entire anterior eye including cornea and adjacent tissues while further processing is done in digital form. The integration of optical and digital techniques allows reliable assessment of the central and peripheral curvatures of the cornea and the curvature of the adjacent limbal and scleral area.

References

1. Kawara T, Corneal topography using moiré contour fringes. *Applied Optics* 1979;18:3675-3678
2. Bell BW and Koliopoulos CL. Moiré topography, sampling theory, and charged-coupled devices. *Optic Letters* 1984;9(5):171-173
3. Wasowski J, Moiré topographic maps. *Opt Comm* 1970;2:321-323
4. Handbook of Non-Topographic Photogrammetry, Karara HM Ed. Chap. 15 Moiré Topography: Systems and Applications. Pekalsky JR and van Wijk MC. Am Soc of Photogrammetry and Remote Sensing, 1987
5. Lipson SG and Lipson H. Optical physics. 2nd edn Cambridge: Cambridge University Press 1981:266-267
6. Jongsma FHM, Ruissen CJ, Lambrecht P, and Vanherle G, Real-time contouring of tooth imprints. *Proc of the ECOOSA '84* 1984;492:500-506
7. Halioua M, Krishnamurthy RS, Liu H, and Chiang FP. Projection moiré with moving gratings for automated 3-D topography. *Appl Opt* 1983;22(6):850-855
8. Tangelder GJ, Slaaf DW, Muijtjens AM, Arts T, Oude Egbrink MA and Reneman RS. Velocity profiles of blood platelets and red blood cells flowing in arterioles of the rabbit mesentery. *Circulation Research* 1986;59(5):505-514
9. Takeda M, Ina H, and Kobayashi S, Fourier-transform method of fringe-pattern analysis for computer-based topography and interferometry. *J of Opt Soc of Am* 1982;72(1):156-160
10. Stultiens BAT, Jongsma FHM, Frequency modulation as an alternative for local phase in 3D corneal topography. *Progress in Biomedical Optics Proc. series, SPIE Proc. of Ophthalmic Technologies IV* JM Parel, Q Ren, A Katzir Ed 22-23 January 1994 Los Angeles, Ca 1994;2126:174-184
11. Hieselaar LJC, Ten Tusscher MPM, Jongsma FHM, Hendrikse F, Reproducibility of a new keratometer. *Vision Research* 34 (supplement, Programme and abstracts Montpellier October 15-19) 1994:94

Chapter 5

Development of a wide field height eye topographer: validation on models of the anterior eye surface

Franciscus HM Jongsma, John de Brabander, Bertho AT Stultiens and Fred Hendrikse
Optometry and Vision Science 1998; 75(1):69-77

5.1 Abstract

Purpose. The aim of this research was to develop a corneal topographer that determines the shape of the entire anterior surface of an eye without assumptions and with uniformly high precision in the center and periphery.

Methods. Based upon a double projection of two sine-wave gratings and analysis of the distortion of the sine-wave gratings due to the corneal-scleral shape, point-by-point measurements of surface elevation were obtained with a sample density equal to the pixel density of the CCD-detector. Using this principle a prototype topographer, called the Maastricht Shape Topographer (MST) was developed. The accuracy and reproducibility of the instrument were evaluated using bispheric models of the anterior surface of the eye.

Results. The precision of height measurements was $0.55\text{ }\mu\text{m}$ in the 10 mm central area and $22.50\text{ }\mu\text{m}$ in the periphery (14 to 19 mm). Precision of the reconstruction of the radius of curvature was 0.0155 mm (0.08D) in the center and 0.0313 mm in the periphery (sclera). Average height reproducibility standard error was $0.03\text{ }\mu\text{m}$ in the center and $2.6\text{ }\mu\text{m}$ in the periphery.

Conclusions. With the MST, unambiguous shape measurements of the entire anterior surface of the eye are possible with accuracy up to clinical accepted standards. The MST is able to measure height over a wide area of 20 mm, with a 6-mm depth of field. The tested prototype of the device can be further improved by the use of custom-made optics in order to increase signal to noise ratio in the periphery of the image. This height topographer could offer a reliable method in cases where shape is of paramount importance, e.g., in (scleral) contact lens fitting and refractive surgery.

Key words: cornea topography, contact lens fitting, sclera, moiré, videokeratography.

5.2 Introduction

Placido disc-based corneal topographers use the cornea as a convex mirror. The raw data in this type of topographer are highly sensitive for slope deviations. In Placido systems, the first Purkinje image, which is formed behind the cornea, is viewed for analysis. Historically, an assumption is made on the location and orientation of the image, and also on the shape that was actually measured. These assumptions, however, may not be applicable. Recently, some Placido systems have reduced the assumptions for identifying the corneal surface to the need of a continuous surface. However, the newer methods rely on relating adjacent measurements, which requires a dense and precise reflection pattern that cannot always be obtained. Because the shape of the cornea determines where the mires will reflect, the reflected image provides different coverage of different corneas, and does not consistently reveal structures outside the cornea.

A way to determine the real shape of the cornea directly, unambiguous and without assumptions, is to measure its local height. There are a variety of modalities to measure local height of objects in general. Most of them cannot be used in optometry because the corneal surface is transparent and the precorneal tear film is specular reflecting.

There exist some techniques of which the feasibility has been proven. The most impressive are those that are based upon interferometry^{1,2}. However, due to the difficulty to align the patient's eye with the axis of the instrument and the extreme sensitivity to movement artifacts, these technologies have not been adopted in clinical practice so far. With a slitlamp one can obtain a profile from the cornea using Rayleigh scattering from the corneal tissue³. By imaging multiple vertical slits across the whole width of the cornea from a known angle, this technology has been extended to a fully computerized system in the commercially available "Orbscan"⁴. Another alternative to the classical Placido-based topographers is the rasterstereography as is used in the PAR corneal topographers^{5,6}. This system uses a grid pattern composed of horizontal and vertical lines spaced approximately 200 μm apart. The topographic elevation is calculated from an image of the projected grid onto the corneal surface. Because the cornea consists of a transparent structure reflecting the light specular, its surface needs to be made diffusely radiating. This can be done by instilling sodium fluorescein in the precorneal tear film. It has been reported that the stability of the precorneal tear film is affected by fluorescein⁷. Therefore it is advised to perform *in vivo* exposures immediately after blinking. Tear film-dependent techniques do not work on dry eyes or other tearfilm deficiencies. Adding more viscous substances may change the surface shape⁸ but is not necessary for normal tear films. In case no coherent tear film is present, a diffusing membrane may be used⁹. The fluorescent coating technique was already applied in 1979 by Tetsuo Kawara¹⁰ in a corneal topography device that uses moiré contour fringes. Moiré fringes can be observed when two gratings are superimposed (fig. 5.1). This phenomenon can be used to obtain a display of the three-dimensional shape of an object. Kawara¹⁰ used sine-wave gratings in his device (fig. 5.2). A grating (PG) is projected on the fluorescein coated tear film and modified by the corneal shape. The modified grating is then optically projected onto a reference grating (RG) positioned in an intermediate plane in the viewing system. As a result of the interference between the two gratings, moiré fringes are formed and photographed (Ph). As the moiré image consists of

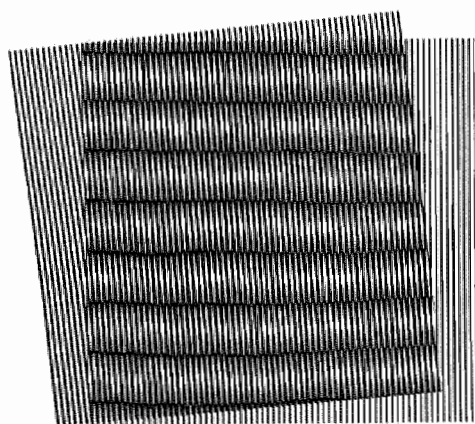


Figure 5.1

When two gratings are superimposed at an angle, a secondary pattern emerges that is called "moiré".

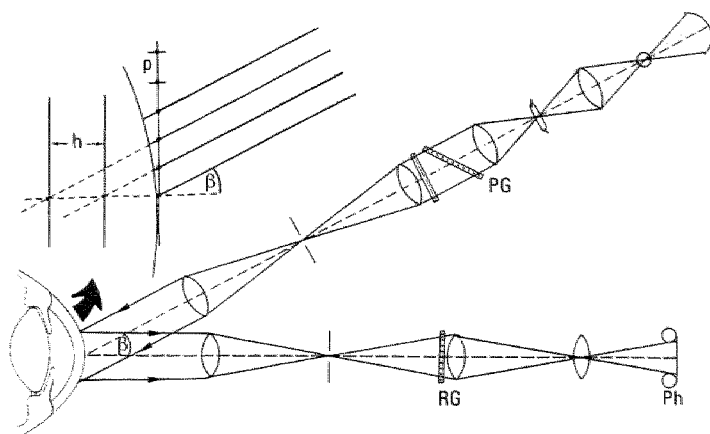


Figure 5.2

Schematic diagram of Kawara's moiré system. The moiré image is located at the reference grid (RG). Lines of equal height are obtained according $h = p/\sin \alpha$ (see insert).

lines of equal height, direct topographic information can be obtained without mathematical assumptions on the measured shape. In order to make magnification independent of distance, a telecentric projection method is applied. This provides an orthoscopic projection of the two grids on the corneal surface. The oblique orientation of the grating with respect to the optical axis of the projector, corresponds with the Scheimpflug correction for oblique projection. Unfortunately this correction method does not compensate for optical aberrations. The location of the moiré contour fringes is precisely determined with micro densitometer traces from photographic recordings. Each measurement point has, according to Kawara, an precision $5 \mu\text{m}$. Although this point accuracy is adequate for clinical practice, the laborious technology requires automation for widespread use.

We used Kawara's design as a starting point for the development of a computer-assisted topographer that is able to determine the shape of the entire anterior surface of the eye without assumptions and with equal accuracy in the center and the periphery. The aim of the study was to test the width and depth of field, validity, and reproducibility of the developed instrument. At this stage bispherical eye models were used that represent the broad range of corneal and scleral curvatures.

5.3 Methods

5.3.1 Design considerations

Projection-type moiré technologies have some inherent limitations.

1. The number of contour lines is dependent upon the spatial frequency and the angular displacement of the gratings used.
2. The spatial frequency of the moiré gratings is limited to the maximum frequency that allows the plus and minus first diffraction orders to pass the aperture of the projec-

tor. When a small slit is applied in the projector the spatial frequency of the projected grid is consequently low. Kawara¹⁰ used about 12 cycles/mm being about the physically maximum possible grid frequency with respect to the required depth of field. By tolerating a blur in the projected image equal to $1/4$ cycle of the projected grating, the modulation of the intensity is reduced to about 54 %. This arbitrary value was used as a boundary condition for the calculation of the required aperture dimensions, in order to obtain a depth of field of 6 mm. The diffraction limit of the projectors can be calculated by determining the width of the slit necessary for passing the + and - first diffraction orders of the grating. The calculation, according to Abbe, assumes a point light source in the projection device. When the dimensions of the light source are also included in the calculation, a slightly smaller aperture can be used. The area limited by the mentioned boundary conditions is given in figure 5.3.

3. Moiré contour fringes are only located at depth intervals of 2π or, when two opposed gratings with the same spatial frequency are applied, of π . This implies a restriction of the amount of measuring points with respect to the uncertainty in each point.
4. To produce moiré difference contours without ambiguity, i.e., no spurious moiré fringes, the image to be sampled must have a spectrum that lies totally within the range of $1/2$ to 1 Nyquist frequency¹¹.
5. The small slit that is required for projecting minute gratings with enough depth of field make projectors in a sensitive moiré system rather light consuming.

The number of measuring points and, consequently the accuracy of a moiré system can be extended by applying a scanning grid¹². Another method is to shift the object during

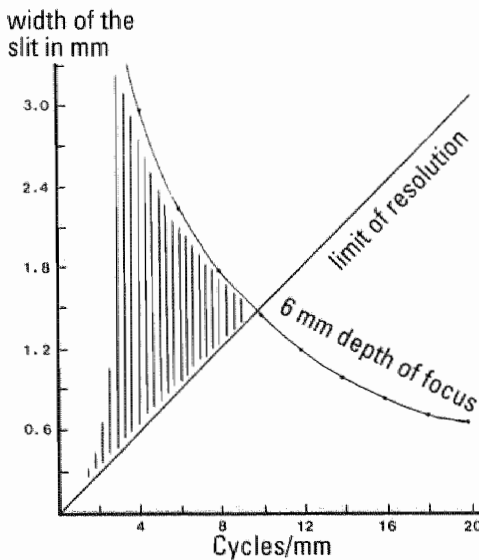


Figure 5.3

Slit width vs spatial frequency of the projected gratings. With 6-mm depth of focus at a 1:1 imaging ratio, only the shaded area is available.

the observation¹³ to reveal the local phase representing the local height of the contour fringes. However, to avoid movement artifacts, exposure times for corneal topography must be in the order of milliseconds, making it difficult to reveal the phase with a sequence of recordings. A mathematical technique for local phase reconstruction is the Fourier-transform method. Phase values can often be obtained, using sophisticated techniques, with an precision approaching $2\pi / 1000$ ¹⁴. A disadvantage of these techniques is that they require moving parts or a series of phase related exposures. With a Fourier-transform analysis using only a single exposure, the image reconstruction is less precise. However, Takeda et. al.¹⁵ developed a method using only a single exposure with better than $2\pi/30$ point precision. Applied to height contouring also the sign of the phase shift can be revealed. This method works best on frequency modulated signals. However, the amplitude modulation inherent to moiré techniques introduces noise. Moiré amplitude modulation can be avoided by using two projections separated in time or by (color)labeling of the gratings for subtraction afterwards. Another possibility is separation in space, which requires two sensors placed in opposite direction of the projection axis of one grating.

5.3.2 The device

With the above mentioned considerations in mind, we started to build a topographic device that could meet the criteria as given in Table 1. This was done at the Maastricht University in the Netherlands. The prototype instrument we present in this paper is therefore referred to as the "Maastricht Shape Topographer" (MST).

Table 1.

Reproducibility and accuracy of height data per given area of 3 bispherical eye models. Standard error of the MST presented as averaged variance and its SD within a set of 5 measurements per model. Difference in measured height presented as the averaged difference and SD over the given area. Note: values are in micrometers.

Area in (mm)	Radius Mold (mm)	Reproducibility: SE MST		Accuracy: Difference in Height Microscope-MST	
		Average (μm)	SD (μm)	Average (μm)	SD (μm)
10	7	0.0182	0.0216	-0.3691	2.9011
10	8	0.0031	0.0017	-0.5509	4.8901
10	9	0.0633	0.0719	0.5479	1.5632
14-19	12	4.6327	8.2248	0.0168	62.4585
14-19	13	3.0249	2.0604	-44.1550	19.8974
14-19	15	0.1891	0.1516	1.0208	13.0182

Figure 5.4 shows an optical schematic of the MST¹⁶. This topographer consist of two lateral telecentric sine-wave grating projectors for the projection of orthoscopic images on the cornea in conjunction with a central orthoscopic viewing system. A rectangular diaphragm (RD), of which its long sides run parallel to the lines of the gratings, is placed in the confocal plane of the orthoscopic projectors. In this way the gratings are projected such that a depth of field of 6 mm with respect to the viewing part is provided. A

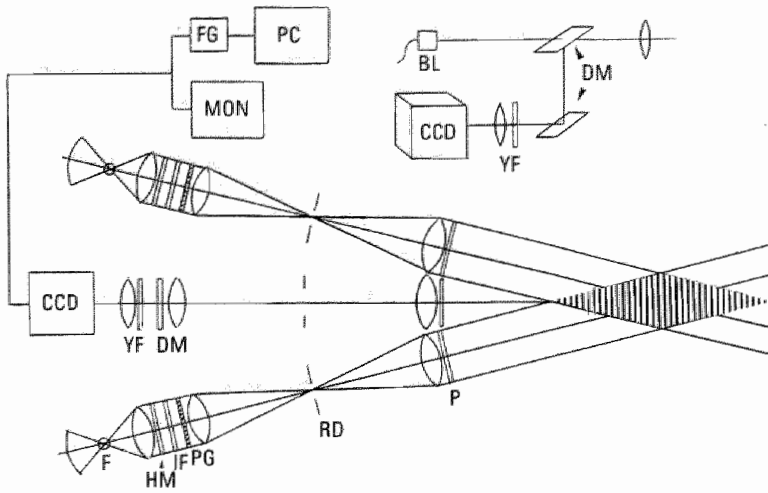


Figure 5.4

Optical schematic of the MST. The flash light in the lateral projectors is filtered by a heat reflecting mirror (HM) and a long pass interference filter (IF) that blocks radiation with a wavelength longer than 480nm. The sine-wave grating (PG) is projected onto the anterior surface of the subject's eye. A vertical slit (RD) serves as the telecentric diaphragm. A crossed polarizer with respect to the polarizers (P) on the projectors is placed in the viewing path in order to suppress specular reflection. Further suppression of unwanted light is obtained by a yellow filter (YF) that is nearly opaque for the excitation light. With dielectric mirrors (DM) the fluorescent light is guided to the camera while the blue led (BL) is visible for aligning the subject's eye (see insert). The CCD camera is connected with a monitor for focusing and a frame grabber (FG) for connection to a PC. The subjects' eye must be placed in the area where the two projected gratings coincide (indicated with vertical parallel lines).

frame transfer CCD camera, with its optical axis bisecting the angle between the two lateral projectors, records the two sequentially flashed images as odd and even line fields respectively. The time interval between the two images is about 8 ms. The images are captured by a 512 x 512 pixel frame grabber (FG) and stored in a PC for analyzing. A pilot monitor (MON) enables rough focusing and centering on the eye. It also displays a composed image after exposure. The lateral projectors have an angular separation with respect to the detector of 18°. Each projector contains a 2.5 cycles/mm grating which is projected on the precorneal tear film with a 1:1 imaging ratio. Thus, a moiré fringe represents a depth interval of about 0.65 mm with respect to a reference plane perpendicular on the optical axis of the sensor. The exposure time is determined by a 0.1-ms flash of light generated by a xenon tube in the projector. Between the flash tube (F) and the grating (PG) a heat reflecting mirror (HM) and an interference filter (IF) are inserted to restrict the radiation load on the eye to that of the blue-green excitation light. The fluorescent images from the modified grating are guided by two dichroic mirrors (DM), that reflect wavelengths longer than 500 nm, to the detector. In order to increase the suppression of the excitation light, a yellow barrier filter (YF) is placed in the viewing optics. Specular reflections are further suppressed by polarizers (P) placed in the projectors in

conjunction with a crossed polarizer in the viewing optics of the sensor. Without the polarizers, a local saturation of the CCD sensor causing loss of data may be introduced by specular reflection. This would prevent unambiguous phase unwrapping necessary for the height reconstruction. The standard UV polarizers were the only components in the device that affected the étendue (matching of the apertures of an optical system) of the projectors and recording system. However, for the above mentioned reasons, this shortcoming was accepted. A blue led (BL) is placed to be able to align the subjects' eye with the optical axis of the sensor. The independent odd and even frames are analyzed separately using Fourier techniques¹⁶, before being combined in a later stage of the reconstruction process.

A diffuse infrared illumination is added to locate the target area. Exact focussing is performed by triangulation with two diode lasers that are mounted onto the projectors. The 0.5 mW output of these diode lasers is filtered by a 1% transmission neutral density filter and focussed on the conjunctiva near the limbal area of the subjects eye by an $f = 160$ mm lens.

The software in the MST for the image reconstruction is based upon Takeda et. al. and extended for use in the MST¹⁷. The surface shape can be displayed either as a three dimensional (x, y, z) contour map or as cross-section. As the three-dimensional mappings are calculated for Cartesian coordinates, the display can be manipulated to enhance particular features such as image subtraction and reset of the center of the reconstruction to relocate the corneal apex.

Because of the oblique projection, the peripheral left part of the left projection and the peripheral right part of the right projection may be out of focus. As both half frames of the tv-system are used for the reconstruction, the missing information from one half frame can be compensated by the other frame.

5.3.3. Calibration and validation of the MST

On a computer-assisted submicron precision lathe (Euro Precision Technology), three bispherical PMMA molds were produced. The total diameter of the molds was 20 mm, the central part representing the cornea had a diameter of 12 mm. One mold had a "corneal" radius of 7mm with a "scleral" radius of 13mm. The other two molds had radii of 8mm/12mm, and 9mm/15mm respectively. From the molds impressions were made with Vinyl Polysiloxane (3M ExpressTM 7301H) that has the property to show autofluorescence when exposed to blue light. Using this material we obtained eye models that are entirely fluorescent, without the need for a coating or application of fluorescein. The model had a flat ground surface perpendicular to the central axis and is fixated in a micro-bench adapter plate (Spindler & Hoyer). To be able to control rotation exactly, the adapter plate was placed in a divided circle rotating mount.

As, according to the manufacturer, some dimensional change may occur during the first 24 h after making the impression, the shape of the Vinyl Polysiloxane eye models was measured one day after molding. To be able to compare MST height values to a solid standard, measurements on the eye model were first carried out with a Leitz microscope. For this, the eye model in its mount was fixed on the microscope table. The z- and x-axes of the microscope were connected to micrometers (Haidehahn Metrotaster 30M, sensor resolution $\pm 0.5 \mu\text{m}$). z Axis measurements were performed with a long free

working distance objective (Leitz UTK 32x / NA = 0.40). The microscope was coupled to a TV-camera showing a 1300x magnified image of the surface of the eye model. In this way focusing (z-axis) was done at an 8- μ m diameter area of the model with a focusing precision 1 μ m. Guided by the monitor image and the Metrotaster readings, the highest point of the eye models was found in an iterative z-x and z-y search. On both sides of the highest point z measurements were taken, thus scanning the whole meridian, at intervals of 500 μ m. After the series of measurements along a meridian was completed, the top was again brought in focus (zero value on the Metrotaster). When in that stage more than 1 μ m refocusing had to be done, the measurement series was rejected. Then the mold was rotated 90° and the measuring procedure repeated.

Because of the contact lens production program of the lathe, the transition area between diameter 10 and 14 mm could not be defined, and therefore measurements in that area are omitted. Hence, we used a 10-mm central area (20 measuring points per meridian) and a peripheral area extending from 14 to 19 mm (22 measuring points per meridian). If we use "central" or "peripheral" in the following text, we refer to these figures.

Directly after the measurement with the microscope, five exposures from each model were made with the MST. Before measuring, the MST was calibrated on a precision length caliber. In order to be able to compare the MST and microscope height measurements, the same meridians (0-180° and 90-270°) were sampled at intervals of 500 μ m. The height data of the MST are recorded after finding the highest point of the eye model in a proces similar to that used with the microscope.

The reproducibility of the MST was tested by analyzing the variance among the five measurements for the three eye models in the center and in the periphery. To compare height measurements, the average value of the five measurements with the MST in each point was compared with the value at the same point obtained by the microscope. To compare radii we computed Axial Radius Of Curvature (AROC) from each measured z value. AROC values were averaged to obtain one value for the central or peripheral part of the eye models.

5.4 Results

5.4.1. Accuracy and precision in height

The accuracy and precision in height is given in table 2. The right part shows the average differences and SD for the central and peripheral parts of the three eye models. From these data it can be seen that the accuracy in the central 10 mm zone is high and the differences between the models are small. The data are consistent and do not statistically differ (Student t-test $p > 0.05$). The 14- to 19 mm peripheral zone shows more inconsistency. Although the differences for radii 12 and 15 are not significantly different from the central part data, they do differ significantly (Student t-test $p < 0.05$) from the data for the 13-mm eye model. Because of the local under exposure caused by the obstructing polarizers, there is remarkable variation in standard deviations for the periphery. The interpretation of differences between average differences is difficult. Also, although the reproducibility of the microscope measurements was within $\pm 1 \mu$ m, the use of the microscope is new and cannot be taken as the accepted "Gold standard".

Table 2.

Averages, SD and differences in radius of curvature of 3 bispherical eye models as calculated from the height data of the microscope and the MST. Note: values are in mm.

Eye Models Mold (r)	Microscope (r)	MST (r)	Difference Microscope-MST	SD	
				Microscope	MST
7	6.9903	7.0250	-0.0347	0.01374	0.01480
8	7.9893	7.9930	-0.0037	0.01191	0.02619
9	8.9256	8.9474	-0.0218	0.03335	0.01346
12	12.0245	11.9846	0.0399	0.04640	0.11998
13	12.9850	12.9261	0.0589	0.00576	0.05266
15	14.9582	14.9492	0.0090	0.01111	0.07565

For these reasons we extended the analysis using the Bland and Altman method¹⁸ for comparing two measuring methods. Fig. 5.5 shows a scatter plot of the average between the microscope and MST height value against the difference between the two measurements. Note that the right part of the plot corresponds to the peripheral (scleral) values. The solid line (-0.0083 mm) shows the overall average with a 95% interval of agreement {shaded area = $\pm 1.96 * 0.0034$ (SD)}. Because of a transition zone between the central and peripheral curves, measurements between 5 to 6.5 mm from the center are elimi-

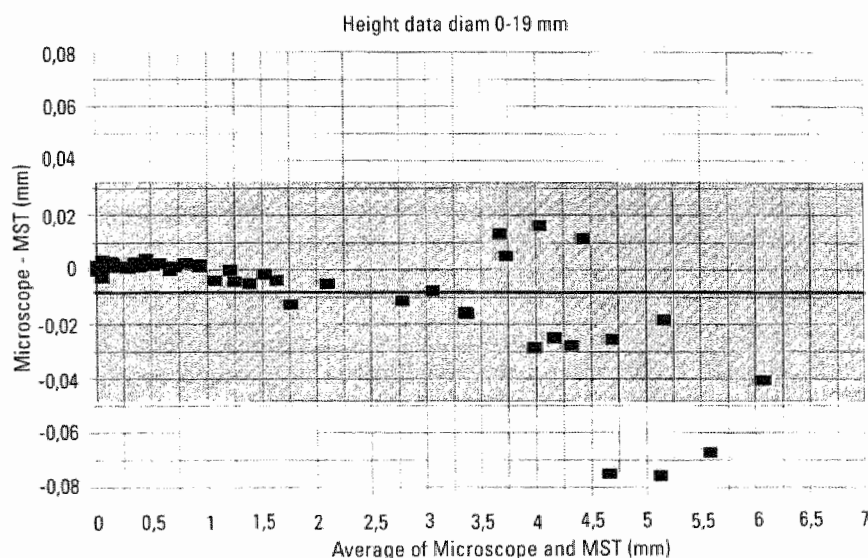


Figure 5.5

Scatterplot of the average between the microscope and MST height values against the difference between the two measurements. The solid line (-0.0083mm) shows the overall average with 95% interval of agreement (shaded area).

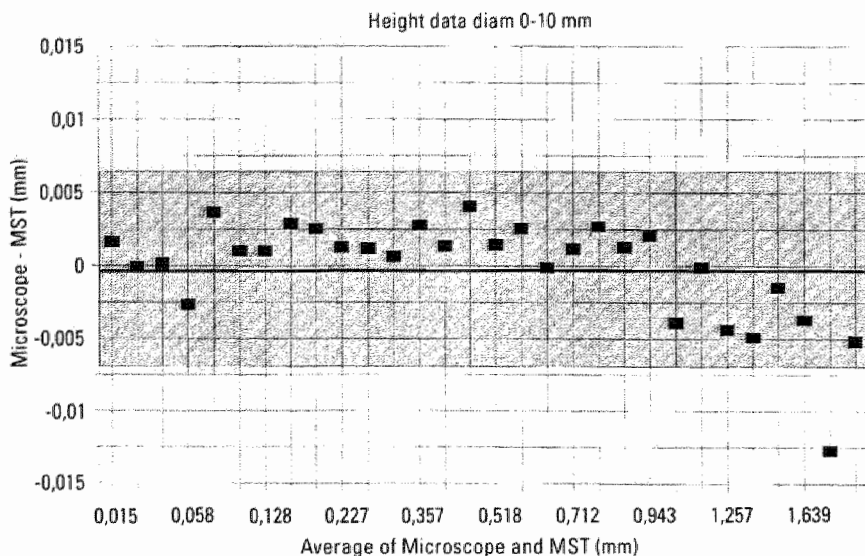


Figure 5.6

Scatter plot of the average between the microscope and MST height value against the difference between the two measurements for the central 10 mm. The solid line (-0.001 mm) shows the overall average with 95% interval of agreement (shaded area).

nated. The data show good agreement within the central 10 mm area with more scatter in the periphery. Fig. 5.6 shows these data in more detail for the central 10-mm (corneal) area only. Here the average difference was -0.000 mm , with SD of 0.00344 .

5.4.2 Reproducibility

Five sequential operator-independent measurements were made, thus without touching the eye model or changing the focusing of the MST. The Reproducibility columns of Table 2 show the reproducibility as average standard error (with its SD) for the whole central and peripheral part of each eye model.

Taken over all eye models, the average standard error in the 10-mm central area was $0.0282\text{ }\mu\text{m}$ (range 0.003 to 0.063) and for the peripheral 14 to 19 mm area $2.6156\text{ }\mu\text{m}$ (range 0.180 to 4.633).

The standard errors show no statistical differences among each other for the individual eye models at the central 10-mm part (Student t-test, $p > 0.05$). For the periphery there is no statistical difference (Student t-test, $p > 0.05$) between the standard error for the 12- and 13-mm eye models. However, both show a statistical difference with the central standard error values and with the standard error found for the 15-mm eye model (Student t-test $p < 0.05$).

5.4.3 Conversion of height values in radius of curvature

AROC was calculated using the microscope height value and the mean MST value in each point ($500\text{ }\mu\text{m}$ intervals). Conversion from height to radius from small sagitta values may

introduce significant error due to the reciprocal relationship between curvature and sag. Therefore, in the central area radii were computed from a point 2 mm from the center. The computed AROC values were then averaged over the area. The variation is given as standard deviation. The same method was used to calculate peripheral radii over an area of 7.0 to 9.5 mm from the center. The results are shown in Table 3. Average reconstruction precision of the radius of curvature of the MST compared to the microscope was 0.0155 mm for the central 10 mm and 0.0313 mm in the periphery (14 to 19 mm). The central (corneal) radius of curvature reconstruction precision may be expressed in diopters. Assuming an index of refraction of 1.3375, the precision 0.08 D.

5.4.4 Depth of field

The entire corneal surface and adjacent tissue can be measured, limited by either the depth of field or the angle of view of the device. For a sine wave projection with a 400 μm period as used in the MST, the depth of field exceeds 6 mm, allowing a significant part of the scleral-conjunctiva tissue to be in focus. Fig. 5.7 shows a cross-section height profile of an eye model and fig. 5.8 shows a cross-section height profile of the anterior eye of one of the authors. The limbal transition area of the eye model separates two bispherical curves. The *in vivo* limbal transition separates the smooth corneal surface from the more irregular scleral-conjunctiva surface. Also the nasal/temporal assymetry can be seen.

5.5 Discussion

A height measuring device, like the MST, has the advantage that the primary data

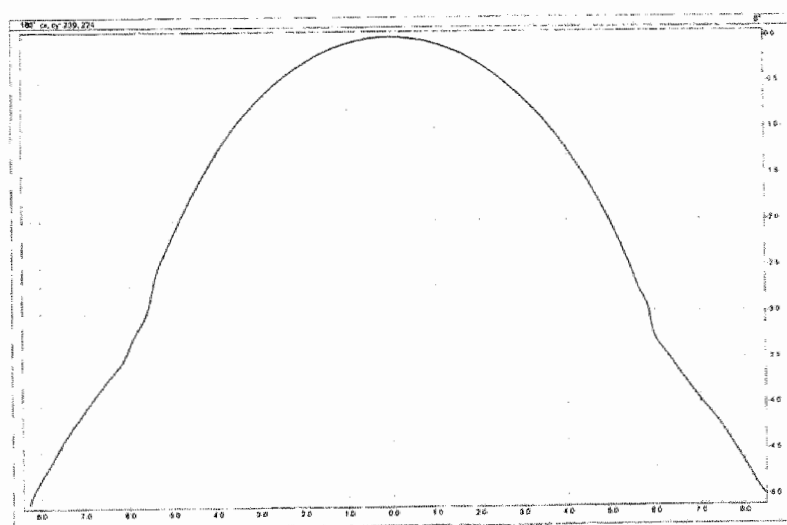


Figure 5.7

Cross section of the surface of a bispherical eye model. Note: x, y, z ratio has been changed for illustrative purpose.

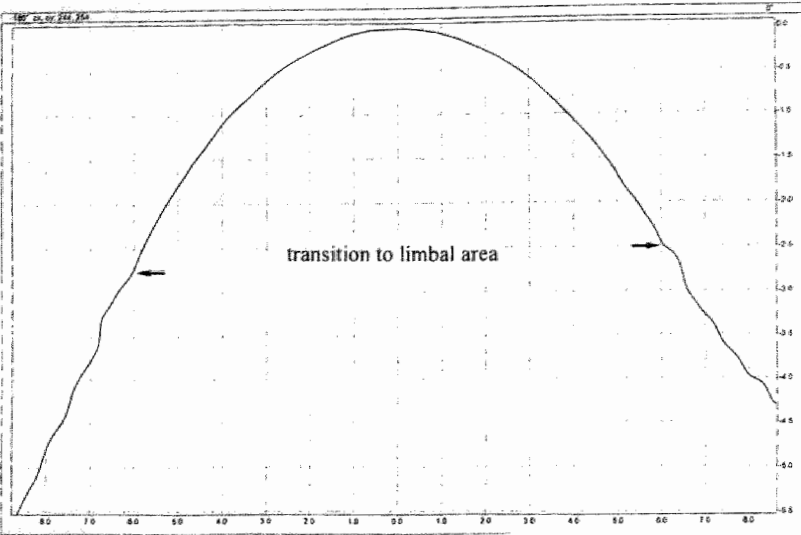


Figure 5.8
Cross section of the anterior surface of the right eye of one of the authors. Note: x, y, z ratio has been changed for illustrative purpose.

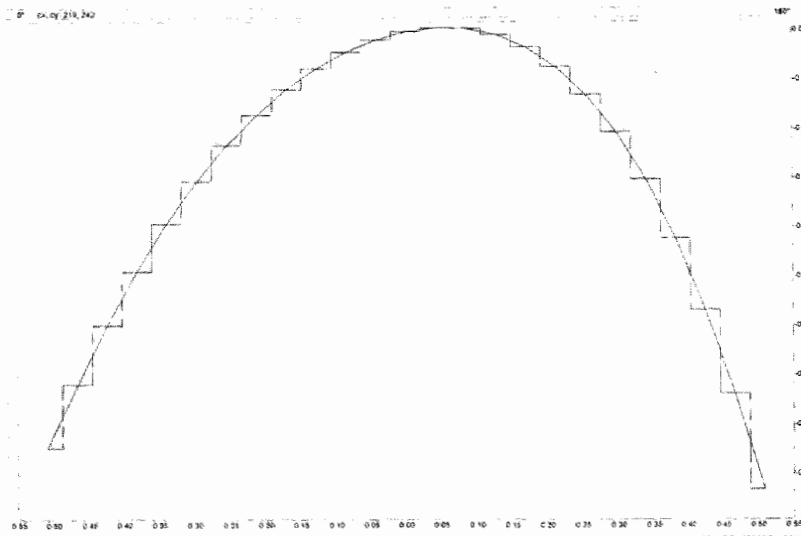


Figure 5.9
Enlargement of a horizontal cross-section of the surface of a living eye. Height values at pixel level are shown for the central part of 1 mm. Note x,y,z ratio has been changed for illustrative purposes.

obtained are non parametric (model free). In the MST the number of measuring points equals the number of pixels of the CCD sensor. A lateral resolution equal to the resolution of the sensor can be obtained. The accuracy and precision of the MST depends on the characteristics of the sensor, the spatial frequency of the gratings, and the calculations to reconstruct the topography. The pixels are correlated using a Fourier transform-based reconstruction algorithm, similar to that of Takeda et al.¹⁵. In this way it is possible to guarantee pixel resolution. This is illustrated in fig. 5.9, showing an enlargement of the central 1-mm area of the 0 to 180° meridian of a living eye. If precision is high throughout the field, the use of subpixel resolution techniques could be of interest to increase local discrimination of shape.

The prototype MST was made of standard components with small diameter polarizers that affected the étendue of the viewing system. In this way some vignetting was introduced that caused poor SNR values for the peripheral measurements (Table 2). To solve this technical problem, custom made polarizers could be used. An other possibility could be the use of a combination of excitation- and barrier filter that have a higher capacity to block the disturbing specular reflection.

Our aim in this study was to validate the MST on the ability to measure height with a large field. For this reason, we restricted measurements to bispherical models representing the entire surface of the eye. On purpose we did not include aspherical and irregular eye models, *in vivo* measurements and inter-observer variability at the present stage. We realize, however, that this should be subject to investigation in further validation and reproducibility testing of the device. This should also include other means of presentation of data like instantaneous radius of curvature, corneal peripheral flattening, astigmatism and irregularity indices.

We have analyzed the data with the standard Student t-test. This follows the method as described by Hanusch et al.¹⁹ From statistical theory, however, it can be argued that the variance at the center and the periphery of the eye models may not follow a normal distribution. An analysis of variance on all data did not show any other conclusions than the Student t-test method. A more sophisticated analysis using the multi variate nature of data according to Viana et al.²⁰ and incorporating more measuring points could possibly resolve this statistical problem. We did not apply this method in the present research because by resolving the technical problem of vignetting as outlined before, the difference in central and peripheral height accuracy would probably be eliminated. Furthermore the prototype of the MST as described in this research has been the basis of a new version under the name "Euclid". In this version technical problems as described here are taken into consideration.

5.6 Summary

With the MST, unambiguous shape measurements of the models representing the anterior eye surface were possible.

The MST has a depth of field of 6 mm, and is able to measure height over the entire 20-mm field. This feature enables the device to measure not only the entire corneal surface but also the limbal and scleral-conjunctiva surface.

This research shows that for the central area of 10 mm the prototype of the MST has sufficient accuracy and precision. For the periphery the device in its present state works satisfactorily in terms of radius but could be further improved on peripheral height accuracy.

Because the MST offers the possibility of extended surface topography measurements over a large field of the anterior eye, its use could be advantageous in cases where shape is of paramount importance, e.g. in (scleral) contact lens fitting and refractive surgery.

Acknowledgement

We thank Dr. D.W. Slaaf of the Departement of Biophysics of the University Maastricht for the hospitality in his Laboratory for Microcirculation enabling us to perform the microscopic measurements. Also we thank Ben Lubberman of Sumipro and George Lo-A-Foe of Euro Precision Technology for their help in fabricating the molds. This study was partly supported by Technisch Ontwikkelings Krediet 91073 from the Ministry of Economic Affairs of the Netherlands.

References

1. Politch J. Optical and long wave holography potential application. *Doc Ophthalmol* 1977;43:165-175.
2. Kasprzak H, Förster WN, von Bally G. Holographic measurement of changes of the central corneal curvature due to intraocular pressure differences. *Opt Eng* 1994;33(1):198-203.
3. Mandell RB. Profile methods of measuring corneal curvature. *J Amer Opt Assoc* 1961;32:627-631.
4. Patent Kera Metrics Inc.
5. Cambier JL, Strods SJ. Method and apparatus for obtaining the topography of an object. Patent PCT/US91/04960, 15 July, 1991.
6. Belin MW. Intraoperative raster photogrammetry, the PAR corneal topography system. *J Cataract Refr Surg Supplement* 1993;19:188-197.
7. Patel S, Murray D, Mc Kenzie A, Shearer DS, Mc Grath BD. Effects of fluorescein on tear film breakup time and on tear thinning time. *Am J Optom Physiol Opt* 1985;62:188-190.
8. Pavlopoulos GP, Horn J, and Feldman ST. The effect of artificial tears on computer-assisted corneal topography in normal eyes and after penetrating keratoplasty. *Am J Ophthalmol* 1995;119:712-722.
9. Lange SR and Thall EH. Method and apparatus for measuring corneal topography, US patent No 4,984,893 Januar 15, 1991.
10. Kawara T. Corneal topography using moiré contour fringes. *Applied Optics* 1979;18:3675-3678.
11. Bell BW and Koliopoulos CL. Moiré topography, sampling theory, and charged-coupled devices. *Optics Letters* 1984;9(5):171-173.
12. Hovanesan JD, Hung YY, and Waidelich W. Moiré contouring of large objects by a scanning technique. *Proc. Laser '77 Optoelectronics*, Munich, Germany, 20-24 June 1977. *Laser* 77,1977:589-597.
13. Jüptner W, Kreis Th, and Kreitlew H. Automatic evaluation of holographic interferograms by reference beam phase shifting. *Proc Soc Photo-Opt Instrum Eng* 1983;398:22-29.
14. Reid GT. Automatic Fringe Pattern Analysis: A Review. *Optics and Lasers in Engineering* 1986;7:37-68.
15. Takeda M, Ina H, and Kobayashi S. Fourier-transform method of fringe-pattern analysis for computer-based topography and interferometry. *J of Opt Soc of Am* 1982;72(1):581-585.
16. Jongsma FHM. System for determining the topography of a curved surface. United States Patent Number 5,406,342, April 11, 1995.
17. Stultiens BATH, Jongsma FHM. Frequency modulation as an alternative for local phase in 3D corneal topography. *Progress in Biomedical Optics Proceedings series, SPIE Proc of Ophthalmic Technologies IV* JM Parel, Q Ren, A Katzir (ed), 22-23 January 1994 Los Angeles, Ca 1994;2126:174-184.
18. Zadnik K, Mutti DO, Bullimore MA. Use of statistics for comparing two measurements methods. *Optom Vis Sci* 1994;71:539-540.
19. Hannush SB, et al. Accuracy and precision of keratometry, photokeratoscopy, and corneal modeling on calibrated steel balls. *Arch Ophthalmol* 1989;1235-1239.
20. Viana MGA, Olkin I, McMahon T.T. Multivariate assessment of computer-analyzed corneal topographers. *J Opt Soc Am* 1993;1826-34.

Chapter 6

Clinical evaluation of the Maastricht shape topographer

6.1 Abstract

To investigate the clinical value of the height measuring Maastricht Shape Topographer (MST) a multicentre clinical evaluation was performed. Compared with a Placido disc-based CAVK, the TMS-1, the MST performed better in height topography of irregular surfaces due to pathology as well as corneal surfaces immediately after refractive surgery. The larger surface area that could be measured with the MST, compared to Placido disc based CAVKs, turned out to be advantageous in morphological measurements of the entire anterior eye.

6.2 Introduction

Three devices were constructed for a multicentre trial. One device was tested in the eye clinic in Maastricht, another in Amsterdam (Academic Medical Centre) and Rotterdam (Eye Hospital Rotterdam), and one was sent to London (St Thomas' Hospital).

The clinical evaluation in London led to a full paper by MC Corbett et al¹. This paper is reproduced and included in this chapter. Some remarks concerning further developments are given.

6.3 Corneal Topography using a New Moiré Image-based System

Melanie C. Corbett, FRCS, David P.S. O'Brart, FRCS, Bertho A.Th. Stultiens, BSc, Frans H.M. Jongsma, John Marshall, PhD

Eur J Implant Ref Surg 1995;7:353-370

Acknowledgements:

Miss Corbett holds The Williams Fellowship for Medical and Scientific Research of The University of London. Mr. O'Brart holds a research fellowship sponsored by The Iris Fund for the Prevention of Blindness.

The authors are grateful to Mr. Malcolm G. Kerr Muir and Mr. Michael G. Falcon for clinical material, Professor F. Hendrikse for his advice, and The Iris Fund for Prevention of Blindness for financial support.

Proprietary Interest:

Frans Jongsma and Bertho Stultiens are the only authors who have a commercial interest in the "Maastricht Shape Topographer", and hold its patent rights.

Running Head:

Corneal topography using a new moiré image-based system.

Abstract

Aim: To describe a new device, the Maastricht Shape Topographer (MST), which uses the principle of moiré interference, to measure corneal shape.

Methods: The Maastricht Shape Topographer (MST) projects two sinewave gratings onto the tearfilm in quick succession, and by local analysis of grating intensity in the image so formed, reconstructs the true corneal shape in terms of height from a reference plane. A total of 262,144 data points are measured in an area $21.5 \times 14.5 \text{ mm}^2$. During a one year period, patients referred for topography had measurements made by the MST and a videokeratoscope. Three cases were selected to demonstrate the advantages of the MST.

Results: Image acquisition by the MST was straightforward, with alignment and focusing being of less importance than in videokeratoscopes. It provided detailed topographic information from the whole corneal area, and from irregular or non-reflective surfaces. The initial reconstruction of the true corneal shape was expressed in terms of height, from which measurements of slope, curvature and power were derived directly.

Conclusions: Height reconstructions made by the MST are particularly useful in certain corneal pathologies and in evaluating the corneal profile after photorefractive keratectomy. Measurement of the ablation surface immediately postoperatively is essential in the study of ablation profiles and postoperative wound healing.

Introduction

Over the last four centuries the development of new techniques for studying corneal topography has been driven by progressive changes in the type of information sought. In the 16th and 17th centuries, scientific curiosity led early investigators to become interested in the cornea and its shape. The first measurements of anterior corneal curvature were made by Scheiner in 1619¹. He held a series of convex mirrors of different curvatures next to the eye until he found one which gave an image of the same size as the image reflected from the cornea.

It became apparent that for good vision, the surface of the cornea should be smooth and regular, and that an image reflected from it should be undistorted. In the 1820's Cuignet developed a keratoscope through which he observed the reflected image of an illuminated target held in front of the patient's cornea. Perhaps the most well-known system that designed by Placido in 1880, which clearly demonstrated the presence or absence of surface irregularities². It consisted of a disc bearing alternating black and white concentric rings; and this pattern still forms the basis of many topography systems today^{3,4}.

Quantification of corneal curvature became possible in 1854 with the development of the keratometer (ophthalmometer) by Helmholtz⁵. His device measured the distance between the images of two pairs of objects (mires) reflected from the corneal surface. This gave the spherocylindrical curvature of the central 3mm of the cornea, in two perpendicular meridians. In order to increase the area of cornea analysed, Javal (1889)

attached a Placido-type disc to his keratometer (keratoscopy), and by photographing the image obtained, Gullstrand (1896) was able to measure the size of the rings⁶. The simple curvature information obtained by such devices was appropriate for contact lens fitting.

With the development of microsurgical techniques for cataract extraction, corneal grafting and incisional refractive surgery, interest turned to the optical power provided by the cornea^{3,4}. Measurements of corneal curvature can be converted to dioptric power using the standard keratometric index^{6,7}. This figure is derived from a number of approximations and extrapolations⁸. It combines the refractive index of the cornea (which is assumed to be uniform throughout its layers⁹), and the negative power of the posterior corneal surface¹⁰.

Recent years have seen the introduction of excimer laser photorefractive keratectomy (PRK), in which a precise depth of tissue is removed from the anterior corneal surface¹¹. For this type of surgery, it is more appropriate that corneal topography should be able to measure the true shape of the cornea, in terms of its height, or elevation¹². Such measures would enable accurate preoperative programming of the depth of tissue to be removed, and assessment of the shape changes caused by wound healing after surgery. From this basic data, corneal slope can be accurately calculated and used to provide corneal curvature or power if required for other applications.

Keratometry, keratoscopy and the techniques derived from them all utilise the principle of reflection¹³, and therefore have a number of inherent limitations. Firstly, they map the corneal surface in terms of slope, and not height. This is because they use the corneal surface as a convex mirror, and view the first Purkinje image. This virtual erect image is formed behind the cornea, in the anterior chamber, almost at the level of the anterior lens capsule. The size of this image is dependent upon the slope of the corneal surface: the steeper the slope, the smaller the radius of curvature, and the smaller the image. In devices using Placido-type discs, the rings follow lines of equal slope. These lines of equal slope will not necessarily follow the same pattern as contours joining points of equal height. For example, in a keratoconic eye with the cone placed inferiorly, a point 1mm above the centre may have the same height (elevation above a reference plane), as a point 3mm below the centre, but the inferior point will have a steeper radius of curvature. Therefore the two points will lie on the same height contour, but not on the same slope contour. This limits the usefulness of conventional reflection-based techniques in PRK and certain corneal pathologies.

The second limitation of techniques relying upon reflection, is that no useful image can be obtained from non-reflective surfaces. This precludes their use in the absence of the epithelium, such as immediately after PRK; and when the epithelium loses its reflectivity, as when oedematous or in band keratopathy and various scarring processes. Thirdly, little quantitative information can be obtained from irregular corneas as it becomes difficult to distinguish the individual rings; for example over ulcers, nebulae, scars and peripheral thinning. The spherical bias inherent in several of algorithms also con-

tributes to errors in the reconstruction of irregular surfaces¹³.

Fourthly, techniques using the principle of reflection cannot make accurate measurements from the whole corneal surface. They fail to take measurements from the very centre of the cornea, which is optically the most important area, and sensitivity is reduced towards the periphery^{14,16}. Neither can information be obtained from the paralimbal cornea, which is the site of a number of surgical incisions, and pathologies such as peripheral corneal thinning and melts.

This paper describes The Maastricht Shape Topographer (MST) which is a new device developed to overcome these limitations in the principals employed by conventional videokeratoscopes. The results of topography performed in specifically selected clinical cases will be shown, to determine whether the instrument can achieve this aim.

Materials & Methods

Optical Principles

The MST used the principle of projection rather than reflection. An image was formed on the surface of the tearfilm in the same way as a slide is projected onto a screen. In contrast to systems using reflection, which measure surface slope, measurements were made in terms of elevation above a mathematical reference plane. The contours therefore followed lines of equal height, rather than lines of equal slope.

Projection techniques have been used in industry for sizing machine parts and depth perception in robotics. Medical applications include measurement of body parts in plastic and reconstructive surgery¹⁷⁻¹⁸. Application of the technique to the cornea was complicated by two factors. Firstly, the cornea is normally transparent and therefore transmits light, resulting in a low signal. Secondly, light is reflected by the surface of the tearfilm, resulting in high noise. For the projected image to be visible, it had to be intensified by improving its signal-to-noise ratio. In the early days of corneal topography, the noise was reduced by applying talcum powder to convert the reflecting tear fluid to an opaque surface. Obviously the application of talcum powder was unacceptable in clinical practice, so attention was turned to increasing the signal. This was achieved by adding fluorescein to the tearfilm to provide image enhancement^{12,18,19}.

There are two methods currently available for analysing a projected image to provide topographic information. The first is rasterstereography or rasterphotogrammetry in which a grid projected onto the tearfilm surface is imaged from a known angle^{17,18,20,21}. The topographic elevation is calculated from the displacement of components within the grid image when projected onto the corneal surface, compared to their known position when projected onto a flat surface. The rasterstereography systems currently available use a square-wave grid, so the number of data points provided by this method is limited by the number of lines.

The second technique involves the analysis of moiré interference patterns^{18,19} (Fig. 1). Moiré interference occurs when two sets of parallel lines are superimposed at different orientations, as seen, for example, when two net curtains overlap. When parallel gratings (Fig. 1A) are projected obliquely onto a cornea, the image on the corneal surface is a series of parallel lines, curved in a similar manner to that seen when using a slit lamp beam (Fig. 1B). Gratings projected from the nasal and temporal sides produce images curved in opposite directions. Addition of these two images results in moiré interference which generates ring-shaped interference fringes visible on the corneal surface (Fig. 1C & 2). These fringes follow contour lines representing points of equal height (Fig. 1D), and can be viewed directly without recourse to mathematical assumptions or computations^{12,19}. The width of the moiré fringes is partially determined by the spatial frequency of the gratings. Their orientation is dependent upon the relative orientations of the two grating images, and therefore the shape of the surface on which they are formed.

The MST optimised topographic analysis by combining elements from both raster-stereography and moiré interference. The number of data points was further increased by the use of sine-wave gratings rather than square-wave gratings. In a sine-wave grating, the intensity varies across each line with a known distribution, whereas in a square wave grating, only the borders of each line can be located. Fourier analysis of a sine-wave grating enabled all the points of the image to contribute to the reconstruction^{22,23}.

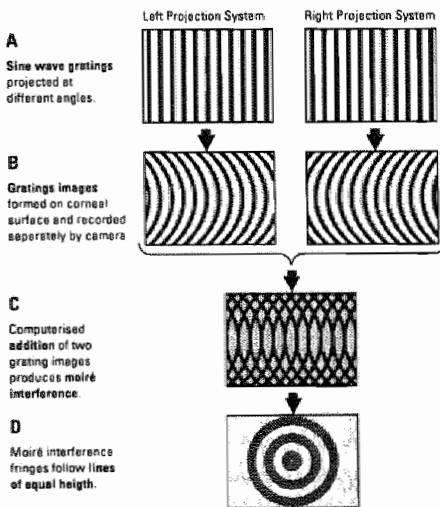


Figure 1.

Diagrammatic representation of the generation of moiré interference fringes. The Maastricht Topographer projected parallel sinewave gratings (A) down its right and left lateral arms. The light approached the cornea obliquely, and therefore the lines of the grating images formed on the corneal surface appeared curved (B). Addition of the two images resulted in moiré interference (C), in which the ring-shaped interference fringes followed contour lines representing points of equal height (D).

The Device

The MST device consisted of (Fig. 3):

1. Customised hardware composed of:
 - a) Two lateral arms along which light is projected on to the cornea;
 - b) Central body housing a CCD camera for recording the corneal image;
2. Slitlamp table on which the above component can be manoeuvred by means of a joystick;
3. Television monitor displaying video images of the cornea;
4. Frame grabber to capture single images;
5. Computer (486 DX personal computer) on which images are stored and analysed.

The two lateral arms of the MST had an angular separation in the horizontal plane of 36° (Figure 4). Each contained a sinewave grating of 2.5 line-pairs/mm which was projected onto the tearfilm by a flash of light generated by a xenon flash tube. Between the flash tube and the grating a filter was inserted to limit the spectral emission to between 380 to 400nm. The illumination sources each emitted a single pulse of 100 μ sec duration, with a delay of 8msec between that from the right and the left arms. It was essential to be able to capture independent images for subsequent analysis, but the time between pulses was minimised to reduce the likelihood of misalignment of the two images due to intervening eye movement. Independent images were required so that the grating pattern of each could be analysed separately using Fourier techniques^{21,23}, before being combined in a later stage of the reconstruction process.

As previously stated, in order to enhance the signal-to-noise ratio, sodium-fluorescein was applied to the tear film. In a similar manner to cameras employed in fluorescein

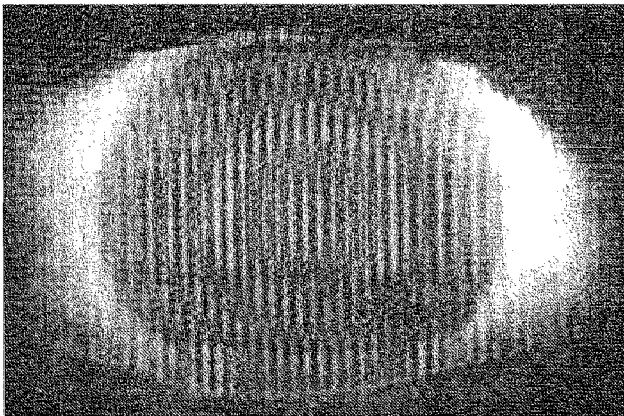


Figure 2.

Circular moiré interference patterns on the corneal surface formed by the computerised addition of two sinewave grating images. The fringes follow lines of equal height, but as there are so few, detailed shape information is provided by computer analysis of the two individual images.

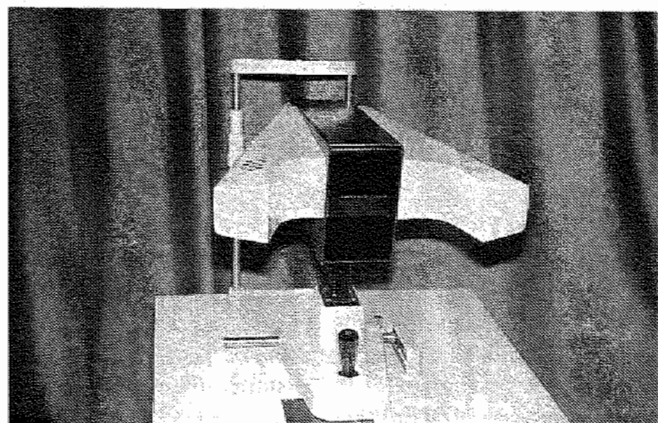


Figure 3.

The Maastricht Shape Topographer (MST) consisted of two lateral arms (white) and a central body (blue) mounted on a slitlamp table. The patients sat at the far side with their head positioned against the strap and chin rest. The MST was connected to a video monitor, frame-grabber and computer.

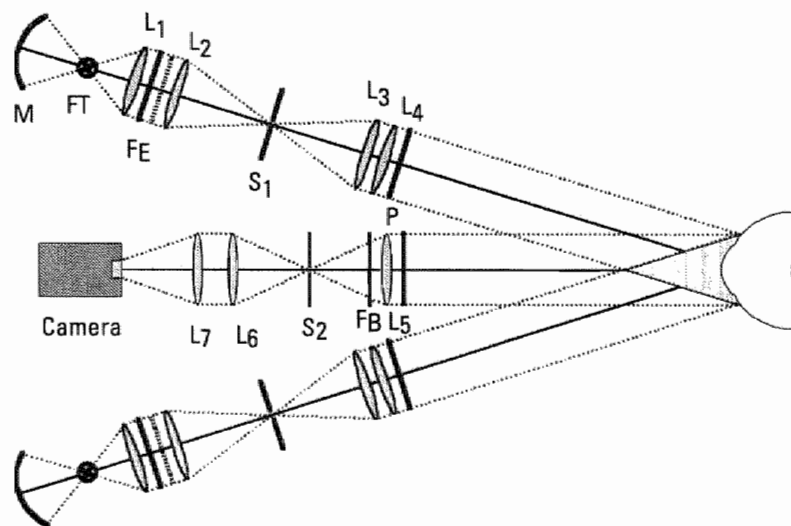


Figure 4.

Optical schematic of the Maastricht Shape Topographer (MST). The two lateral arms projected sinewave gratings on to the corneal surface; the images of which were recorded by a camera in the central body. The two arms have an angular separation of 36° in the horizontal plane. Light from a xenon flash tube (FT) was reflected by a concave mirror (M) and passed through a collimating lens (L1), excitation filter (FE) and sine wave grating (G). A convex lens (L2) projected the light through a slit (S1) which selected zero and first order. Two further lenses (L3 and L4) projected the grating orthoscopically through a polarising filter (P) onto the surface of the eye (E). Light emitted from the fluorescein in the tearfilm passed through polarising (P) and barrier filters (FB). A lens (L5) projected the light onto a slit to improve the depth of focus, and two further lenses (L6 and L7) formed the objective for the CCD camera (C).

angiography, the MST incorporated excitation (380-480nm) and barrier ($> 480\text{nm}$) filters to optimise observation of the image. The final image was further enhanced by the use of polarising filters to reduce degradation due to reflections.

The CCD camera was housed in the central body of the MST. Its axis bisected the angle between the two lateral arms. It recorded separately the image of each of the two gratings. The temporal separation of the flashes was timed in such a way that the frame grabber recorded the images on the first and second halves of a TV frame. This can be visualised as being recorded on the odd and even scan lines. Each pixel represented a point on the cornea. There were 512×512 data points (total of 262,144, each with 256 grey levels) in an imaged area $21.5 \times 14.5\text{mm}^2$ when the cornea was in focus, giving a lateral resolution of $42 \times 29\mu\text{m}^2$. This was independent of the distance from the cornea, because firstly, the imaging system received parallel light²² and secondly, the cornea was focussed at a fixed distance from the camera. The precision of the height measurement at any individual pixel was $5\mu\text{m}$, but when the height of each point is analysed with respect to the overall corneal shape, the precision can be improved to better than $1\mu\text{m}$. The depth of focus of the total imaged area is greater than 6mm. This enables the whole cornea to be imaged, from apex to limbus.

Disturbances occasionally occurred within the image due to the reflection of light from the cornea or iris. These were minimised by using digital filters and redundancy techniques. Such techniques also allowed enhancement of images where part of one of the pair is poor²².

The corneal shape determined the spacing, orientation and position of the grating lines imaged on its surface, and therefore the measured image was a modulated function of the projected grating. Addition of the two grating-images produced moiré interference patterns (Fig. 1 & 2) in which the zero-crossings corresponded to corneal points of equal height. However, the rings of the moiré interference pattern were considerably wider apart than were the lines of the gratings from which they arose, and therefore they alone cannot be used to make a detailed reconstruction. Since the recorded images were a special case of phase-modulated gratings, an alternative means of reconstructing the corneal surface was possible. The corneal height modulated the phase and frequency of the grating, and therefore a modified phase demodulation algorithm using fourier techniques could reconstruct the corneal surface in detail^{22,24}.

The surface shape could be displayed with current software in three different forms, typical examples of which (to be described later) are illustrated:

1. two-dimensional contour map (Figure 5c),
2. three-dimensional wire net (Figure 5d),
3. cross-sections obtained from any part of the image at any axis (Fig. 7d).

These representations required less experience for their interpretation than did the maps of videokeratoscopes, because the contour lines were the same as those on a geographical map.

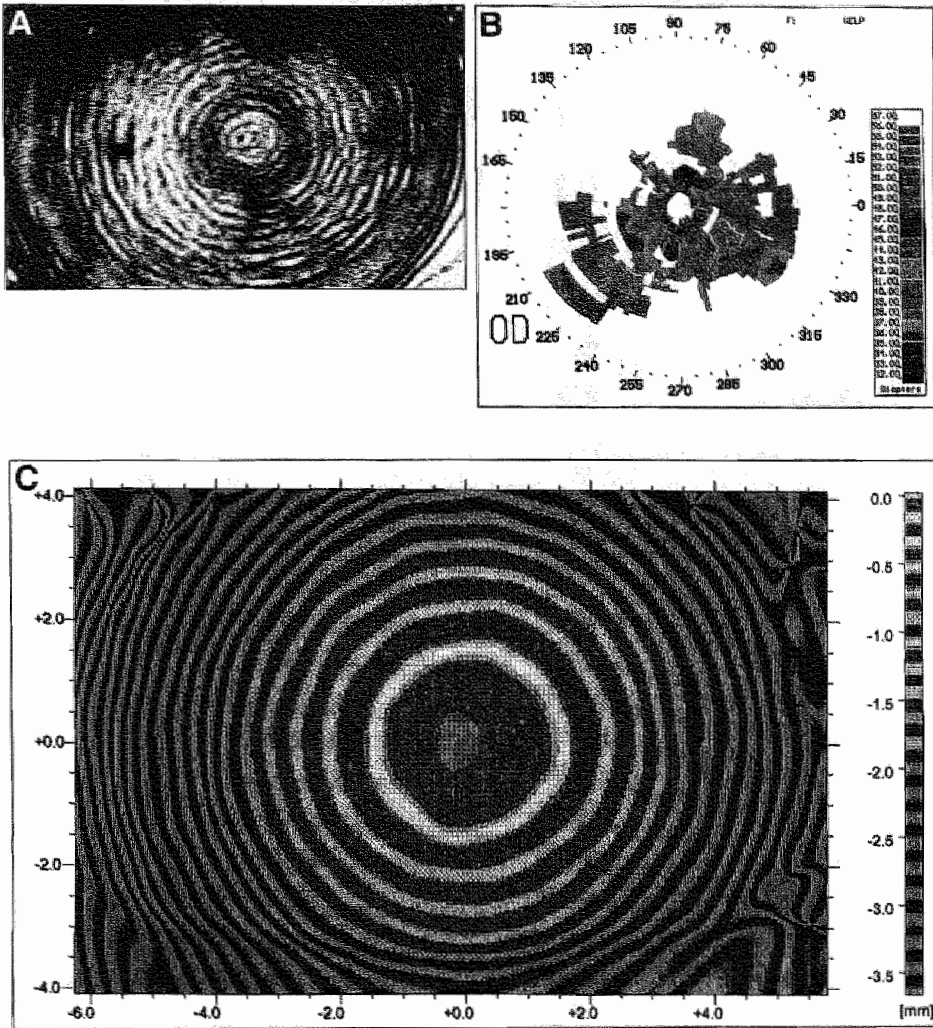
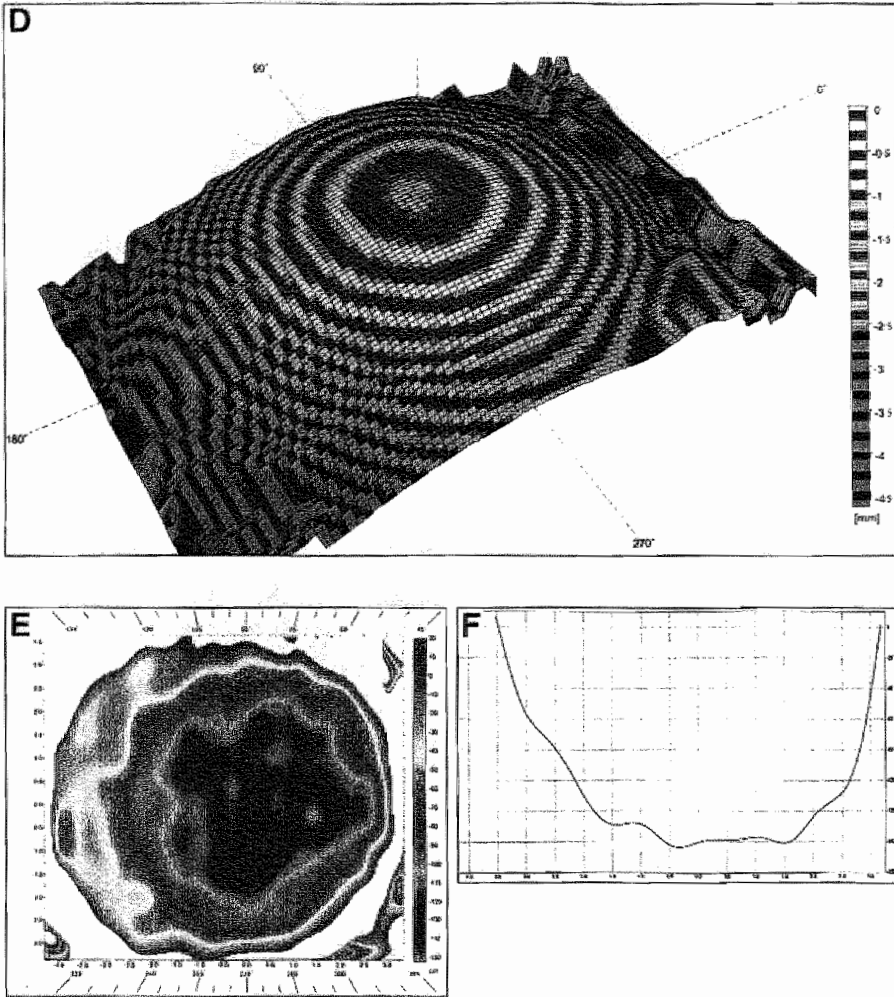


Figure 5.

Corneal topography taken by the TMS-1 videokeratoscope (a,b) and Maastricht Topographer (c-f) immediately after -6.00D 6mm excimer laser photorefractive keratectomy. In the absence of a reflective corneal surface, the quality of the mires on the videokeratograph (a) was too poor for any meaningful topographic information to be obtained from the colour-coded map (b). In contrast, the Maastricht Topographer was able to accurately measure the true corneal shape in terms of height (mm) above a reference plane, as shown by the two-dimensional (c) and three-dimensional (d) reconstructions. On the two dimensional map, the x and y axes give the coordinates of the positions of the corneal points, in mm relative to the centre. The position of the centre may be relocated manually. On the three-dimensional map, the axes are marked. On both maps the scale gives the corneal height (z-axis) in mm. Subtraction of the postoperative from the preoperative corneal height generated difference maps (e,f). The two-dimensional difference map (e) shows the change in corneal height, and is plotted using a colour-scheme similar to that of the TMS-1. The cross-section (f) showed the ablation profile. Removal of the epithelium (about $60\mu\text{m}$) and ablation of the underlying stroma ($78\mu\text{m}$) gave a maximum change in height of $140\mu\text{m}$. The irregularity of the surface was caused by mucus and epithelial debris in the tearfilm.



The display could be manipulated to enhance particular features. Reconstructions could be subtracted from a sphere to accentuate surface asphericity. Alternatively, one reconstruction could be subtracted from another to show change in shape of a single cornea over time, for example, as a result of surgery (Fig. 5e & f). The centre of the reconstruction could be reset to relocate the corneal apex.

Having obtained the definitive shape of the cornea, maps of the surface slope (Fig. 6c) and radius of curvature (Fig. 7c) were directly calculated. These accentuated the appearance of local irregularities of the corneal surface. As in keratometry and keratoscopy, radius of curvature could be converted to dioptric power using the Standard Keratometric Index^{6,7}, but as in other devices, this included estimates of the corneal

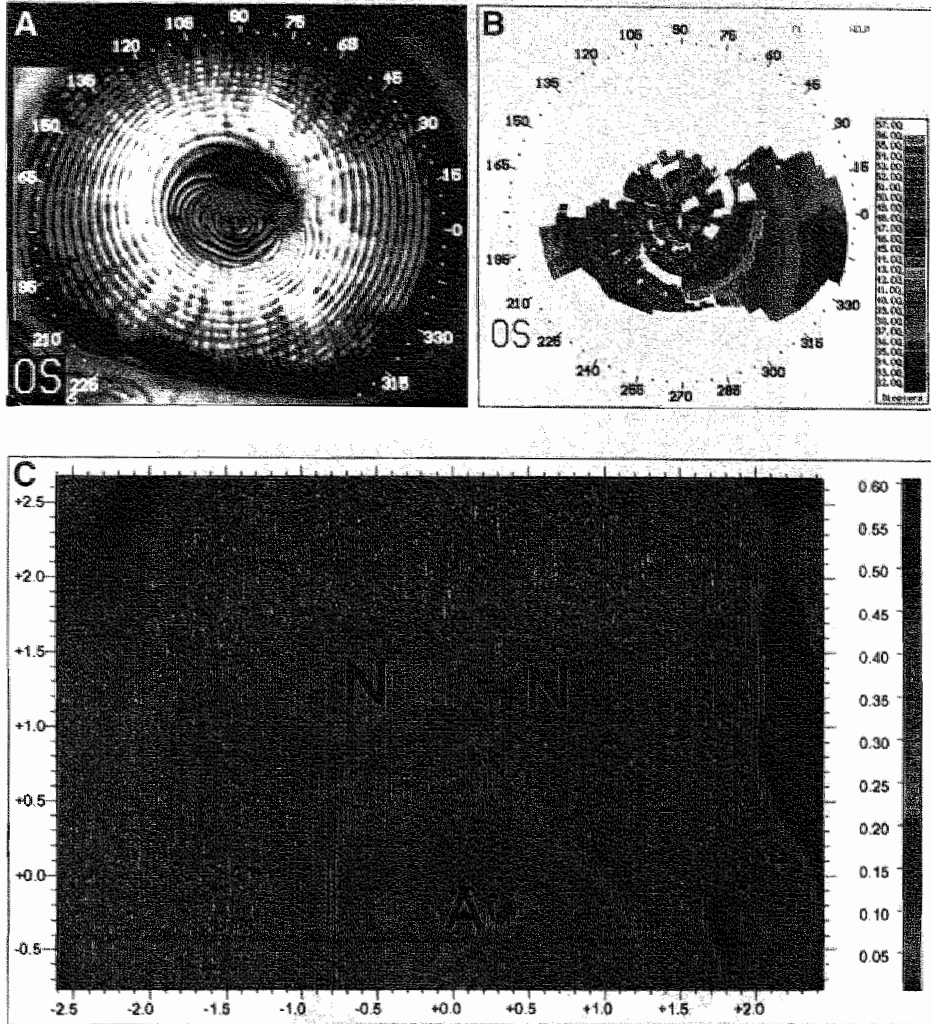


Figure 6.

Topography of a cornea with keratoconus measured by the TMS-1 videokeratoscope (a,b) and Maastricht Topographer (c). The videokeratography mires (A) were narrowed inferiorly in association with the apex of the cone, and were highly distorted just superior to the centre of the cornea due to the presence of two proud nebulae. The colour-coded contour map (b) correspondingly showed inferior steepening, but no information could be obtained from the areas where the mires were too distorted. In contrast, the Maastricht Topographer (MT) was able to reconstruct the irregular surface in detail (c). In order to highlight the irregularities, the topography was plotted in terms of surface slope, and a high-powered view concentrated on the central cornea. The x and y axes give the coordinates of the positions of the corneal points, in mm relative to the centre. The scale gives the corneal slope (0 = horizontal, 1 = vertical). The slope of the cornea was almost horizontal over the apex (A) of the cone. It then became increasingly vertical more peripherally, although it remained relatively horizontal over the two nebulae (N).

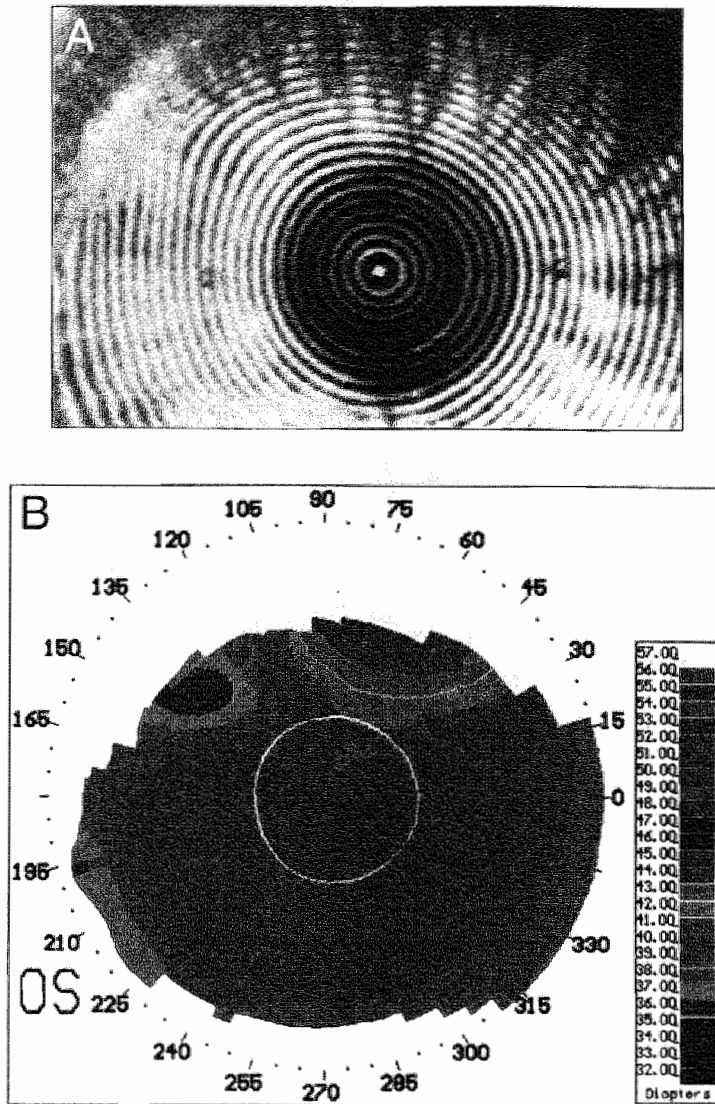
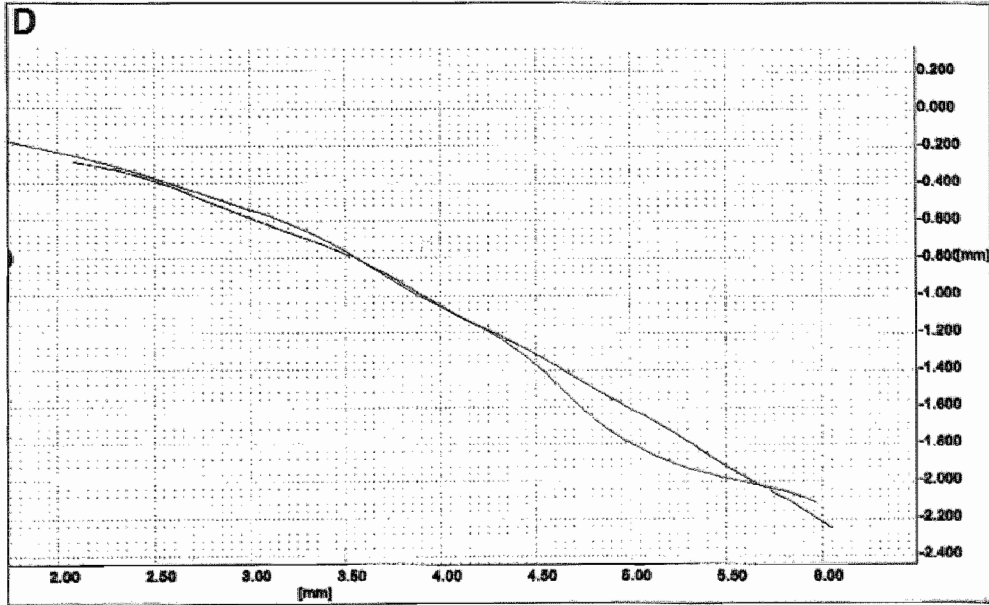
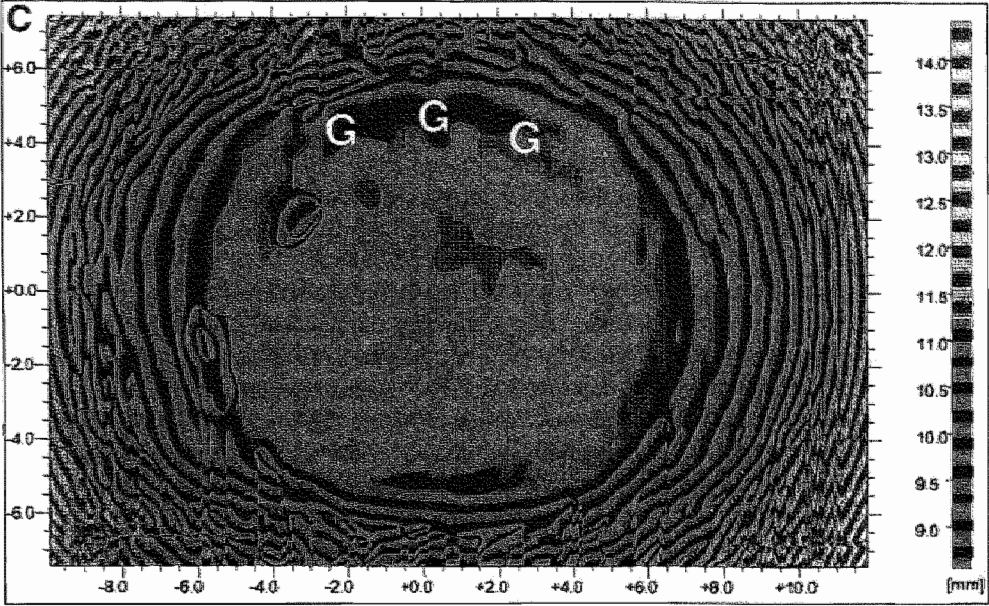


Figure 7.

Topography of a cornea with Terrien's marginal degeneration measured by the TMS-1 videokeratoscope (a,b) and Maastricht Topographer (c,d). Peripheral corneal thinning caused a gutter which was most marked between 60° and 135° on the superior cornea about 1mm from the limbus. On the videokeratograph (a) the left hand end of the gutter could be seen as an area in which the mires became fused and indistinct. The colour coded map (b) provided accurate information about the optical effect of the peripheral changes on the central cornea, but provided no data about the topography at the site of the pathology in the paralimbal area. In contrast, the Maastricht Topographer obtained data from an area 21.5 x 14.5 mm. The radius of curvature map (c) accurately located the position of the gutter (G). A cross-section (d) of the corneal shape (height, mm) through the affected area (90°, red) compared to one through an unaffected area (0°, black) showed that the gutter was 1.5mm wide and 175µm deep.



refractive index and the posterior corneal curvature, and assumed that the cornea is spherical.

Image Acquisition

One drop of Fluorescein 1% was routinely applied to the tear film immediately prior to image acquisition. The patient then fixated the blue target light in the body of the machine, and in so doing, aligned their visual axis with the videocamera.

Focusing was achieved by the operator superimposing the images of two helium-neon aiming beams on the limbus. This was performed as a two-stage procedure. Initially rough focusing was obtained by directly viewing the images of the lasers on the tearfilm. The operator then turned to the television and approximately centred the cornea on the screen. Fine focusing was then performed whilst viewing the television screen, by means of the joystick. To avoid distortion and degradation of the diagnostic image, the beams of the focusing lasers were automatically occluded during capture of the video images.

In an early prototype of the MST, visible radiation was used to illuminate the eye during focusing and alignment. In individuals with lightly-pigmented irides, reflection and back-scattering of light from the iris surface produced distortion of the grating image. In order to avoid pupillary constriction and minimise the effect of iris pigmentation, the use of infrared radiation was introduced with a videocamera sensitive in this spectral domain.

Clinical Cases

During a one year period, patients referred for topography from the corneal, refractive and general clinics had measurements made with both the MST and the TMS-1 videokeratoscope (Computed Anatomy). Three cases have been selected to demonstrate the performance of the MST in situations where the information provided by a conventional videokeratoscope was inadequate:

1. Immediately after PRK.
2. Keratoconus with two proud nebulae;
3. Terrien's marginal degeneration²⁵;

Results

Image Acquisition and Analysis

The acquisition of images was straightforward and usually took less than one minute. Focusing and centration was much less critical for the MST than for videokeratoscopes. In some patients with lightly pigmented irides, accurate information could only be obtained over the pupillary area. In the few of those with naturally small pupils, it was sometimes necessary to resort to mydriatic agents to enable the paralimbal cornea to be reconstructed.

One disadvantage of the current system was the inadequacy of the computer, which required about three minutes to reconstruct the topography, then took a further minute to make the slope and curvature calculations.

Clinical Cases

The following three cases highlighted specific advantages of the MST.

Case 1 (Fig. 5)

Immediately following PRK, the exposed stroma with limited fluid coverage constituted a poorly reflecting surface. As a result, no useful information was obtained using the TMS-1 videokeratoscope, but image acquisition by the MST was facilitated. The MST reconstructed the elevation of the cornea from a reference plane, in millimetres, and represented it by two and three dimensional maps. Subtraction of the postoperative topography from the preoperative data showed the depth and profile of the tissue removed by the excimer laser. Subtraction of the immediate postoperative topography from subsequent images was used to quantify the wound healing response⁴³.

Case 2 (Fig. 6)

In the patient with keratoconus, the apex of the cone was inferiorly, and just above it, were two proud nebulae. In this area, the TMS-1 videokeratoscope could not distinguish the individual rings of the mires, so the reconstruction was missing or inaccurate. In contrast, the MST could reconstruct the irregularities in detail, to show the position of the apex of the cone, and the presence of the two nebulae. The appearance was accentuated in two ways. Firstly, the topography was represented in terms of corneal slope, which is the first derivative of corneal height. Secondly, the zoom function was used to provide a high-powered view of the area of interest.

Case 3 (Fig. 7)

In the patient with Terrien's marginal degeneration, peripheral corneal thinning had caused a gutter about 1mm from the limbus, which was most marked between 60° and 135° on the superior cornea. The TMS-1 videokeratoscope accurately determined the optical effect of the peripheral pathology on the central cornea, but could not obtain topographic data from sufficiently far peripherally to reconstruct the gutter. The MST made measurements from an area 21.5 x 14.5 mm², which includes the optical axis and the limbus; and the accuracy of the reconstruction was approximately uniform across this whole area. Therefore the full extent of the peripheral gutter was mapped, and its effect on the central cornea also demonstrated. Cross-sections of the corneal height in the affected and unaffected meridians showed the exact location and profile of the gutter. In the vertical meridian, the gutter affected an annulus 4.25mm to 5.75 mm from the centre of the cornea. It was 1.5mm wide, and 175µm deep. Serial measurements accurately monitored the course of the condition.

Discussion

Although videokeratoscopy is becoming a widely available technique for measuring corneal topography, it is perhaps timely to reevaluate what is required from topography systems, and the ability of current systems to fulfil these needs. Systems vary in the features which they incorporate, but their value should be assessed in terms of the benefits that they confer in the clinical and research settings.

The shape of the corneal surface can be described in a number of ways, some of which result directly from measurements of the corneal surface, and others of which can be calculated from these values²⁶. The two direct measurements in common clinical use are the surface height (measured by the MST, and rasterstereography, holography and interferometry techniques) and the surface slope (used by videokeratoscopes to measure radius of curvature)¹⁸. Slope (and therefore radius of curvature) can be calculated from height measurements, but the reverse is not true. This is because slope is the first derivative of height, but direct measurements of slope do not contain information about the position of the measured slope in the z-axis. Once measurements have been made by either of these methods, mathematical computation can be used to express the results in terms of corneal power, curve-fitting equations, wave front analysis, surface irregularity, surface asymmetry, etc. The limitation of using these derivatives is that they make a number of approximations and assumptions which reduce the accuracy with which they represent the original data^{8,27}.

To date, corneal topography has been largely used in patients undergoing surgery involving the cornea. Applications include preoperative screening and planning of surgery, and postoperatively, the routine management of patients and the diagnosis of problems. It has been claimed by some to be of limited value, and by others to be a necessity²⁸. Corneal topography certainly provides more information about the corneal surface compared to the traditional techniques of refraction, pinhole and hard contact lens acuities, keratometry, Placido disc examination and photokeratoscopy³. However, it is important to consider for each application, how much information is required, how the measurements should be made, and in what form the results are best presented.

Height versus Curvature Measurements

First we will consider whether radius of curvature as provided by videokeratoscopes is sufficient, or whether measurement of corneal height is necessary, in a number of different clinical situations. The aim of preoperative screening is to detect irregular astigmatism, subclinical keratoconus and contact lens warpage in an eye that appears normal when examined by traditional methods^{29,30}. These conditions can be adequately detected by measurements of corneal curvature; and although this requires the analysis of more than the four points provided by keratometry, considerably fewer points are probably required than provided by videokeratoscopes. In contrast, the planning of surgery requires detailed reconstruction of the cornea³¹. The mapping of astigmatism, for example prior to astigmatic keratotomy or cataract extraction, can again be performed by measurement of radius of curvature. However, the corneal height is more

important in irregular corneas when knowledge of the true corneal shape is required. Examples include: phototherapeutic keratectomy (PTK) when a precise height of tissue needs to be ablated to make the corneal surface smooth; the fitting of therapeutic contact lenses when the posterior lens surface has to encompass all protuberances on the anterior corneal surface; and perhaps in the grafting of asymmetric corneas, such as in keratoconus.

Postoperatively, the routine management of patients, such as suture adjustment, requires only location of the astigmatism³², which can be performed with sufficient accuracy using measurements of radius of curvature. The diagnosis of postoperative problems can also frequently be made using radius of curvature, for example a decentred optical zone following photorefractive keratectomy³³⁻³⁵, or a multifocal cornea following radial keratotomy (RK)^{3,36}. However, quantification of these abnormalities, such as the extent of the decentration or irregularities of wound healing after PRK, are more accurately performed using a height-based system.

Measurement of corneal height is of considerably more value than radius of curvature in a number of research fields. The surface of the normal cornea is known to be very complex³⁷, but measurements of corneal height will map its true shape and its normal variations. It will also help in the understanding of the correlation between corneal topography and visual function^{36,38}. Knowledge of the true corneal shape is important when developing or modifying surgical procedures, such as epikeratophakia³⁹, relaxing incisions⁴⁰ or wound construction in cataract surgery⁴¹⁻⁴³.

One field in which it is essential to measure corneal height, is photorefractive keratectomy. The refractive outcome of this procedure is highly dependent upon the precise depth of tissue removed by the ablation process, and the amount of newly-synthesised tissue laid down on this surface during wound healing⁴¹. Corneal height measured immediately postoperatively provides information about the spatial uniformity of the excimer laser beam, and the profile of the ablation. Subtraction of the immediate postoperative topography from subsequent maps quantifies new tissue production at intervals during the healing process⁴⁴. Measures such as these are important in characterising the wound healing response, and objectively comparing the results of different ablation profiles or postoperative drug treatments.

Now that it is possible to measure the true corneal shape in terms of height, the applications of the excimer laser could be extended to include the treatment of irregular astigmatism. The corneal shape map could be used to lathe an individualised erodible mask whose shape is complementary to that of the cornea. As the mask is ablated, more corneal tissue is removed from the high areas than the lower areas, thereby creating a more spherical or normally-shaped surface. This technique would be particularly useful in the retreatment of decentred ablation zones, and conditions such as keratoconus. However, such cases require symmetry in the wound healing processes if these shape changes are to be maintained.

At the present time, the use of topography in contact lens fitting and corneal pathology is of secondary importance to its role in corneal surgery. In the case of contact lens fitting, this is probably because keratometry provides an adequate measure of corneal curvature in the majority of cases. However, in complex cases with irregular corneas (for example the case of keratoconus with two nebulae described earlier), more detailed information may be required, and this includes a knowledge of the true corneal shape measured in terms of height.

Topography may be seldom used in cases of corneal pathology because the information about radius of curvature currently provided is of little use in patient management. In irregular corneas such as these, height information is more useful, as demonstrated by the case of the peripheral corneal thinning. Monitoring of a condition over time (for example the size or depth of a gutter or ulcer) can guide management decisions, although in many cases, the clinical signs will still be of major importance.

Measurements of Irregular & Non-reflective Surfaces

A second reason for the limited application of videokeratoscopy to corneal pathology is that the technique can not obtain useful information from irregular or non-reflective surfaces. A projection-based system such as the MST is therefore required to determine the true morphology of a number of corneal pathologies, and may give us some insight into their nature and progression.

One important benefit arising from the ability of MST to make measurements from non-reflective surfaces, is the information obtained about the corneal surface immediately after photorefractive keratectomy. This is necessary in any topographic investigation of ablation profiles or postoperative wound healing. It could potentially also provide a means of measuring the shape of the corneal surface during the ablation procedure itself and during other surgical procedures⁴⁵⁻⁴⁶. This may be useful in the tailoring of treatments to individual patients.

Number and Position of Data Points

Although the accuracy of a system depends to some extent on the number of data points⁴⁷, this must be balanced by the time taken for analysis, and the cost of the equipment⁴⁸. Any system should therefore aim to use as few data points as is clinically necessary. However, as demonstrated during the development of visual field technology⁴⁸, the appropriate number of data points and their optimum position is not always easy to determine⁴⁹. The central cornea is obviously the area with most influence on visual function; but the peripheral cornea is a common site for surgical incisions and corneal pathology.

No measurements are made from the very centre of the cornea by either keratometry or videokeratoscopy⁴⁵. These techniques may therefore fail to detect the presence of small surface irregularities which could have a dramatic impact on vision. Neither can they be used in the detailed study of the optical zones induced by refractive surgery. In contrast, the MST can easily image this visually-important area by projecting a grating onto its surface.

Keratometry uses four points on an annulus about 3mm in diameter, to measure the corneal curvature in two perpendicular meridians. This information is frequently sufficient for contact lens fitting⁷, and in straight forward cases, is used to calculate the power of intraocular lenses⁵⁰.

Most videokeratoscopes have 15-38 rings, whose image positions are analysed along 256-360 meridia, giving a total of 6,000 to 11,000 data points within an area 11mm in diameter³. Preoperative screening^{29,30} and the routine postoperative management of corneal sutures⁵¹ probably require simpler equipment with fewer data points covering the same area; whereas for planning the site of incisional surgery, the detail provided is appropriate. The MST uses 262,144 data points, from which very detailed reconstructions can be made, but more work needs to be performed to determine which points can be disregarded if less detail is required.

As surgical technology improves and there is greater interest in the technique, as well as the site of wound construction, it is becoming increasingly important to be able to study the shape of the corneal periphery. For example, there is still much debate concerning how radial keratotomy wounds exert their effects⁵², and the mechanics of the increasingly large variety of incisions used in cataract surgery⁴¹⁻⁴³. These applications of corneal topography require that, firstly, measurements are made from the peripheral cornea, and secondly, that the reconstructions made from those measurements are sufficiently accurate.

Videokeratoscopes measure the power of spherical test objects with an accuracy of 0.25D within an area equivalent to the central 70% of the corneal surface; but their accuracy falls off peripherally¹⁵. When measuring radially aspheric surfaces, which are more representative of the normal cornea³⁷, accuracy declines very fast in the periphery, dropping to below 3D outside a 4mm radius¹⁴. This occurs as a result of the spherical bias in the assumptions used when calculating the tangential (global) radius of curvature³⁷⁻⁵³. The peripheral accuracy of videokeratoscopy may be improved by the development of new algorithms⁵³⁻⁵⁴, shape fitting (for example, subtracting the corneal shape from a sphere)²⁴, calculating the instantaneous (local) radius of curvature¹⁴, or by matching mathematical equations to the corneal shape. The MST has two advantages over videokeratoscopes in this respect. Firstly it images an area 21.5 x 14.5 mm², and therefore makes measurements from the entire corneal surface, including the limbus. Secondly the accuracy of the reconstruction is approximately uniform across this whole area, thereby providing a detailed map of the shape of the corneal periphery as well as the centre. The accuracy and reproducibility of the MST is at least comparable to that of videokeratoscopes⁵⁵. However, for the former test objects need to be mat, but for the later they are reflective. Therefore direct comparison is not possible with the same test specimen.

Accuracy of the Reconstruction

When any measuring equipment is under development, there is a tendency to strive to maximise accuracy, on the assumption that higher accuracy will provide better results. Precise measurements are frequently needed in research laboratories, but not neces-

sarily in the clinical setting, where the accuracy required of a machine is dependent upon its applications. The majority of clinical topography is currently performed for pre-operative screening, the planning of incisional surgery, routine postoperative followup and the diagnosis of complications. In most cases, the level of accuracy provided by modern videokeratoscopes appears to be sufficient.

However, the accuracy of the reconstruction will be reduced in the presence of small errors in the focusing or alignment of the videokeratoscope relative to the eyes⁶. Although correct positioning in most models is aided by the superimposition of laser spots or cross-hairs, or by use of an autofocus facility, inaccuracies still occur. These arise because videokeratoscopes make a number of assumptions concerning the position and orientation of the cornea. They assume that the visual axis is centred on the machine axis; the centres of curvature for all reflecting points are on the optical axis¹⁴; and that the apex of the cornea is the correct distance from the film plane (ie: focused). No correction is made for the altered position of the corneal apex after refractive surgery⁵⁷. Corneal position orientation and focusing is less important in the MST as the sine-wave gratings are projected using parallel light, and the surface is reconstructed from the position of the points relative to each other and the mathematical reference plane, rather than at an absolute position in space. Therefore the MST is potentially less prone to operator error.

One clinical area in which highly accurate measurements are likely to become essential is excimer laser surgery. The use of corneal topography as a template for treatment requires an accuracy much greater than has previously been necessary for diagnostic roles. The excimer laser removes $0.25\mu\text{m}$ tissue per pulse, so perhaps this is the order of magnitude required.

As topography systems become more accurate, it has to be considered how the tearfluid influences measurements. Techniques dependent upon either reflection or projection methods image the air-tearfluid interface rather than the surface of the corneal epithelium. They rely upon the assumption that the tearfluid is a thin layer of uniform thickness covering the entire surface from which measurements are made. Early measurements estimated a tearfilm thickness of about $7\mu\text{m}$ ⁸, which would have negligible effect on the corneal curvature or power²⁶, and is well below the sensitivity of currently-available videokeratoscopes which have an precision of 0.25D in the central region. However, more recent studies have found the tearfilm to be thicker, with some reports claiming $40\mu\text{m}$ ⁵⁹; and its uniformity is unknown. Therefore the tearfilm could potentially affect topography, particularly as measurement techniques become more sensitive. This degree of sensitivity is now achievable, as demonstrated by the MST, which has an axial resolution of at least $5\mu\text{m}$, and can reconstruct the inferior tear meniscus. The viscosity of the tearfluid may serve to integrate out microundulations in the corneal surface by being thicker over depressions, and thinner over protuberances. However, this is unlikely to be of clinical importance, as it is the air tear-fluid interface which is the major refractive surface of the eye.

Disadvantages of the MST

One of the disadvantages of the MST is that it requires the instillation of fluorescein, and it is not known whether this exerts an effect on the tearfilm thickness and distribution. Fluorescein is currently necessary to provide image enhancement and improve the signal-to-noise ratio. In about 5% of patients it is also necessary to instil mydriatics to reduce signal to noise problems caused by scatter from lightly pigmented irides. Both of these problems could be overcome by the use of optical radiation of wavelengths with low penetrance in the superficial layers of the cornea. For example the use of a brief sub-damage threshold pulse of low intensity ultraviolet radiation at 193nm would provide a good image on the surface, with little or no scatter because of its high absorption. However, it would be difficult to process such an image because videocameras have relatively low sensitivity in this spectral domain. Further, cataractogenic wavelengths and irradiance thresholds would need to be avoided. Similarly, radiation in the infrared could be employed, but again imaging would be difficult and equipment costly.

In order for any device to be of value in the busy clinical setting, it is essential that the information provided can be obtained quickly and easily, and presented in a simple form which is easy to apply clinically. Image acquisition by the MST is straight forward, but a three minute delay in viewing the reconstruction is unacceptable. This could be addressed in two ways. Either the current computer could be retained, with reduction of the number of data points analysed; or alternatively, a faster computer would be necessary. In a research environment, the latter solution is preferable. With the recent application of new generation computer technology, the processing time has been reduced to less than 15 seconds.

With the development of new topography systems and methods of data analysis, there is an increasing number of ways in which topographic information is presented. Each presentation format may have its individual merits, but there could be considerable benefits in developing a standard format⁶⁰⁻⁶² which could be chosen as a presentation option in all systems. Most surgeons are familiar with the colour-coded contour maps in the form developed by Klyce and colleagues⁶³, and therefore the same colour-scheme is provided as an option on the MST (Fig. 5e). At this time of rapid expansion in the field of corneal topography, we should perhaps be considering whether this is the most useful format. We should also consider whether more than one standardised format will ultimately be required to present the wealth of information which can now be obtained about corneal topography. Given the problems which occurred in developing standards in electrophysiology and perimetry, the need for an internationally-agreed system may be rapidly approaching.

References

1. Scheiner C. *Oculus Hoc est: fundamentum opticum*. Innsbruck, 1619.
2. Placido A. Novo instrumento de exploracao da cornea.. *Periodico d'Ofthalmologica Practica*, Lisbon. 1880; 5: 27-30.
3. Wilson SE, Klyce SD. Advances in the analysis of corneal topography. *Survey Ophthalmol* 1991; 35: 269-77.

4. Morrow GL, Stein RM. Evaluation of corneal topography: past, present and future trends. *Can J Ophthalmol* 1992; 27: 213-25.
5. von Helmholtz H. In: Graefe's Archiv fur Ophthalmologie. Vol 2. 1854; 3.
6. Gullstrand A (1911) in Helmholtz's treatise in physiological optics volumes I and II (Appendix); Ed: JPC Southall, 1962, Dover, New York.
7. Bennett AG. Use of the keratometer. In: Optics of contact lenses. ADO publishing, London. 1974, 16-8.
8. Roberts C. The accuracy of 'power' maps to display curvature data in corneal topography. *Invest Ophthalmol Vis Sci* 1994; 35: 3525-32.
9. Patel S. Refractive index of the mammalian cornea and its influence on pachymetry. *Ophthalmic & Physiological Optics* 1980; 7: 503-6.
10. Patel S, Marshall J, Fitzke FW. Shape and radius of posterior corneal surface. *Refract Corneal Surg* 1993; 9: 173-81.
11. Trokel SL, Srinivasan R, Braren B. Excimer Laser Surgery of the Cornea. *Am J Ophth* 1983; 96: 710-715.
12. Kawara T. Corneal topography using moiré contour fringes. *Applied Optics* 1979; 18: 3675-3678.
13. Corbett MC, O'Brart DPS, Saunders DC, Rosen ES. The assessment of corneal topography. *Eur J Implant Ref Surg* 1994; 6 (2): 98-105.
14. Roberts C. Characterisation of the inherent error in a spherically-biased corneal topography system in mapping a radially aspheric surface. *J Refract Corneal Surg* 1994; 10: 103-11.
15. Hannush SB, Crawford SL, Waring GO, Gemmill MC, Lynn MJ, Nizam A. Accuracy and precision of keratometry, photokeratoscopy, and corneal modeling on calibrated steel balls. *Arch Ophthalmol* 1989; 107: 1235-9.
16. Hannush SB, Crawford SL, Waring GO, Gemmill MC, Lynn MJ, Nizam A. Reproducibility of normal corneal power measurements with a keratometer, photokeratoscope, and video imaging system. *Arch Ophthalmol* 1990; 108: 539-44.
17. Warnicki JW, Rehkopf PG, Arra RC, Stuart JC. Corneal topography using a projected grid. In: Corneal topography. Measuring and modifying the cornea. Eds: Schanzlin DJ, Robin JB. Springer-Verlag 1992; 25-32.
18. Corbett MC, Marshall J, O'Brart DPS, Rosen ES. New and future technology in corneal topography. *Eur J Implant Ref Surg*, 1995; 7: 372-386.
19. Varner JR. Holographic and moiré surface contouring. In: Holographic non-destructive testing. Ed: Erf R. 1974; 105-147.
20. Arffa RC, Warnicki JW, Rehkopf PG. Corneal topography using rasterography. *Refract Corn Surg* 1989; 5: 414-7.
21. Belin MW, Litoff FK, Strods SJ, Winn SS, Smith RS. The PAR technology corneal topography system. *Refract Corn Surg* 1992; 8: 88-96.
22. Takeda M, Ina H, Kobayashi S. Fourier-transform method of fringe-pattern analysis for computer-based topography and interferometry. *J Optical Soc Am* 1982; 72: 156-60.
23. Jongsma FHM, Laan FC, Stultjens BATH. A moiré based corneal topographer suitable for discrete Fourier analysis. *Proc Ophthal Tech* 1994; 2126: 185-92.
24. Stultjens BATH, Jongsma FHM. Frequency modulation as an alternative for local phase in 3D corneal topography. *Proc Ophthal Tech* 1994; 2126: 174-84.
25. Wilson SE, Lin DTC, Klyce SD, Insler MS. Terrien's marginal degeneration: corneal topography. *Refract Corn Surg* 1990; 6: 15-20.
26. Corbett MC, Marshall J. Current and future technology in corneal topography. *Eur J Implant Refract Surg* (in press).
27. Mandell RB. Corneal power correction factor for photorefractive keratectomy. *J Cat Refract Surg* 1994; 10: 125-8.
28. Thornton SP. Clinical evaluation of corneal topography. *J Cat Refract Surg* 1993; 19 (Suppl): 198-202.
29. Wilson SE, Klyce SD. Screening for corneal topographic abnormalities before refractive surgery. *Ophthalmol* 1994; 101: 147-52.
30. Madea N, Klyce SD, Smolek MK, Thompson HW. Automated keratoconus screening with corneal topography analysis. *Invest Ophthalmol Vis Sci* 1994; 35: 2749-57.
31. Gibraltar R, Trokel SL. Correction of irregular astigmatism with the excimer laser. *Ophthalmol* 1994; 101: 1310-5.
32. Corbett MC, Shun-Shin GA, Awdry PN. Keratometry using the Goldmann tonometer. *Eye* 1993; 7: 43-6.
33. Lin DTC. Corneal topographic analysis after excimer laser photorefractive keratectomy. *Ophthalmol* 1994; 101: 1423-39.
34. Cavanaugh TB, Durrie DS, Riedel SM, Hunkeler JD, Leshner MP. Topographical analysis of the centration of excimer laser photorefractive keratectomy. *J Cat Refract Surg* 1993; 19 (Suppl): 136-43.
35. Spadea L, Sabetti L, Balestrazzi E. Effect of centring excimer laser PRK on refractive results: a corneal topography study. *Refract Corn Surg* 1993; 9 (Suppl): S22-5.
36. McDonnell PJ, McClusky DJ, Garbus J. Corneal topography and fluctuating visual acuity after radial keratotomy. *Ophthalmol* 1989; 96: 665-70.
37. Corbett MC, O'Brart DPS, Saunders DC, Rosen ES. The topography of the normal cornea. *Eur J Implant Ref Surg* 1994; 6 (5): 286-97.
38. Dingeldein SA, Klyce SD. The topography of normal corneas. *Arch Ophthalmol* 1989; 107: 512-8.
39. Arffa RC, Klyce SD, Busin M. Keratometry in epikeratophakia. *J Refract Surg* 1989; 2: 61-4.
40. Lundergan MK, Rowsey JJ. Relaxing incisions: corneal topography. *Ophthalmol* 1985; 92: 1226-36.
41. Martin RG, Sanders DR, Miller JD, Cox CC, Ballew C. Effect of cataract wound incision size on acute changes in corneal topography. *J Cat Refract Surg* 1993; 19 (Suppl): 170-7.

42. Kock DD, Haft EA, Gay C. Computerized videokeratographic analysis of corneal topographic changes induced by sutured and unsutured 4mm scleral pocket incisions. 1993; 19 (Suppl): 166-9.
43. Hayashi K, Nakao F, Hayashi F. Corneal topographic analysis of superolateral incision cataract surgery. *Cat Refract Surg* 1994; 20: 392-99.
44. Corbett MC, Verma S, Prydal JI, Pande M, Oliver KM, Patel S, Marshall J. The contribution of the corneal epithelium to the refractive changes occurring after excimer laser photorefractive keratectomy. *Invest Ophthalmol Vis Sci* 1995; 36: S2.
45. Thall EH, Lange SR. Preliminary results of a new intraoperative corneal topography technique. *J Cat Refract Surg* 1993; 19 (Suppl): 193-7.
46. Ediger MN, Pettit GH, Weiblinger RP. Noninvasive monitoring of excimer laser ablation by time-resolved reflectometry. *Refract Corn Surg* 1993; 9: 268-75.
47. Sanders RD, Gills JP, Martin RG. When keratometric measurements do not accurately reflect corneal topography. *J Cat Refract Surg* 1993; 19 (Suppl): 131-5.
48. Suzuki Y, Araie M, Ohashi Y. Sectorization of the central 30° visual field in glaucoma. *Ophthalmol* 1993; 100: 69-75.
49. Vass C, Menapace R. Computerised statistical analysis of corneal topography for the evaluation of changes in corneal shape after surgery. *Am J Ophthalmol* 1994; 118: 177-84.
50. Cuaycong MJ, Gay CA, Emery J, Haft EA, Koch DD. Comparison of the accuracy of computerized videokeratoscopy and keratometry for use in intraocular lens calculations. *J Cat Refract Surg* 1993; 19 (Suppl): 178-81.
51. Strelow S, Cohen EJ, Leavitt KG, Laibson PR. Corneal topography for selective suture removal after penetrating keratoplasty. *Am J Ophthalmol* 1991; 112: 657-65.
52. Simon G, Ren Q. Biomechanical behaviour of the cornea and its response to radial keratotomy. *J Refract Corn Surg* 1994; 10: 343-56.
53. Wang J, Rice DA, Klyce SD. A new reconstruction algorithm for improvement of corneal topographical analysis. *Refract Corn Surg* 1989; 5: 379-87.
54. Dingeldein SA, Klyce SD, Wilson SE. Quantitative descriptors of corneal shape derived from the computer-assisted analysis of photokeratographs. *Refract Corn Surg* 1989; 5: 372-8.
55. Patel S, Corbett MC, O'Brart DPS, Marshall J. Inter-observer and test-retest reliabilities of three corneal topographers. *Invest Ophthalmol Vis Sci* 1994; 35: 2194.
56. Wang J, Rice DA, Klyce SD. Analysis of the effects of astigmatism and misalignment on corneal surface reconstruction from photokeratoscopic data. *Refract Corn Surg* 1991; 7: 129-40.
57. Maguire LJ, Klyce SD, Sawelson H, McDonald MB, Kaufman HE. Visual distortion after myopic keratomileusis. Computer analysis of keratoscope photographs. *Ophthalmic Surg* 1987; 18: 352-6.
58. Mishima S. Some physiological aspects of the precorneal tearfilm. *Arch Ophthalmol* 1965; 73: 233.
59. Prydal JI, Campbell FW. Study of Precorneal Tear Film Thickness and Structure by Interferometry and Confocal Microscopy. *Invest Ophthalmol Vis Sci* 1992; 33: 1996-2005.
60. Wilson SE, Klyce SD, Hussein ZM. Standardized color-coded maps for corneal topography. *Ophthalmol* 1993; 100: 1723-7.
61. Siegel IM. Standardized color-coded maps for corneal topography. [letter] *Ophthalmology* 1994; 101 (5): 795.
62. Gailitis RP, Lipsitt KL. Standardized color-coded maps for corneal topography. [letter] *Ophthalmology* 1994; 101 (5): 795.
63. Maguire LJ, Singer DE, Klyce SD. Graphic presentation of computer analysed keratoscope photographs. *Arch Ophthalmol* 1987; 105: 223-30.

6.4 Further developments

The clinical evaluation on which the preceding article "Corneal topography using a new moiré-based system" is based, proved to be invaluable for the design considerations for an commercial device. Some disadvantages mentioned, such as the unacceptably long reconstruction time, necessary to visualize an image, could be eliminated. One drawback, inherent to the technique used, the requirement to instill fluorescein, remained. In this respect the Placido disc-based CAVK is certainly superior to the fluorescein-based device. It is still not known whether fluorescein exerts an effect on the tear film thickness and distribution, this aspect certainly needs further research. Instilling fluorescein might be avoided by applying a wavelength for which the corneal tissue is non-transparent e.g. the 193 nm laser line as is suggested in the Corbett et al.'s article. However, succes of this technique is not guaranteed, because absorption of this wave length depends strongly on tissue temperature. In photorefractive surgery, part of the

opacity of the tissue is obtained due to the high temperature during the impact of the laser pulse. When low light intensities are used e.g. for imaging purposes, transparency increases². The excimer laser can be used to produce light of this wavelength, however, the optical quality of the excimer laser radiation is poor.

6.5 Further clinical validation

Besides the evaluation in Londen, the MST was also used to quantify surgical ablation on 7 patients in Rotterdam (Oog Ziekenhuis Rotterdam), a patient with an corneal ulcer was followed in Maastricht (University Hospital Maastricht) where also 5 normal eyes and 32 pathological eyes were measured to test inter- and intra-observer variation in measuring corneal curvature. In another trial, the transition from cornea to sclera was reconstructed of 30 normal and 10 keratoconus eyes.

6.5.1 The subtraction modality

Differential measurements could be obtained by subtracting successive maps to quantify new tissue production during the healing process after refractive surgery. During in situ laser keratomileusis (LASIK), ablation profiles to correct -10.5 to 14.5 dioptres were successfully measured³. Evaluation showed that the difference between planned and achieved ablation depth was in three out of four eyes within 10 μm . In 3 out of 7 eyes, however, peripheral measurements were illegible, possibly due to stromal absorption of fluorescein.

6.5.2 Localization of irregularities

A corneal ulcer was monitored during four months. Visibility of the measurements was enhanced by using the local radius of curvature as mark. The lateral localization of the ulcer's central part in the monthly measurements was reproducible within $\pm 40 \mu\text{m}$, being the camera pixel size projected on the corneal surface. However, quantification of the ulcer's volume turned out to disagree with other clinical findings⁴.

6.5.3 Reproducibility of curvature determination

Six measurements of 5 normal eyes were made by 5 observers. Also 32 pathological eyes ranging from keratoconus to cornea plana were measured. The mean standard deviation of the inter-observer variation varied from 0.04 to 0.08 mm corneal curvature, whereas the mean standard deviation of the intra-observer variations varied from 0.03 to 0.08 mm⁵.

6.5.4 Wide field measurements

Multi-meridional cross sections of 30 normal and 10 keratoconus eyes were reconstructed over a cross section of 19 mm. We found that the transition from cornea to sclera (limbal area) is much flatter than would be expected from comparing corneal with scleral curvatures. Only a boundary between smooth (corneal) tissue and more or less irregular (conjunctival) tissue was observed⁶.

References

1. Corbett MC, O'Brart DPS, Stultiens BAT, Jongsma FHM, and Marshall J. Corneal topography using a new moiré image-based system. *Eur J Implant Ref Surg* 1995;7:353-370
2. Pettit GH, and Ediger MN. Corneal-tissue absorption coefficients for 193- and 213-nm ultraviolet radiation. *Appl Opt* 1996;35(19):3386-3391
3. de Brabander J, Odenthal MThP, Jongsma FHM, Beekhuis WH. Corneal height and corneal power change measurements in lasik patients, using Euclid and TMS-1 corneal topography systems. *Inv Ophthalmol Vis Sci ARVO abstract book* 1996:S559.
4. Jongsma FHM, Laan FC, Stultiens BATH. A moiré-based corneal topographer suitable for discrete Fourier analysis. *Proc Ophthal Tech* 1994;2126:185-192
5. Nuijts RM, de Brabander J, Hieselaar LC, Odenthal MTh, Stultiens BA, and Jongsma FH. Curvature, height and slope in corneal topography. *Inv Ophthalmol Vis Sci ARVO abstract book* 1996:S557
6. de Brabander J, Nuyts RMMA, Stultiens BAT, and Jongsma FHM. Height measurements of the corneal-scleral profile. *Inv Ophthalmol Vis Sci ARVO abstract book* 1997:S1090

Chapter 7

Concluding remarks



7.1 Introduction

In this chapter the modalities of the MST are discussed and the findings of the literature research and the experiments are used to place the developed anterior eye topographer in the context of alternatives. Information about conversion of height values into parametrical values such as axial radius of curvature or dioptres is given. The chapter closes with some remarks on future research.

7.2 Height measurements of the entire eye anterior surface

The development of the Maastricht Shape Topographer has shown that the shape of the entire anterior eye surface can be measured with clinically relevant accuracy. Kawara's moiré keratometer was chosen as the basis for this development as with his device he obtained a precision in height of $5\text{ }\mu\text{m}$. Although his precision, when expressed as curvatures as is often used in clinical practice, is less than obtained with a Placido disc-based device, it offers an advantage that the surface itself is measured rather than a reflected image. Specular reflection, when applied on irregular surfaces including undulations and transitions from convex to concave curvatures, results in reflected virtual upright images and real upside-down images. These images are superimposed and cannot be separated afterwards. In contrast, measurement of height contours on the surface itself includes any surface feature that lies within the method's spatial resolution. The spatial resolution can be improved by using the projected fringes itself rather than the moiré contours. With Fourier analysis the intensity variations as a result of projected fringes on the anterior eye can be frequency analysed. In this way higher frequencies than the carrier frequency allow lowering of the spatial frequency of the fringes. This offers the opportunity to increase the measuring volume to the entire anterior eye.

If the corneal radius of curvature needs to be known, a precision within 0.1 mm is clinically acceptable. (it requires at a sagittal position of 2 mm a precision of $3\text{ }\mu\text{m}$ in height and corresponds to 0.5 dioptre (see fig. 7.1). A 0.05 mm radius of curvature precision can be obtained by shifting the aforementioned point to approximately 2.4 mm .

The precision of the MST based on the fringe analysis technique described is limited by detector noise and calculation technique (see chapter 4 of this thesis). An important feature is that the measurement is independent of any assumption made regarding the shape to be measured.

Reshaping corneal surfaces, especially when using a computer-assisted photorefractive surgery device, requires accurate assessment of the corneal surface preferably in Cartesian coordinates. The current MST matches these requirements as it delivers more than 10^5 data points to reconstruct the eye's shape. These topographic data are also valuable in contact lens manufacture. In the future these data, using some appropriate interface, may be directly used to design and produce contact lenses.

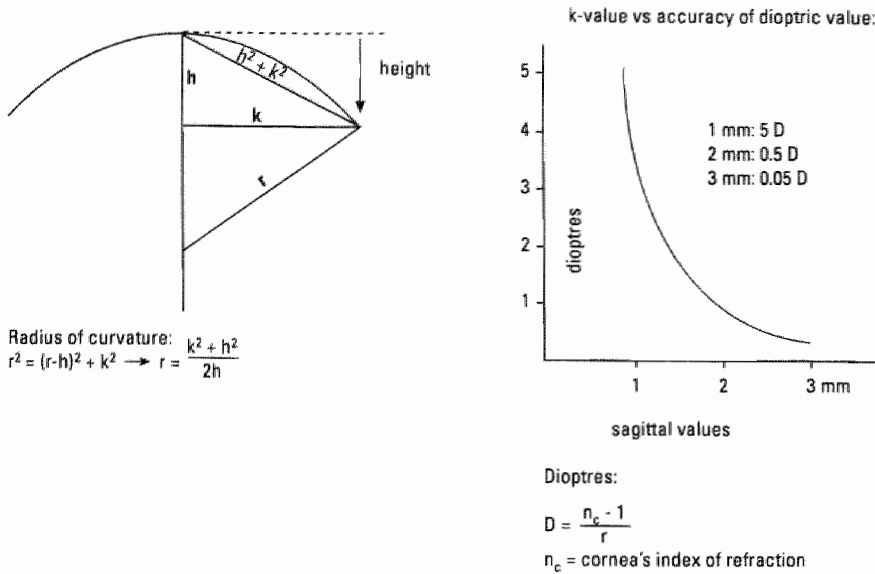


Figure 7.1

Conversion steps from height into radius of curvature into dioptries. For a sagittal value $k = 2.4$ at $r = 7.8$ mm, a $\pm 3 \mu\text{m}$ error of the MST (the average found for 3 different radii of phantom axial radius of curvature found in chapter 5) results in ± 0.25 D.

7.3 Limitations of height topography

Height topography measurements give direct insight into the shape of the entire anterior eye but this technique is less sensitive in the detection of small global deformations. When you look at an image by an ancient window reflected, the minute slope variations on the surface causes a considerable distortion of the reflected rays. In this way the weak undulations of the glass surface are clearly visualized. Starting from height data it is much more difficult to visualize such undulations. The same holds true for the mirrored images from the corneal surface. Central slope deviations can be easily detected and reasonably accurately expressed in radius of curvature by the Placido disc-based CAVK. In contrast, beyond 1 mm from the visual axis on the cornea the MST may cause 5% error in axial radius of curvature. Therefore, the MST becomes an interesting tool when shape rather than radius of curvature must be measured, or when apical axial radius of curvature can be estimated on the basis of other measurements.

7.4 Presentation of height data

Because the corneal surface is the most important optical surface of the eye, real shape data are essential. For other applications, however, a quick global presentation in terms of sphere-cylinder values are required. For this, a software program has been developed

to subtract spherical or elliptical shapes from the measured corneal shape. Local differences from the general shape such as cavities, deformations like in pterygium, ulcers, scars and transitions with corneal transplants, are clearly visualized in these mappings or differential mappings after subtracting a reference shape.

These fitting and subtraction techniques can be used on the exact height data resulting in extra shape information. In normal corneal astigmatism, this information reveals a unique picture of the real astigmatic component.

Additional possibilities of the MST

As the MST maps the tear film surface, this device may also be useful for the analysis of the precorneal tear film. Here, synchronizing flash illumination by LEDs with the 25 Hz video field frequency may allow one to detect when and where discontinuities appear, for instance due to break up of the tear film.

Excimer corneal laser ablation can be complicated by unpredictable impact of the laser pulses due to local differences in hydration. A height measuring topographer could be used here as an intra-operative device that provides possibly real time feedback on the corneal surface. However, fluorescein cannot be used intra-operatively because of possible unwanted interactions with the unprotected stromal tissue. Still the transparent and specular reflecting cornea could be mapped if light is used with a wavelength for which corneal tissue is highly absorbing. The induced backscattering in the corneal superficial layers may be adequate to replace the fluorescent light. Interfering specular reflection could be suppressed by crossed polaroids.

7.5 Predicting contact lens fitting and behaviour

With the availability of exact height data and submicron contact lens production technology, a new era in contact lens fitting has started. Our first experiments with designing contact lenses from height topography have made us realize how little we know about the mechanical behaviour of the eye - contact lens system. Today, extra information from height data could be valuable for improved design of contact lenses on an individual basis. However, there is a lot more to know than only shape of the cornea to achieve an optimal fit. For example, the conditions of the precorneal tear film that controls a variety of physiological and optical demands. Little is known about the influence of the contact lens on the tear film's fluid dynamics. To reach the point of implementing an intelligent expert system able to guide the practitioner will require additional research efforts.

7.6 The MST compared to Placido disc-based CAVKs

Since Placido invented his disc in 1880, the instruments based on his idea have had an increasing success, and the majority of present day keratometers are indeed based on the Placido disc. It is certainly not true that with the MST the Placido disc-based devices have become obsolete. On the contrary, they are the most convenient devices to obtain

easily and quickly good measurements from most corneal surfaces. There are still interesting developments in this field. New, and more accurate algorithms are being developed^{1,2}. It has been claimed that with adequate algorithms the central corneal shape can be reconstructed with an accuracy in the nm range rather than the μm range³. A remarkable example is the development of a reflection-based device which exploits properties of Pseudo Random Binary Arrays (PBRA). Encoded in a coloured stimulus pattern, the PRBA contributes to a robust measurement technique with uniquely characterized positions. With such a stimulus it is not necessary to use the assumption that reflection occurs in meridional planes⁴.

The power of the MST lies where the corneal surface is irregular or when the measurement must be extended to the peripheral parts of the cornea and the adjacent tissues. In this respect the research question, the starting point for the study, can be answered in a positive way. It is possible to measure without mechanical contact the entire corneal surface and also part of the adjacent tissues.

7.7 Further research

Little is known about the tear film fluorescein interaction. Fluorescein might influence tear film break ups⁵ and controversy exists in the literature on this topic⁷. Could this influence the height measurement adversely? Further study on tear film fluid behaviour and the interaction between corneal surface and contact lens is now facilitated by the availability of reliable shape data. This could lead to micro-hydrodynamic models that in turn can further improve the process leading to safe and comfortable contact lenses for both normal and abnormal corneas.

With eye shape topography and other optical evaluation methods, we are now in principle able to design the front surface of the contact lens for an optimized image quality. However, the eye is a complex optical system, the contact lens is relatively thick and pupil effects must be incorporated. This calls for the development of an extended opto-mechanical eye contact lens model. Recent ray tracings of the MST optics indicated a systematic error in height measurements particularly toward the periphery of the image. This was caused by residual spherical aberration of the projector's achromats, despite the aplanatic configuration. It can be compensated mathematically, but also optically. By using ray tracing technology we have found an improved (Scheimpflug) correction angle. Implementing this angle into the MST will increase the depth of focus of the projectors but unfortunately it does not reduce the residual spherical aberration.

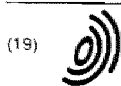
References

1. Rand RH, Howland HC, and Applegate RA. Mathematical model of a Placido disc keratometer and its implications for recovery of corneal topography. *Optom Vis Sci* 1997;74(11):926-930
2. Klein SA. Corneal topography reconstruction algorithm that avoids the skew ray ambiguity and the skew ray error. *Optom Vis Sci* 1997;74(11):945-962
3. Stultiens BAT. Generic description of topography reconstruction of reflection-based corneal topographers. Accepted for publication in *Optom Vis Sci*.

4. Vos FM, van der Heijde GL, Spoelder HJW, van Stokkum IHM, and Groen FCA. A new PRBA-based instrument to measure the shape of the cornea. *IEEE Trans Instrum Meas* 1997;46(4)
5. Mengher LS, Bron AJ, Tonge SR, Gilbert DJ. Effect of fluorescein on the pre-corneal tear film stability. *Curr Eye Res* 1985;4:9-12
6. Patel S, Murray D, McKenzie A, Shearer DS, McGrath BD. Effects of fluorescein on tear breakup time and on tear thinning time. *Am J Optom Physiol Opt* 1985;62:188-190
7. Cho P, Brown B, and Lau C. Effect of fluorescein on the tear Stability of Hong Kong-Chinese. *Optom Vis Sci* 1996;73(1): 1-7

Appendix

European patent EP o 551 955 B1 1997



Europäisches Patentamt

European Patent Office

Office européen des brevets



(11) EP 0 551 955 B1

(12) EUROPEAN PATENT SPECIFICATION

(45) Date of publication and mention
of the grant of the patent:
13.08.1997 Bulletin 1997/33

(51) Int. Cl.⁵ A61B 3/107, G01B 11/24

(21) Application number: 93200102.7

(22) Date of filing: 15.01.1993

(54) System for determining the topography of a curved surface

System zur Bestimmung der Topographie einer gekrümmten Oberfläche

Système pour déterminer la topographie d'une surface courbée

(84) Designated Contracting States:
BE CH DE DK ES FR GB IT LI NL SE

(30) Priority: 15.01.1992 NL 9200071

(43) Date of publication of application:
21.07.1993 Bulletin 1993/29

(73) Proprietor:
EUCLID MEDICAL INSTRUMENTS Inc.
NL-6200 AE Maastricht (NL)

(72) Inventor: Jongsma, Franciscus Hermanus Maria
NL-6235 BX Ulestraten (NL)

(74) Representative: de Bruijn, Leendert C. et al
Nederlandsch Octrooibureau
P.O. Box 29720
2502 LS Den Haag (NL)

(56) References cited
DE-A- 4 007 502 FR-A- 2 254 781
FR-A- 2 292 213

- SPIE-ECOOSA vol. 492, 1984, Amsterdam NL, pp. 500-506; F.H.M. JONGSMA et al.: "Real-time contouring of toothimprints"
- APPLIED OPTICS vol. 18, no. 21, 1 November 1979, New York US, pp. 3675-3678; T. KAWARA : "Corneal topography using moiré contour fringes"
- NOUVELLE REVUE D'OPTIQUE, vol. 6, no. 2, October 1975, Paris FR, pp. 67-86; P. BENOIT et al.: "Characterization and control of threedimensional objects using fringe projection techniques"

Note: Within nine months from the publication of the mention of the grant of the European patent, any person may give notice to the European Patent Office of opposition to the European patent granted. Notice of opposition shall be filed in a written reasoned statement. It shall not be deemed to have been filed until the opposition fee has been paid (Art. 99(1) European Patent Convention)

Printed by Rapin & Co., Luxembourg
2 16 13 2 4

EP 0 551 955 B1

EP 0 551 955 B1

Description

The invention relates to a system for determining the topography of a curved surface, comprising a projection device for projecting patterns of lines on the surface, which projection device includes two independent light projectors disposed at an angle relative to each other, each projector having a projection optical axis and including a grating having parallel straight lines, wherein each grating is positioned at a right angle to the projection optical axis of its projector, and a rectangular diaphragm having the long sides parallel to the lines of the grating, and a detection device for registering an image formed on the curved surface. Such systems are used, *inter alia*, in the case of the so-called keratometer for determining the external shape of the human eye, in particular the curvature of the external surface of the cornea, for example for measuring for contact lenses and accurately determining the topography of the cornea before and after surgery.

These systems can also be used in manufacturing and checking curved objects.

With the known commercially available photokeratometer the radius of curvature of the cornea is measured locally by comparing mirrored measurement figures on the interface between air and lacrimal fluid with test figures.

Places of equal slope can be mapped in this way. In the interpretation of such registrations, without previous knowledge of the object, errors cannot be ruled out. Only a limited area of the cornea is measured.

Unequivocal registrations of the topography of the surface of the cornea can be obtained with the keratometer of the type which is described in an article by Tetsuo Kawara, "Corneal topography using moiré contour fringes", in *Applied Optics*, Vol. 18, pp. 3675-3678 (Nov. 1979). Such a keratometer makes use of moiré contour lines, which are lines of equal height. For this purpose, the reflecting surface of the cornea is transformed into a perfectly diffusely radiating surface, through the application of a fluorescein film, as is necessary for said moiré technique. The fluorescent light of the fluorescein film is used to form the image, while the excitation light (which through specular reflection could distort the image) of the projection device, consisting of a single projector, is filtered out. In order to achieve the accuracy for a spherical surface which he claimed, Tetsuo Kawara used a grating with approximately 12 line pairs per millimetre (lp/mm) which, because of a narrow slit-shaped diaphragm in the projection device having optical compensation for the slanting projection angle relative to the viewing axis of the keratometer and a small enough diaphragm of the camera with the required depth of field, forms an image on the reference grating of the camera.

Due to the slanting projection angle, the camera "sees" a superimposed pattern of a projected grating slightly deformed by the convex cornea and the reference grating. The spatial beat between the gratings, which becomes visible as an interference phenomenon, is known as moiré. This interference image represents lines of equal height. Since in this moiré arrangement a multiplication contrast is obtained, the height lines can be read directly from the photographs. Translation of these height lines into three meridional profiles produces information on the local radius of curvature of the cornea.

A serious general limitation of the moiré projection system described is that, on the one hand, sufficient depth of field is required, for which a small diaphragm is needed, while, on the other hand, the height contour interval must be as small as possible, which only a grating with a large number of lp/mm can provide. The system described by Tetsuo Kawara is therefore diffraction limited. A higher resolution can be obtained only at the expense of the depth of field, or by increasing the projection angle of the grating relative to the optical axis of the camera. With a small depth of field the whole cornea is not mapped in one exposure, and a larger projection angle than approximately 18° produces an image which can no longer be interpreted visually, on account of the occurrence of optical artifacts. In the case of the instrument described the height lines are displayed at the position of the reference grating instead of being located on the surface to be registered, which means that the flexibility of the instrument with regard to variation of image scale and image angle is low. The sign of the slope is not known (from previous knowledge is derived as "convex"). The product of Tetsuo Kawara's keratometer is a photograph. The translation of the height lines thus recorded into local radius of curvature, eccentricity etc. has to be carried out from there.

The dependence on very fine gratings in order to keep the moiré contour interval (= measuring point) limited, could be removed in principle if, instead of the intensity distribution of the moiré image, the local phase of the projected grating were used as the measuring point.

Moiré height lines of a surface of an object are formed by the relative phases between the projected grating and the reference grating. The height lines will shift due to shifting of one of the gratings, with the result that a continuous phase measurement at one measuring point is possible. The intensity variation is then a measure of the phase variation. The measuring sensitivity and the accuracy then increase greatly. Since the movement device of the moving grating is known, the sign of the slope can be determined. In the case of the keratometer, on account of unavoidable eye movements, it is hardly possible to carry out such a dynamic measurement.

However, in the examination of surfaces of other objects, such as dentures, the use of a device is known from an article by F.H.M. Jongsma et al., "Real-time contouring of tooth imprints", in *SPIE*, Vol. 492, pp. 500-506, ECOOSA 1984, in which two interference patterns are projected at an angle relative to each other by means of an interferometer. Planes which are at right angles to the bisectrix of the angle and are alternately diffusely illuminated or contain more or less highly contrasting line patterns are thereby produced in the space in which the two light beams intersect. The dis-

EP 0 551 955 B1

tance between these parallel planes is equal and depends on the angle between the light beams and the distance between the lines in the projected grating pattern. If an object is now placed in this space, it alternately intersects the diffusely illuminated planes and the planes with the images of the grating pattern. As a result of this, intersection lines become visible on the object, which lines have a constant height difference from each other, although due to the summation effect the contrast of the two intensities is very low. In order to make said height lines visible, a spatial (optical) or temporal (electronic) filtering such as that described in above article by Jongsma et al. must therefore still be used.

A disadvantage of moiré images is that it is not possible to determine the sign of the slope other than from previous knowledge of the object. One method of overcoming this problem is described in French patent application No. 2,292,213 of 21 November 1974. This patent application describes a method in which two moiré projections are compared with each other. These moiré registrations are produced in such a way that the reference plane of the second moiré registration is displaced over a distance which is smaller than half the moiré contour distance. Double contours with alternating small and larger intervals are thus produced. The contours are labelled with a colour, for example by making use of a yellow and a blue grating. The result is then a colour registration with the relatively small contour intervals yellow - blue or blue - yellow. The information of the sign of the slope is contained in the combination of distance and colour.

Another form of colour labelling is described in German patent application No. P 40 075 028 of 9 March 1990. This patent application describes how two gratings of different colours are projected simultaneously on the object from different angles. The two gratings can be processed in the detection system separately by means of a colour separation mirror. The angle and the orientation of the slope relative to the sensor can then be calculated from the local spatial grating frequency on the object. What is essential in this system is the mechanical linking of the two gratings lying in one plane, so that their phase relation is fixed. As a result of this, by displacement of the gratings the noise can be averaged, while the height contours do not change position.

If unambiguous external shape information on the moist and reflecting surface of the cornea is desired, use can be made of the fluorescence technique described in the article by T. Kawara, in order to convert this reflecting surface into a Lambertian radiator. In these conditions, when there is a well-defined illumination, the local emission can then be calculated. In order to obtain a moiré contrast, use can be made of the projection technique known from an article by J. Wasowski, "Moiré topographic maps", in Opt. Communications, Vol. 2, pp. 321-323, 1970, by means of a projector of the type described by Kawara. If lasers which are suitable for this are available, it is also possible to choose the interferometer described by Wasowski as the grating producer, or another interference system can be used.

The invention aims at obviating the earlier mentioned problems in the prior art. This is realized, according to the invention, in that the projection device comprises, in each projector, a flash light source synchronised in sequence with the detection device, and in that the detection device comprises a frame grabber for separately registering a projected grating of each projector in said sequence, respectively, for digital image analysis to obtain the topography of the curved surface. Hereby the system is implemented such that an additive moiré pattern is produced. In a further embodiment a pilot monitor in conjunction with an electronic filter is provided for real-time visualizing this moiré pattern, the detection device being implemented for registering the image without moiré interference, suitable for discrete Fourier analysis.

The invention is explained in greater detail with reference to an example of an embodiment shown diagrammatically in the drawings, in which

Fig. 1 shows diagrammatically a system according to the invention;

Fig. 2 shows the projection of the intensity function on the x-axis through object $c(x)$;

Fig. 3 shows an electronic real-time filtered viewfinder image;

Fig. 4a, 4b and 4c respectively show a complete TV picture and the separate components from which it is composed, the first half raster (fig 4b) and the second half raster (fig 4c);

Fig. 5 shows a digitally obtained phase reconstruction of a TV line, and

Fig. 6 shows a 2-D reconstruction of a half TV raster of a spherical surface.

On account of the gain in sensitivity and accuracy which can be achieved with phase detection, a calculation program has been developed, in which the local phase of a projected grating on the surface to be measured is calculated relative to a reference plane at right angles to the optical axis of the sensor. Since the carrier wave itself, and not the modulation of the carrier wave, is now the basis for extracting the information, it is possible to work with relatively coarse gratings which permit correspondingly larger diaphragms. In this way it becomes possible, without causing too great a radiation load for the eye, to use a high-resolution TV camera, such as a CCD camera, which permit real-time digitising of the images through the use of a frame grabber.

The cornea to be measured is mobile and cannot be fixed, with the result that the collection time has to be very short (shorter than the integration time of a TV camera). Moreover, a part of the image can be lost through local over-exposure, due to reflection on the cornea.

These problems can be solved by making use of a TV camera, like a CCD camera, and two flash tubes synchronised with the camera such as is indicated in Fig. 1. The first tube is synchronised in the end of the first half raster

EP 0 551 955 B1

period, and the second at the beginning of the next half raster. The total integration time is now limited to the flash times and the flash interval. Since the two flash exposures produce an independent picture independently of each other (but linked in time), one picture can supplement the information which has been lost in the other picture, for instance caused by local disturbances like undesired reflections, too strong defocussing, etc. This situation is achieved in the case of the double flash technique described, in which it is possible, for example, first to analyse the odd TV lines and then to analyse the even lines.

The system for use in the invention, as indicated in Figure 1, comprises two projectors 3 set up at an angle with the optical axis 1 of a camera 2. Both projectors contain a slide or grating 4 containing a line pattern of about five line pairs per mm, which lines run at right angles to the plane through the projection axes. As described above, by projection of two line patterns at an angle, diffusely illuminated planes and planes with more or less highly contrasting raster images are produced alternately in the space 12 in which the two light beams cross, which images produce a height line or contour chart on intersection by an object.

The eye to be examined is treated with Na-fluorescein in Hypromellose-Bourbonville®, a substance which is also used as a replacement for natural tear moisture in the case of "dry eyes". Hypromellose serves as a solvent for Na-fluorescein. Blinking a few times causes the Na-fluorescein to be absorbed in the tear film, following which the registration can be taken.

For accurate measurements of the cornea contours, in which the liquid film must have a uniform thickness, use can be made of Healon®, which has a low molecular weight, and in which Na-fluorescein is dissolved, as known, for example, in the case of cornea plastic with the aid of excimer lasers.

Projection lamps 5 are used as the light source in the projectors. In order to "freeze" rapid eye movements, use can be made of flash lamps 6 which are synchronised with the TV camera, and which then temporarily replace the continuous lamps in the projectors. Filters are fitted between the lamps and the slides, which filters reflect (7) the heat of the light source and reflect (8) all colours except blue-green, so that the radiation load on the eye is restricted to that of the blue-green excitation light. For projecting the grating, the projection device is provided with a projection objective 10. Placed in the focal plane of this projection objective at the side where the object lies is a rectangular diaphragm 9, of which the long sides run parallel to the lines of the grating. The aperture of the diaphragm along the narrow side is small enough to project five line pairs per mm with sufficient depth of field. The relatively large aperture of the diaphragm along the long side contributes to the desired light intensity of the height line map.

The distance setting takes place with the aid of an image on a pilot monitor, on which after analog filtering concentric rings appear on the cornea (Fig. 3) which cornea is imaged totally in the depth of focus of the cornea image.

A yellow-band stop filter 11 is fitted in front of the camera, which filter blocks the blue excitation light and transmits only the yellow emitted light.

The unfiltered moiré image at the location of each CCD camera contains pixel information on the spatial coordinates x , y and z . With the aid of digital image processing it is possible to make the shape of the cornea visible in detail, for example as an axial section or as a three-dimensional structure. In order to obtain both a high axial and a high lateral resolution, the ring pattern such as that obtained after electronic analog filtering is not used as the starting point, but instead the unfiltered TV picture is analysed TV line by line.

As soon as the instrument is set, a frame grabber sees to the digitisation and the transmission of the signal to the monitor coupled to a computer. There the signal is analysed line by line (Fig. 4). This takes place both for the left-hand projection and for the right-hand projection in the calculation, possibly simultaneously. In this way any missing information in one image can be supplemented through the other image. This also applies to defocussing effects, which in the case of the two projections are left-right opposed.

One method for analysing signals is to use Fourier analysis. A condition for this analysis is that the signal is not overmodulated, as is unavoidable in the case of a moiré contrast. The TV pictures registered can be regarded as being phase-modulated, the height of the object to be measured being modulated in the phase of the projected grating.

Figure 2 shows in a one-dimensional manner how the grating is modulated and projected, in which:

- $a(x)$ = perpendicular line of $p(x)$ through the origin
- $\{Z(x)\}$ = collection of perpendicular lines of $p(x)$ with an intersection point with $c(x)$; β
- φ = projection angle
- $p(x)$ = intensity function axis with O as origin
- α = distance between $a(x)$ and any line of $Z(x)$ representing the original phase angle produced by the raster
- β = abscis value of the intersection point with $c(x)$ representing the phase angle which comes about after projection

The diaphragm setting, passes the first and zeroth order, with the result that the intensity can be characterised by:

$$i(\alpha) = A \sin(\omega_0 \alpha) + d \quad (1)$$

EP 0 551 955 B1

where

- ω_0 : raster function
 A : amplitude
 d : D.C. shift

The projected modulated wave form then acquires a shape of the type:

$$i(\beta) = A \sin [\omega_0 (\cos(\varphi) \cdot \beta + \sin(\varphi) \cdot c(\beta))] + d \quad (2)$$

where

- $c(\beta)$ = height of the object written as function,
 φ = projection angle.

Note that $i(\beta)$ is the image measured with the camera.

The phase, thus the height of the object, can be reconstructed from the modulated wave form $i(\beta)$ by means of the Fourier transform. In principle, the following steps are necessary to reconstruct the height:

$$I(\omega) = F\{i(\beta)\} \quad (3)$$

$$Y(\omega) = D\{I(\omega)\} \quad (4)$$

$$y(\beta) = F^{-1}\{Y(\omega)\} \quad (5)$$

$$T \cdot c(\beta) = \arg(y(\beta)) \wedge T \cdot c(\beta) + k \pi = T \cdot c(\beta) \quad k \in \mathbb{Z} \quad (6)$$

where:

- T : constant factor
 $F\{\}$: forward Fourier transform
 $F^{-1}\{\}$: backward Fourier transform
 $D\{\}$: demodulation transform
 $\arg(\)$: argument/phase of a complex number/series
 k : constant, element of \mathbb{Z}

A data processing system will carry out these operations in discrete form. For the discrete Fourier transform there is a very suitable method which reduces the number of calculations required. This is the so-called Fast Fourier Transform (FFT). In analogy to the one-dimensional analysis technique described, there is the possibility of carrying out a two-dimensional analysis. Since the two-dimensional Fourier transform comprises two one-dimensional transforms which can be carried out independently of each other, the same method as that mentioned in formula (3), (4), (5) and (6) applies.

For determining radii of curvature of a demodulated image it is possible to use, inter alia, elliptical or polynomial curve fitting. A method for this is, for example, Gaussian elimination. Eccentricity, astigmatism and the like can be determined or calculated from these fittings. The determination of fittings can also be carried out in a one-dimensional or a two-dimensional manner. For both transform technique and fitting technique the two-dimensional method is more accurate, because in principle all measured image points are brought into relation with each other, which corresponds to reality. Measuring errors are also averaged out more effectively or are even eliminated in this way. In order to achieve further improvements, digital filter techniques will be required.

For an example of above processing reference is made to Figures 5 and 6, in which a digitally obtained phase reconstruction of a (pilot) monitor line (projection on a spherical surface) and a two-dimensional reconstruction of a half TV raster of a spherical surface are respectively shown. In figure 6, the contours can now be adjusted with intervals as desired. Details - such as a defect in the model top left - can thus be visualised.

In the above explained technique the lateral horizontal resolution is determined by the band width of the TV system or by the resolution of the frame grabber, and no longer by the fringes of the moiré pattern, which as a beat pattern by definition have a much lower lateral resolution. The vertical resolution is determined by the number of TV lines. Apart

EP 0 551 955 B1

from being used as a keratometer, on account of the absence of the need for having previous knowledge of the object to determine the sign of the slope, the system can also be made suitable for determining the three-dimensional shape of other objects such as contact lenses, dentures, models and industrial objects. Advantageously, the system can be used such that by means of digital processing of the height contours already calculated the requested information for, for example, an optician, contact lens specialist, ophthalmologist or technician becomes available.

The system according to the invention can be used for determining a curved surface, in which an accurate height line or contour pattern with a high lateral resolution is the basis for obtaining the required data, as needed, for example, for fitting contact lenses or for surgery in the ocular media. When the system is used as a keratometer, a height line map can be created on the cornea, comprising the whole cornea, and the detection device will also be designed in such a way that the whole height line map is available in real time in digital form for further data processing, with the result that an accurate determination of the central and peripheral curvature of the cornea becomes possible.

This is obtained through the fact that the above system includes a projection device provided with two projectors disposed at an angle relative to each other, each positioned at right angles to the plane through the projection axes and a rectangular diaphragm, of which the long sides are parallel to the lines of the grating.

Through the use of these projectors, diffusely illuminated planes and planes with more or less highly contrasting grating images can be obtained, which when intersected by an object produce a highly contrasting moiré contour or height line map after analog or digital processing of the signal.

A radiation load which is acceptable for the eye to be examined will be produced by making use of a relatively large diaphragm aperture from the detector side, even when using the required blue-green excitation light.

The angle at which projection takes place depends on the slope or curvature of the surface to be examined. Through the nature of the data processing, considerably larger projection angles are possible than in the case of direct formation of moiré images, while the sensitivity gain compared with respect to the direct moiré system also makes very small angles effective. In the case of the keratometer a real-time moiré image is created by means of an analog electronic filter, for a setting and viewfinder image.

In addition, in particular in the case of keratometers, the light source used for the viewfinder image is a lamp with slit shaped filament or slit shaped gas discharge, which is projected in vertical orientation on the vertical slit-shaped diaphragm of the projector. In order to minimise the thermal load of the projection device and in order to keep the light load of the eye low, relatively coarse gratings are projected, which gratings can still be projected with sufficient depth of field when the diaphragm aperture is large. The detection device can be embodied such that the definition of the height line map takes only a short time, with the result that possible movements of the eye during the exposure do not adversely affect the quality of the registration.

Through specular reflections of the surface of the object, differences can occur in the intensities of the two grating images, with the result that the derivation of the phase height of the gratings from the local intensity is jeopardised, and so also is the formation of the height line map.

Providing the object with a fluorescent layer prevents specular reflections in the case of this method. Use is made of a continuous light source which radiates light with a wavelength which causes emission in a fluorescent substance applied to the object. A substance which is suitable for this is Na-fluorescein, of which the optimum excitation wavelength, depending on the solvent, is 460 to 510 nm (blue-green) and the emission wavelength is 520 - 560 nm (yellow). The projection device is fitted with a filter which transmits only light of the excitation wavelength, and in the detection system there is a filter which transmits only light of the emission wavelength. The interfering influences as the result of reflections of the excitation light are removed through this latter filter. In the case of the keratometer embodiment, the viewing axis and optical axis of the keratometer can be aligned as follows. The person to be examined is asked to fix the eye on a light source, the optical axis of which coincides with the optical axis of the instrument. The operator of the keratometer ensures then that this light source reflected by the eye goes into the centre of the image.

Claims

1. A system for determining the topography of a curved surface, comprising a projection device for projecting patterns of lines on the surface, which projection device includes two independent light projectors (3) disposed at an angle relative to each other, each projector having a projection optical axis and including a grating (4) having parallel straight lines, wherein each grating is positioned at a right angle to the projection optical axis of its projector, and a rectangular diaphragm (9) having the long sides parallel to the lines of the grating, and a detection device for registering an image formed on the curved surface, characterised in that the projection device comprises, in each projector, a flash light source (6) synchronised in sequence with the detection device, and in that the detection device comprises a frame grabber for separately registering a projected grating of each projector in said sequence, respectively, for digital image analysis to obtain the topography of the curved surface.
2. A system according to claim 1, wherein the detection device comprises a TV-camera (2) and a synchronizer means for triggering the flash light source (6) of the first projector at the end of a first half TV-raster period and for triggering

EP 0 551 955 B1

the flash light source of the second projector at the beginning of a second half TV-raster period, respectively, the flash light sources illuminating a complete TV-raster wherein the half rasters are adapted to complement each other afterwards.

- 5 3. A system according to claim 2, wherein the detection device further comprises a data processor for analyzing the image to obtain a height function, according to Fourier transform, demodulation, and inverse Fourier transform, on one or more half TV-rasters simultaneously in a one or two dimensional manner for reconstructing the topography
- 10 4. A system according to claim 1, wherein each light projector further comprises a continuous light source (5), wherein the continuous and flash light sources are slit shaped such that the continuous light and flash light is projected from the projectors in a vertical orientation through the rectangular diaphragm.
- 15 5. A system according to claim 4, wherein the detection device comprises an analogue contrast filter and a pilot monitor, whereby the analog filter emphasizes additive height contours in real time on a topography image which is displayed on the pilot monitor
6. A system according to claim 1, wherein the projectors of the projection device are each disposed at an angle ranging from 10° to 45°.
- 20 7. A system according to claim 1, wherein each projector comprises a grating projecting objective (10), the rectangular diaphragm (9) being placed in a focal plane of the objective.
8. A system according to claim 3, wherein the projectors are angled to cause the projected gratings to intersect on the curved surface, wherein the frame grabber is capable of distinguishing the intersecting gratings and separately registering the gratings for individual digital analysis via the data processor.
- 25 9. A system according to claim 1 to 8, for use as a contact lens fitting device.
10. A system according to claim 1 to 8, for use as a keratometer.

Patentansprüche

- 35 1. System zu Bestimmung der Topographie einer gekrümmten Oberfläche, mit einem Projektionsgerät zum Projizieren von Mustern aus Linien auf die Oberfläche, wobei das Projektionsgerät zwei unabhängige Lichtprojektoren (3) enthält, die in einem Winkel zueinander angeordnet sind und deren jeder eine optische Projektionsachse hat und ein Gitter (4) mit parallelen geraden Linien enthält, wobei jedes Gitter in einem rechten Winkel zur optischen Projektionsachse des betreffenden Projektors positioniert ist, und eine rechteckige Blende (9), deren lange Seiten parallel zu den Linien des Gitters verlaufen, und mit einer Erfassungseinrichtung zum Aufnehmen eines auf der gekrümmten Oberfläche gebildeten Bildes, dadurch gekennzeichnet, daß das Projektionsgerät in jedem Projektor 40 eine Blitzlichtquelle (6) aufweist, die in ihrer Sequenz mit der Erfassungseinrichtung synchronisiert ist, und daß die Erfassungseinrichtung einen Einzelbild-Aufgreifer aufweist, um in der besagten Sequenz jeweils ein projiziertes Gitter eines jeden Projektors gesondert aufzunehmen, für digitale Bildanalyse zum Erfahren der Topographie der gekrümmten Oberfläche.
- 45 2. System nach Anspruch 1, in welchem die Erfassungseinrichtung eine Fernsehkamera (2) und eine Synchronisatoreinrichtung aufweist, um die Blitzlichtquelle (6) des ersten Projektors am Ende einer ersten Fernseh-Halbrasterperiode zu triggern und die Blitzlichtquelle des zweiten Projektors am Beginn einer zweiten Fernseh-Halbrasterperiode zu triggern, wobei die Blitzlichtquellen einen vollen Fernsehtraster beleuchten, worin die Halbraster zu späteren gegenseitigen Ergänzung ausgelegt sind.
- 50 3. System nach Anspruch 2, in welchem die Erfassungseinrichtung ferner einen Datenprozessor für eine Analyse des Bildes aufweist, um eine Höhenfunktion gemäß Fourier-Transformation, Demodulation und inverser Fourier-Transformation an einem oder mehreren Fernseh-Halbrastern gleichzeitig in ein- oder zweidimensionaler Weise für die Rekonstruktion der Topographie zu erhalten.
- 55 4. System nach Anspruch 1, in welchem jeder Lichtprojektor ferner eine Gleichlichtquelle (5) enthält, wobei die Gleichlicht- und Blitzlichtquellen spaltförmig sind, so daß das Gleich- und Blitzlicht von den Projektoren in einer vertikalen Orientierung durch die rechteckige Blende hindurch projiziert wird.

EP 0 551 955 B1

5. System nach Anspruch 4, in welchem die Erfassungseinrichtung ein analoges Kontrastfilter und einen Pilotmonitor aufweist, wobei das analoge Filter additive Höhenkonturen in Realzeit auf einem am Pilotmonitor wiedergegebenen Topographiebild hervorhebt.
6. System nach Anspruch 1, in welchem die Projektoren des Projektionsgerätes jeweils in einem Winkel im Bereich von 10° bis 45° angeordnet sind.
7. System nach Anspruch 1, in welchem jeder Projektor ein gitterprojizierendes Objektiv (10) aufweist und die rechteckige Blende (9) in einer Brennebene des Objektivs angeordnet ist.
8. System nach Anspruch 3, in welchem die Projektoren so im Winkel angeordnet sind, daß sich die projizierten Gitter an der gekrümmten Oberfläche durchschneiden, wobei der Einzelbild-Aufgreifer fähig ist, die sich durchschneidenden Gitter zu unterscheiden und die Gitter, für individuelle digitale Analyse mittels des Datenprozessors, getrennt aufzunehmen.
9. System nach Anspruch 1 bis 8 zur Verwendung als Vorrichtung zur Kontaktlinsenanpassung.
10. System nach Anspruch 1 bis 8 zur Verwendung als Keratometer.

Revendications

1. Système pour déterminer la topographie d'une surface courbe, comportant un dispositif de projection pour projeter des configurations de lignes sur la surface, dispositif de projection qui comprend deux projecteurs de lumière indépendants (3) disposés sous un certain angle l'un par rapport à l'autre, chaque projecteur ayant un axe optique de projection et incluant un réseau de diffraction (4) présentant des lignes droites parallèles, dans lequel chaque réseau de diffraction est placé à angle droit par rapport à l'axe optique de projection de son projecteur, ainsi qu'un diaphragme rectangulaire (9) dont les grands côtés sont parallèles aux lignes du réseau de diffraction, et qu'un dispositif de détection pour enregistrer une image formée sur la surface courbe, caractérisé par le fait que le dispositif de projection comporte, dans chaque projecteur, une source de lumière flash (6) synchronisée en séquence avec le dispositif de détection et que le dispositif de détection comporte un dispositif de saisie rapide d'une image complète pour enregistrer, séparément et respectivement, un réseau de diffraction projeté de chaque projecteur en ladite séquence, pour analyse numérique de l'image pour obtenir la topographie de la surface courbe.
2. Système selon la revendication 1, dans lequel le dispositif de détection comporte une caméra TV (2) et un moyen de synchronisation pour déclencher la source de lumière flash (6) du premier projecteur à la fin d'une première demi-trame de balayage TV et pour déclencher la source de lumière flash du second projecteur au début d'une seconde demi-trame de balayage TV, respectivement, les sources de lumière flash éclairant ainsi une trame complète de balayage TV, les demi-frames étant prévues pour se compléter l'une l'autre ensuite.
3. Système selon la revendication 2, dans lequel le dispositif de détection comporte en outre un processeur de données pour analyser l'image pour obtenir une fonction des lignes de niveau, en fonction de la transformation de Fourier, d'une démodulation et d'une transformation inverse de Fourier, sur une, ou plusieurs, des demi-frames de balayage TV simultanément, en monodimensionnel ou en bidimensionnel, pour reconstruire la topographie.
4. Système selon la revendication 1, dans lequel chaque projecteur de lumière comporte en outre une source de lumière continue (5) dans lequel les sources de lumière, continue et flash, sont en forme de fente de sorte que la lumière continue et la lumière flash sont projetées par les projecteurs à travers le diaphragme rectangulaire, selon une orientation verticale.
5. Système selon la revendication 4, dans lequel le dispositif de détection comporte un filtre de contraste analogique et un moniteur pilote, ce par quoi le filtre analogique accentue des courbes de niveau additives en temps réel sur une image topographique qui apparaît sur le moniteur pilote.
6. Système selon la revendication 1, dans lequel les projecteurs du dispositif de projection sont disposés chacun sous un angle allant de 10° à 45° .
7. Système selon la revendication 1, dans lequel chaque projecteur comporte un objectif de projection à réseau de diffraction (10), le diaphragme rectangulaire (9) étant placé dans un plan focal de l'objectif.

EP 0 551 955 B1

8. Système selon la revendication 3, dans lequel le projecteurs font un certain angle pour faire en sorte que le réseaux de diffraction, projetés, s'intersectent sur la surface courbe, dans lequel le dispositif de saisie rapide d'une image complète est capable de distinguer le réseaux de diffraction d'intersection et d'enregistrer séparément les réseaux de diffraction pour analyse numérique individuelle au moyen du processeur de données.

5

9. Système selon les revendications 1 à 8, pour emploi comme dispositif d'ajustement de lentilles de contact.

10. Système selon les revendications 1 à 8, pour emploi comme kératomètre.

10

15

20

25

30

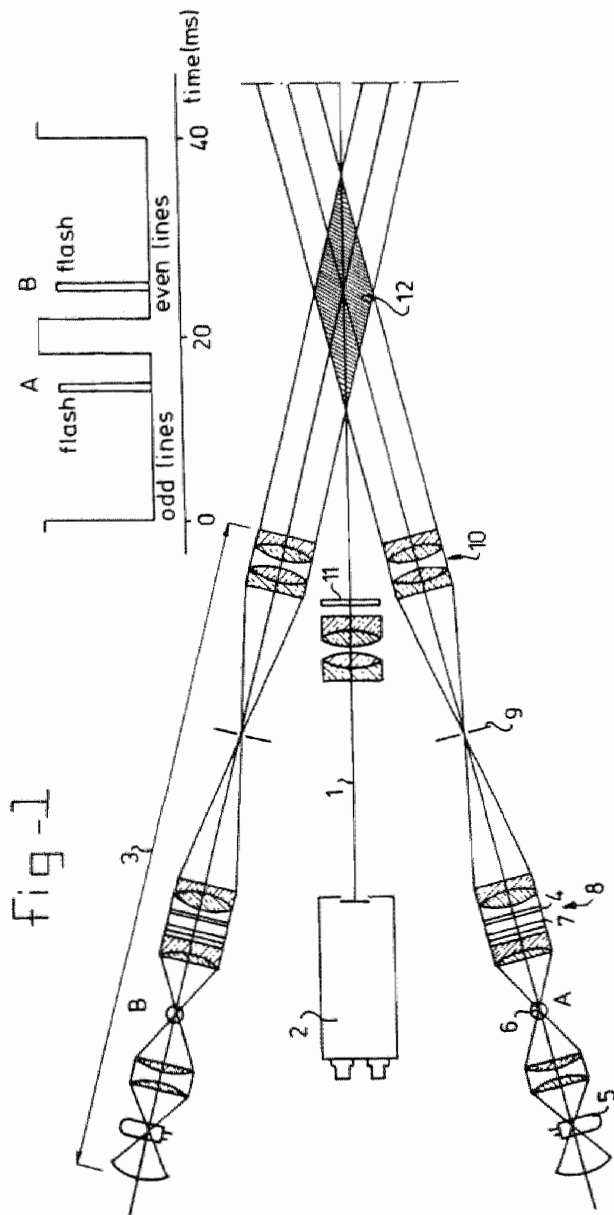
35

40

45

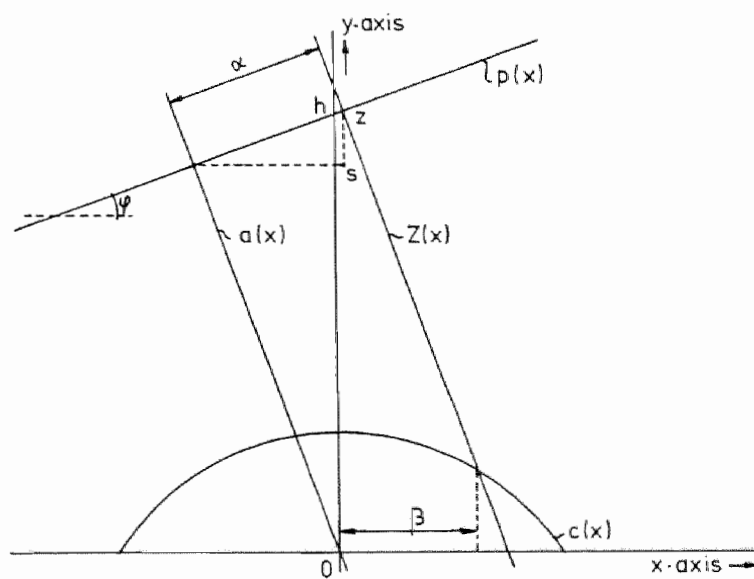
50

55



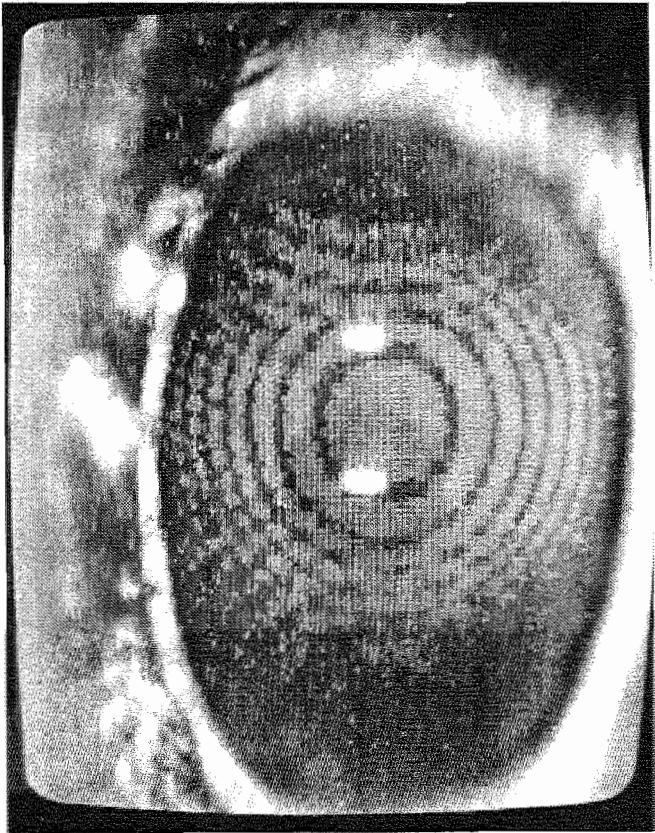
EP 0 551 955 B1

fig-2



EP 0 551 955 B1

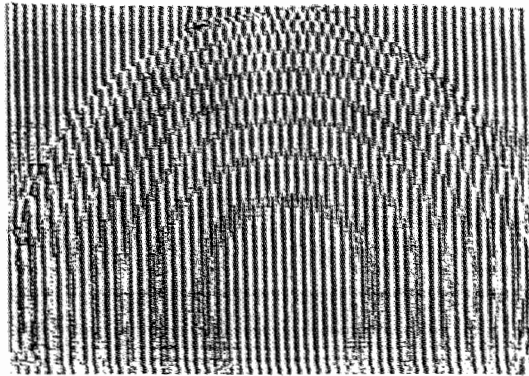
Fig - 3



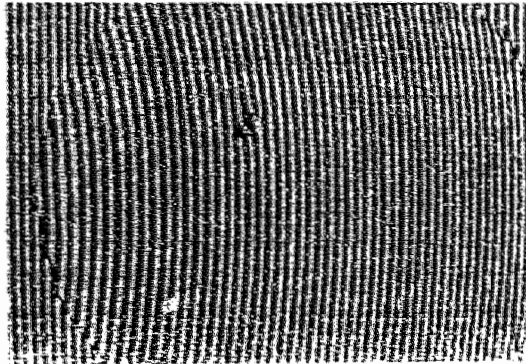
EP 0 551 955 B1

fig - 4

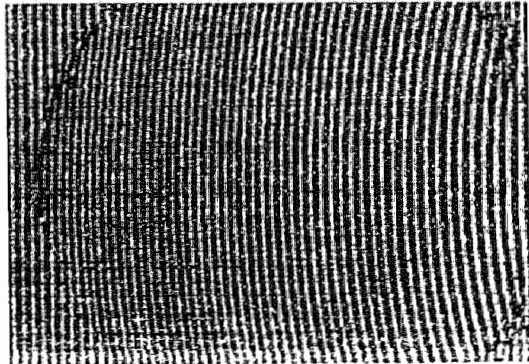
a



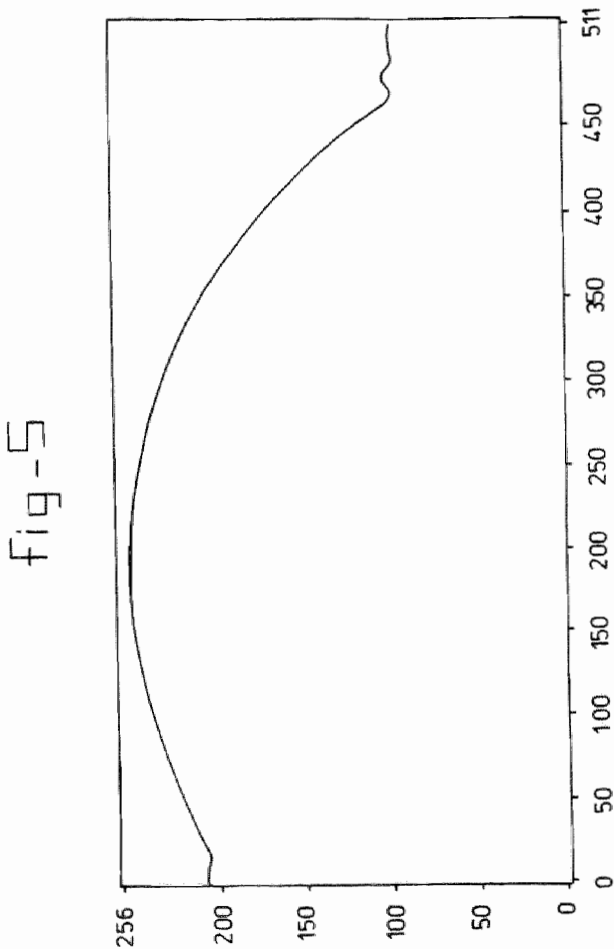
b



c

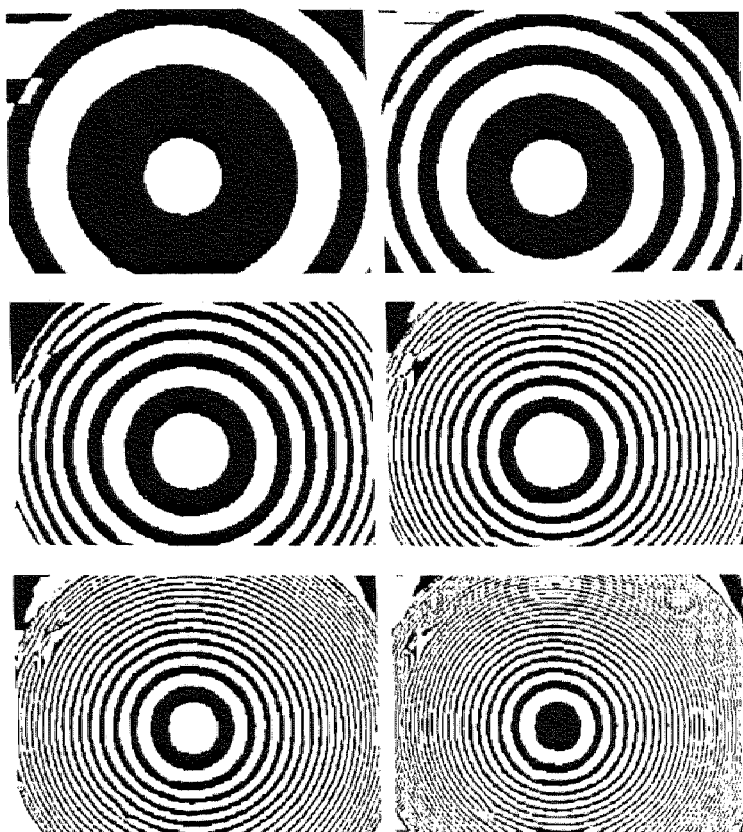


EP 0 551 955 B1



EP 0 551 955 B1

fig - 6



List of symbols and abbreviations

AROC	Axial Radius Of Curvature
AU	Arbitrary Units
TBUT	Tear film Break Up Time
CAVK	Computer Assisted Video Keratometer
CCD	Charge Coupled Device, a light sensitive chip used in miniature video cameras
depth of field	The distance in the object space through which satisfactory definition can be obtained when the lens is in focus for a particular distance
depth of focus	The distance in the image space through which an allowable blur circle of a point in the objectspace can be obtained
diffraction limited	An optical system that is called "diffraction limited" has reached boundaries of resolution determined by the wave character of light
D	Dioptre. Unit of refractive power of a lens expressed as the reciprocal of its focal length in meters
eccentricity	A measure for the cornea's peripherally decreasing curvature
frame grabber	Interface from camera to computer
FWHM	Full Width Half Maximum
IR	InfraRed
IROC	Instantaneous Radius Of Curvature, radius of corneal curvature that not necessarily coincides with the axial radius of curvature. In this thesis also referred to as "local radius of curvature".
LED	Light Emitting Diode
lp/mm	line pairs per mm
LS	Large molecular Strip
LU	Large molecular Unit
m	meter
meridian	A line through the assumed visual axis of the subject and optical axis of the topographer oriented in a certain direction to indicate the position of surface features such as height, axial or local radius of curvature etc.
mire	light emitting pattern of which the reflection on the corneal surface is used to estimate the corneal radius of curvature
ml	millilitre
moiré	Pattern that can appear when two periodic patterns are superimposed
MST	Maastricht Shape Topographer, a topographer that measures the height of the anterior eye with respect to a reference plane
μm	Micrometer (m^{-6})
NA	Numerical Aperture, the half angle of the cone of light departing from the focal plane, accepted by the objective lens
nm	Nanometer (m^{-9})

opacity	Opacity is defined as the ratio between fluorescent yield at 40 μm layer thickness and maximum fluorescent yield (found at thicker layers)
orthoscopic	Corrected for distortion due to obscuring the perspective relation between the picture elements representing the object
OSPCO	Object SPecular COherent
OSPIN	Object SPecular INcoherent
PC	Personal Computer
PIDIFCO	Projected Image DIffuse COherent
PIDIFIN	Projected Image DIffuse INcoherent
PISACO	Projected Image ScAttering Coherent
PISAIN	Projected Image ScAttering INcoherent
PISDIFIN	Projected Image SPecular and DIffuse INcoherent
PISPCO	Projected Image SPecular COherent
PISPIN	Projected Image SPecular INcoherent
PISHIN	Projected Image SHadow INcoherent
pixel	Picture element
Placido disc	A flat disc with concentric black and white circles
Purkinje image	Virtual image, seen when a pattern is reflected by the eye
Scheimpflug	Scheimpflug correction. An optical technique to provide critical focus for projections that are obliquely oriented to the optical axis of the viewing system
snapshot device	A device in which all data are gathered simultaneously
SNR	Signal to Noise Ratio
SS	Small molecular Strip
SU	Small molecular Unit
telecentric	Telecentric lens. A compound lens so constructed that the aperture stop is located at the front focus. In this way the exit pupil is at infinity.
TGI	Twyman-Green Interferometer
tv	television
UV	UltraViolet

Summary

Introduction

The optical part of the eye consist of a succession of transparant tissues with different refractive indices. The first transition, from air to tear film, causes the largest optical density step and the tear film coated cornea is therefor the most important refracting surface.

Considerably progress has been made in the optical correction of this first surface by refractive surgery as well in manufacturing of contact lenses. Modern computer assisted lathes are able to made, besides spherical and aspherical fittings, torical (barrel shaped) fittings and corrections and fittings that are extended to the shape of the adjacent tissues (limbal area and sclera). With these developments the demand for a topographer that can measure the topography of the entire anterior eye has become important.

The aim of this study concerns the development and evaluation of an instrument that can fulfill this task. Measurement should also be feasible on irregular corneal and adjacent surfaces.

The thesis consist 7 chapters and an appendix consisting the patent in which the developed anterior eye topographer is described.

In the first chapter the aims of this study are defined and the principles employed in the construction of the "Maastricht Shape Topographer" (MST) are presented.

The second chapter presents an overview of scientific literature- and patent-research and describes a large number of corneal topography techniques. These techniques are categorized in 12 groups according to their use of light source and light matter interaction. The MST is also included in this scheme.

The MST uses sodium fluorescein as a fluorescent agent to alter the specular reflecting surface in a diffusely radiating surface. The characteristics of this label investigated with phantom studies and investigated under *in vivo* circumstances are described in chapter 3.

In chapter 4 a description of the patent on the MST is given to elucidate the complicated original text. The MST collects height data from the anterior eye, by means of stereoscopically projected, parallel fringes that are recorded with a CCD camera placed between the two projectors. The resolution in heighth is $\pm 5 \mu\text{m}$ and the lateral resolution is about $40 \times 30 \mu\text{m}^2$, being the size of a camera pixel (picture element) projected on the eye.

Chapter 5 demonstrates the technical performance of the MST, using simplified eye models. The aim was to validate the ability of the MST to measure height over a wide area. Phantom studies and one *in vivo* study on a human eye show that meridians (cross-sections) of 17 mm wide could be measured.

A clinical evaluation of the MST has been performed at the St. Thomas' Hospital in London, UK. This study is described in chapter 6. Measurements were carried out on patients with corneal pathologies and patients who underwent photorefractive surgery. The measurements were made with both the MST and a commercially available Purkinje image-based Computer Assisted VideoKeratometer (CAVK). Some preliminary results of clinical evaluation in Rotterdam and Maastricht are presented.

In the last chapter the nature and accuracy are discussed from the on the surface local-

ized measurements with the MST vs the measurements done with an on specular reflection based system.

Samenvatting

Samenvatting

Het optisch gedeelte van het oog bestaat uit een opeenvolging van transparante weefsels met verschillende brekingsindex. De eerste overgang, van lucht naar traanfilm, veroorzaakt de grootste optische dichtheids stap, reden waarom het met een traanfilm bedekte hoornvlies het belangrijkste brekende oppervlak is.

Zowel op het gebied van micro-chirurgische oogheelkundige technieken als op het gebied van de fabricage van contactlensen is er de laatste decennia een aanzienlijke vooruitgang geboekt. Moderne computergestuurde draaibanken kunnen nu naast sferische- en asferische-pasvormen ook torische (tonvormige) pasvormen maken alsmede correcties en pasvormen die zijn uitgebreid om ook aan te sluiten op de aangrenzende weefsels als de overgang van hoornvlies naar het oogwit ("limbus") en het oogwit zelf ("sclera"). Door deze ontwikkelingen is er behoefte ontstaan aan een topograaf die de vorm van het gehele voorste oogsegment kan meten.

Het doel van dit onderzoek is de ontwikkeling en evaluatie van een instrument dat deze taak kan vervullen. Ook onregelmatige hoornvlies- en aangrenzende-oppervlakken moeten gemeten kunnen worden.

Het proefschrift bevat 7 hoofdstukken en een appendix waarin het octrooi van de topograaf is opgenomen.

In het eerste hoofdstuk worden de doelen van het onderzoek gedefinieerd en de gebruikte principes voor de ontwikkeling van de "Maastricht Shape Topographer" (MST) uitgelegd.

In het tweede hoofdstuk wordt een overzicht gegeven van het wetenschappelijk literatuur- en octrooi-onderzoek en er worden een groot aantal technieken beschreven. Deze technieken zijn onderverdeeld in 12 groepen overeenkomstig het gebruik van de lichtbron en de licht - materie interactie. In dit overzicht is de MST eveneens opgenomen.

De MST gebruikt fluoresceïne als middel om het spiegellend reflecterende traanoppervlak om te vormen tot een diffuus stralend oppervlak. De eigenschappen van fluoresceïne onder laboratorium omstandigheden en *in vivo* zijn onderzocht en beschreven in hoofdstuk 3.

In hoofdstuk vier wordt een beschrijving van het octrooi op de MST gegeven om de gecompliceerde originele tekst te verduidelijken. De MST verzameld hoogte-gegevens van het voorste oogsegment, door middel van stereoscopisch geprojecteerde, evenwijdige franjes die met een CCD-camera die tussen de twee projectoren in geplaatst is worden opgenomen. De locale hoogte resolutie is $\pm 5 \mu\text{m}$ and de laterale resolutie is ongeveer $40 \times 30 \mu\text{m}^2$, overeenkomstig de afmeting van een CCD pixel (picture element) geprojecteerd op het oogoppervlak.

Hoofdstuk 5 laat aan de hand van vereenvoudigde oogmodellen de technische kwaliteit van de MST zien. Het doel was om na te gaan of de MST de hoogte over een groot gebied kan meten. Metingen aan de modellen en in een *in vivo* meting aan een humaan oog tonen aan dat meridianen (doorsneden) over een 17mm gebied kunnen worden verkregen.

Een klinische evaluatie van de MST was verricht aan het St. Thomas' Hospital in Londen. Deze evaluatie is beschreven in hoofdstuk 6. Ogen van patiënten met hoornvlies aandoeningen en van patiënten die fotorefractaire chirurgie ondergingen, waren

onderwerp van dit onderzoek. De metingen werden zowel met de MST gemaakt als met een commercieel verkrijgbare computer ondersteunde topograaf die gebaseerd is op spiegeling van concentrische ringen (Placido schijf techniek) via de traanfilm. Tevens zijn in dit hoofdstuk enkele eerste resultaten van klinische evaluaties uitgevoerd in Rotterdam en Maastricht beschreven.

In het laatste hoofdstuk worden de op het oogoppervlak gelocaliseerde MST metingen vergeleken met metingen verricht met een op spiegelende reflectie gebaseerd systeem.

Dankwoord

Dankwoord

Allen die hun bijdrage aan dit promotiewerk leverden bedanken lijkt mij een loffelijk streven. Voor een 4 jaar durende promotie periode is het aantal hulpverleners nog te overzien. Voor het corneatopografie project dat reeds in 1985 startte is dit aanzienlijk lastiger. Daarom begin ik met de op deze plaats met de hier niet met name genoemden te bedanken.

De tijdspanne waarin dit proefschrift tot stand gekomen is kent twee stromen, een academische en een medisch-technische stroom. De bron van de academische stroom is prof. dr Martin van Gemert. Beste Martin jij was de eerste die mij met het stoutmoedig plan om te promoveren confronteerde. Dat heeft nogal wat onrust bij me veroorzaakt waarvoor ik je zeer dankbaar ben. Prof.dr Fred Hendrikse heeft me actief geholpen om deze onrust weg te werken en het pad gebaad tot toelating tot de academische promotie. Beiden zijn dan ook tot mijn vreugde mijn promotor geworden. Om deze weg in te slaan als niet academicus is lastig. Gelukkig heeft dr Herman Kingma mij de eerste beginselen bijgebracht om tot de samenstelling van dit proefschrift te komen.

De bron van de medisch-technische stroom is ir Bas Naastepad, toenmalig directeur van de Stichting Medische Technologie. Bas heeft mij in 1985 gevraagd om een "keratometer" te ontwikkelen. Ver stroomopwaards tijdens een PAOG bijeenkomst kwam ik Margo Beintema, oogarts tegen, die me een lift terug aanbood en me aanmoedigde de banden met de Afdeling Oogheelkunde in Annadal verder aan te halen. Zonder Bas en Margo was ik, veel later, niet in de gelegenheid geweest om dit boekje te schrijven. Dankzij de hulp van Klaas de Boer kon al gauw een eerste prototype getest worden. Bas Peters, nu inmiddels drs ing, was mij behulpzaam met de validatie van deze voorloper van de "Maastricht Shape Topographer". In een latere fase droegen de HTS studenten Etienne van Daelen, Hans van der Logt en Emile Goosens hun steentje bij. Na de aanvankelijk voorspoedige technische voortgang kwam er een periode van stagnatie. Het bleek zeer lastig om op basis van het analoog werkende apparaat een commerciële partner te vinden. Drs John Vossen, dr Loek Kreukels, drs, later dr René Vleugels, dr Nick Sassen en drs Erik Boom speelden hierin, uiteindelijk met succes, een actieve rol.

Het CvB van de toenmalige RL en de respectievelijke voorzitters van de Afdeling Oogheelkunde, prof.dr Wiel Lamers en prof.dr Fred Hendrikse, hebben er ruimhartig voor gezorgd dat een financieel moeilijke periode werd overbrugd. Hierdoor kon onder leiding van René Vleugels een professioneel prototype gebouwd worden.

Mijn toenmalige kamergenoot dr George Willems opperde het idee om Fourier analyse voor de dataverwerking te gebruiken. Hier ging drs ing Fons Laan enthousiast mee aan de gang en wist ondanks de werkzaamheden verbonden aan zijn promotie, de eerste Fourier analytisch berekende hoogtekaarten te produceren. Prof.dr John Marshall, hoofd van de Eye Clinic in het St. Thomas' Hospital in Londen was geïnteresseerd geraakt in onze topograaf en bood ons hulp aan bij de klinische evaluatie. Het was aan ing Bertho Stultiens te danken dat een compleet werkend apparaat op tijd voor verscheping naar Londen gereed kwam. Hierbij werd hij ondersteund door een klein team, waaronder Hans van der Voort, die de mechanica verzorgde. Klaas Ferweda, industrieel vormgever zorgde voor een originele behuizing in prachtig grijs en blauw zoals de kleuren van een Citroën uit de 60er jaren.

Bertho werd zo geboeid door het onderwerp, dat hij zich, tot grote vreugde van de evaluatiegroep in Londen, ook met de wetenschappelijke kanten van het onderzoek ging bezig houden. Daarnaast bleek Bertho's interesse in de zakelijke kanten waar hij echter minder enthousiaste respons ontving. Ik ben er trots op dat hij uiteindelijk voor de wetenschap gekozen heeft en nu een proefschrift mag voorbereiden met corneatopografie als onderwerp bij prof.dr N. Ehlers in Århus, Denemarken.

Dr Melanie Corbett van het St Thomas Hospital in Londen heeft met haar klinische evaluatie van de MST een onmisbare bijdrage aan het onderzoek geleverd. Dat laatste geldt ook, en mogelijk in nog sterkere mate, voor drs John de Brabander. John heeft zich als contactlensspecialist in het Academisch Medisch Centrum te Amsterdam intensief met het aanpassen van bijzondere contactlenzen op bijzondere ogen m.b.v. de MST beziggehouden. Ook John werd door het heilige vuur gegrepen en heeft zich nu geschaard bij het Maastrichtse team. Hij heeft nu, als eerste medewerker van het Eye Research Institute Maastricht, de MST geïncorporeerd in zijn promotieonderzoek "Met het oog op contactlenzen". John heeft ook op andere wijze een bijdrage geleverd aan de totstandkoming van dit proefschrift. Vooral tijdens het schrijven kon ik vaak met hem overleggen over de vorm en inhoud van mijn dissertatie. Eveneens betrokken bij de klinische validatie van de MST was Titia Hieselaar, toen nog oogarts in opleiding. Ook is zij actief geweest bij de verkoop van de licentierechten op het octrooi door met succes een demonstratie van de MST in Washington te verzorgen. Ik denk nog met veel plezier aan ons zonnige weekend met Erik Boom in Washington terug.

Ook de vele hulpvaardige handen uitgestoken vanuit de Instrumentele Dienst van de UM, ik denk hierbij in het bijzonder aan Jeroen Hameleers die menig probleem voor me kon oplossen, waren onmisbaar om het project tot een goed einde te brengen. De ondersteuning van Ellen Timmermans, Sasscha Nix, Marian Jansen en Chantal Rosier tijdens de afronding van mijn promotiewerk had ik niet graag gemist. In deze periode heeft ook Marion Meulendijks zich onderscheiden door, ondanks haar drukke werkzaamheden met oogheelkundige fotografie, ons toe te staan om de spleetlamp af en toe grondig te verbouwen voor ons onderzoek.

Soms is het een verrassende kleinigheid die iemand bijdraagt. Ik denk hierbij aan Puck Muller die een van haar prachtige ravezwarte haren ter beschikking stelde voor de wetenschap.

Ten slotte dank ik allen die mijn proefschrift kritisch hebben gelezen en van commentaar voorzien in het bijzonder mijn promotor Martin van Gemert die hiervoor zelfs een week van zijn vakantie opofferde. In dit kader wil ik ook de anonieme referenten van de in dit proefschrift opgenomen artikelen danken evenals ir A. Plaisier, die mij geholpen heeft met het schrijven van het octrooi en de verdediging van de conclusies voor de Europese, Amerikaanse en Japanse "examiners".

Een fase waarvan het belang door mij aanvankelijk onderschat werd, was de beoordeling door de beoordelingscommissie. Vele waardevolle opmerkingen mocht ik ontvangen van de externe inhoudsdeskundigen dr ir Chris Velzel en dr Rob van der Heijde. De interne beoordelaars prof.dr Luc Snoeckx, prof.dr ir Arnold Hoeks en in het bijzonder prof.dr Wim Hermens, voorzitter van de commissie, hebben er in aanzienlijke mate aan bijgedragen dat dit proefschrift ook voor "leken" wat toegankelijker werd. Tenslotte heeft Bob Wilkinson mijn Engels ontcijferd en in echt Engels omgezet.

De vormgeving van het proefschrift is op een hoger plan gekomen dankzij Peggy Bisschoff wat betreft algemene lay out en Geertjan van Zonneveld die de omslag ontwierp.

Als laatste in deze chronologische opsomming wil ik mijn lieve Magda bedanken voor haar altijd weer opgewekte morele ondersteuning tijdens mijn promotiewerk ondanks de vele avonden en enkele nachten die ik soms letterlijk maar vaak figuurlijk "niet thuis" was.

Curriculum vitae

Curriculum vitae

Franciscus Hermanus Maria Jongsma was born in the Hague on May 21, 1938. In 1962 he received the certificate for Technical and Scientific Photography at the School of Photography and Phototechnique, the Hague. He is presently scientist at the University Hospital and staff member of the Department of Ophthalmology, University Maastricht/University Hospital Maastricht.

He is married to Magdalena Wenderickx and is father of two daughters, Hanneke and Sophia.

List of publications

Papers

- Jongsma FHM. Liquids with a very low ultrasound propagation velocity. *Ultrasonics* 1979;17(5):233
- Jongsma FHM, Van de Bogaard AEJM, Van Gemert MJC and Hulsbergen Henning JP. Is closure of open skin wounds accelerated by argon laser exposure? *Lasers in surgery and Medicine* 1983;3:75-80
- Sterenborg HJCM, de Rijke ThM, Wiersma J, Erckens RC and Jongsma FHM. High-speed photographic evaluation of endoscopic lithotripsy devices. *Urol Res* 1991;19:381-385
- Van den Biesen PR, Jongsma FHM, Tangelder GJ, Slaaf DW. Shear rate and hematocrit dependence of fluorescence from retinal vessels in fluorescein angiography. *Ann. Biomed. Eng.* 1994;22:456-463
- Goossens ELJ, Reutelingsperger CPM, Jongsma FHM, Kraayenhof R, Hermens WTh. Anxin V perturbs or stabilises phospholipid membranes in a calcium dependent manner. *FEBS Letters* 1995;359:155-158
- Corbett MC, O'Brart DPS, Stultiens BATH, Jongsma FHM, and Marchall J. Corneal topography using a new moiré image-based system. *Eur. J. of Implant & Refractive Surgery* 1995;7:353-369 (Dissertation, Chapter 6)
- Van den Biesen PR, Jongsma FHM, Tangelder GJ, Slaaf DW. Yield of fluorescence from Indocyanine Green in plasma and flowing blood. *Ann. Biomed. Eng.* 1995;23:475-482
- Jongsma FHM, Erckens RJ, Wicksted JP, Bauer NJC, Hendrikse F, March W and Motamedi M. Confocal Raman spectroscopy system for noncontact scanning of ocular tissues: an in vitro study. *Opt Eng* 1997;36(11):3193-3199
- Jongsma FHM, de Brabander J, Hendrikse F, and Stultiens BAT. Development of a wide field height eye topographer: Validation on models of the anterior eye surface. *Optom Vis Sci* 1998;75(1):69-77 (Dissertation, Chapter 4)
- Jongsma FHM, de Brabander J and Hendrikse F. Review and classification of corneal topographers. *Lasers Med Sci* (In press. Dissertation, Chapter 2)

Patents

- Jongsma FHM. System for determining the topography of a curved surface. United States Patent 5,406,342 April 11 1995
- Jongsma FHM. System for determining the topography of a curved surface. European Patent EP 0 551 955 B1 1997
